EXPECTED POSITION ERROR FOR AN ONBOARD SATELLITE GPS RECEIVER

THESIS

Anthony S. Williams, 1st Lieutenant, USAF

AFIT-ENY-MS-15-M-029

DEPARTMENT OF THE AIR FORCE
AIR UNIVERSITY

AIR FORCE INSTITUTE OF TECHNOLOGY

Wright-Patterson Air Force Base, Ohio

AFIT-ENY-MS-15-M-029

EXPECTED POSITION ERROR FOR AN ONBOARD SATELLITE GPS RECEIVER

THESIS

Presented to the Faculty

Department of Electrical and Computer Engineering

Graduate School of Engineering and Management

Air Force Institute of Technology

Air University

Air Education and Training Command

in Partial Fulfillment of the Requirements for the

Degree of Master of Science in Electrical Engineering

Anthony S. Williams, B.S.E.E.

1st Lieutenant, USAF

March 2015

AFIT-ENY-MS-15-M-029

EXPECTED POSITION ERROR FOR AN ONBOARD SATELLITE GPS RECEIVER

THESIS

Anthony S. Williams, B.S.E.E.
1st Lieutenant, USAF

Committee Membership:

Dr. Alan Jennings, PhD
Chairman

Dr. Eric D. Swenson, Ph.D.
Member

Dr. Marshall E. Haker, Ph.D.
Member

Abstract

The Global Positioning System (GPS) constellation provides ranging information that delivers inexpensive, high precision positioning for terrestrial users. Satellites in Low Earth Orbit (LEO) can use an onboard GPS receiver resulting in meter-level navigation solution accuracy. There are limitations to using GPS for positioning for satellites above LEO. The number of GPS satellites whose signal can be received decreases as the receiver's altitude approaches that of the GPS constellation. Above the GPS constellation, the available GPS signals for ranging will originate from satellites on the opposite side of Earth. This research calculates the available GPS signals to the receiver and determines the expected position error, while considering the effects from low signal to noise ratios, poor geometry, and signal shift caused by high relative velocity.

Acknowledgements

I would like to acknowledge both Dr. Jennings and Maj Haker for taking on the role of being my advisor and as well as committee member at various times during this research effort. I was able to make it this far thanks to their guidance. I would also like to thank my ANT classmates. I learned a great deal more through the debates, discussions, and overall conversations that took place throughout these 18 months. I would gladly redo this experience and much more if I was allowed to have classmates like you all again! I also want to acknowledge the AFIT Summer 2014 interns Arnett, Wagner, and Dieterle for all their work in creating the MATLAB GUI and configuration of the RF signal simulators. Last, but not least, I would like to thank my friends and family members for keeping me sane and smiling throughout this experience.

Anthony S. Williams

Table of Contents

Page

List of Figures

List of Tables

EXPECTED POSITION ERROR FOR AN ONBOARD SATELLITE GPS RECEIVER

I. Introduction

1.1 GPS Based Orbit Determination

The first NAVSTAR Global Positioning System (GPS) was launched in 1978 and has quickly become the leading tool for Position, Navigation, and Timing (PNT) applications worldwide. GPS receivers have become relatively inexpensive and terrestrial users of GPS are capable of obtaining centimeter level accuracy. The low cost, reliability, and success rate of GPS for PNT on Earth drove the desire for space based application. Benefits of implementing the already operational GPS system for on-board orbit determination are listed below [3]:

1. Reduced amount of ground stations required for operation.
2. Scheduling of ground station operation data collection made easier and can be done in advance
3. Reduced cost from the reduction of ground stations
4. Orbit determination automation possible
5. Multiple satellite formation flying possible

When the receiver remains close to the Earth's surface, there is little change to the expected GPS coverage compared to a ground user. GPS signals still originate from above, Earth obstructs all the signals from underneath, and the ionosphere still

affects the signal. Depending on the altitude, the user may not be affected by the troposphere but there are other consumer based challenges, such as the requirement for an unlocked GPS receiver plus the issue of handling increased Doppler magnitudes compared to ground users. Concerns about the GPS coverage environment increase when the receiver's altitude approaches or surpasses the orbital altitude of the GPS constellation. When planning for GPS utilization at or above the GPS orbital altitude, issues such as lower signal strength from increased range, error sensitivity due to poor geometry, and effects of increased GPS satellite-to-receiver relative velocity have to be considered.

1.2 Problem Statement

The GPS antenna is designed with Earth coverage as the main focus so it uses a directional beam antenna to focus its transmit power over Earth's hemisphere. The area of this 'main beam' is located between GPS and Earth, and has some spillage over Earth's edge. The availability of GPS Space Vehicles (SVs) decreases as a user approaches and even surpasses the GPS's constellation altitude due to being outside of the GPS main beam's area. Instead of relying on GPS signals that lie between the GPS SV and Earth, users above the GPS constellation depend on the main beam spillage originating from the opposite side of Earth. Multiple issues need to be reviewed when relying solely on GPS signals originating from the opposite side of Earth. These issues include limitations on the number of available satellites due to Earth obstruction; increased error caused by lower signal strength; and decreased GPS angle of separation relative to the user, leading to poor geometry. Conventional tools for position determination and position error sensitivity, such as the Newton-Raphson Least Squares algorithm and the Dilution of Precision (DOP) metric, are evaluated for applicability in these scenarios.

1.3 Research Contributions

The goal of this research effort is to investigate the error expected when calculating position with a GPS receiver onboard a subject SV in seven different orbital altitudes. Position error is estimated at each point in the desired satellite's orbit. The orbits of interest for calculating position error include those located below as well as above the GPS constellation, for example Low Earth Orbit (LEO) and Geostationary Orbit (GEO). This research will take into account User Equivalent Range Error (UERE), signal strength degradation due to distance, and the effects of Doppler resulting from the high velocity of the spacecraft near perigee. Effects of the GPS antenna sidelobes will also be considered when determining GPS signals available to the user at each time step. This thesis outlines a process for evaluating expected GPS accuracy tailored to the concerns of satellite orbits.

1.4 Thesis Overview

The purpose of this research is to evaluate the magnitude of errors observed when using GPS for positioning at different select orbits. To better understand the problem, a look at orbit characteristics, the GPS constellation, existing errors affecting GPS, existing position determination algorithms, and other relevant topics are presented in Chapter II. Chapter II ends with the introduction of the resources used in this research. The methodology behind the construction of the simulation to investigate this problem and all underlying assumptions made in this research are discussed in Chapter III. Chapter IV describes the results from the simulations of seven different scenarios. Finally, Chapter V wraps everything together and gives ways to build on the results of this thesis.

II. Background

2.1 Introduction

The goal of this chapter is to provide the reader with background information about orbits in space, GPS, and some existing methods for either using GPS to determine position or reducing errors involved with GPS. A brief overview of different orbits will be described with GPS reception in mind, followed by an overview of the current GPS constellation. Afterwards, errors affecting the GPS signal are reviewed before presenting the position estimation method and error sensitivity method to be tested with this research. Finally, other known methods for position estimation and error reduction will be given.

2.2 Orbits

Low Earth Orbit.

Low Earth Orbit (LEO) is a stable path around Earth with an altitude between 80 km and 2,000 km [2]. The orbital velocity for satellites in LEO average around 27,500 km/hr [17] resulting in an orbital period of approximately 90 min. LEO contains altitudes that are within the GPS antenna main beam's intended area of effect, so obtaining multiple GPS satellites in view for position determination is not an issue. The increased velocity compared to a terrestrial user will increase the range of Doppler values seen at the receiver. Doppler range is one limiting factor in choosing suitable GPS receivers.

Higher Orbits.

There are two orbits at altitudes higher than LEO that are of interest in this research: Medium Earth Orbit (MEO) and GEO. GEO is characterized by being at

an altitude of 35,786 km and having an orbital period equal to the Earth's rotational period [2]. The MEO falls between LEO and GEO, and has an altitude between 2,000 km and 35,786 km with an orbital period between 90 min and 24 hrs [2].

Satellites operating in MEO and GEO encounter more issues with GPS-based position determination than those in LEO. One of the major differences in comparison with LEO is the location of the GPS satellites available to the user. For a user located above the GPS constellation, the GPS signal originates from beneath the user, versus overhead in the case for terrestrial and LEO users of GPS [18]. GPS signals that are capable of reaching the user will originate from the opposite side of Earth or from the antenna side lobes of nearby GPS SVs. Figures 2.1 and Figure 2.2 illustrate the potential GPS transmit beams available for a user whose orbital altitude is above that of the GPS constellation.

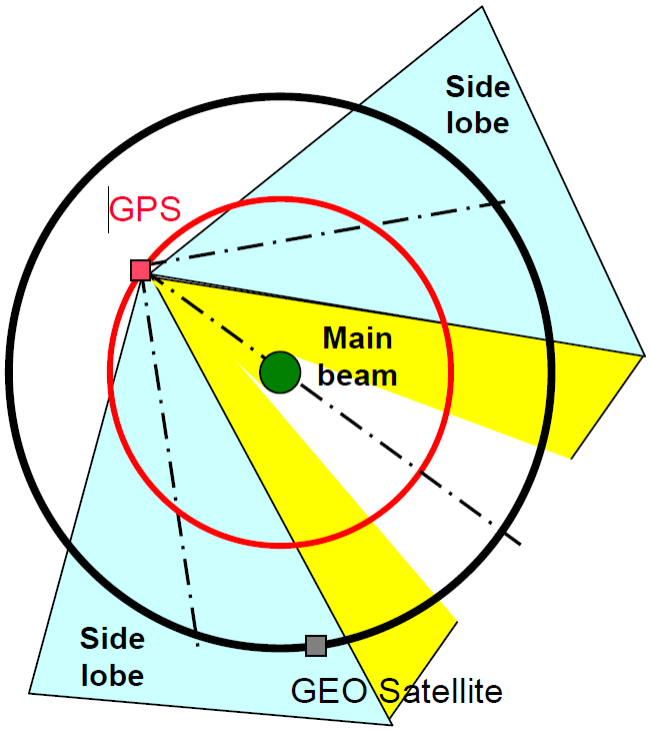

Figure 2.1. Potential GPS Beams Available at GEO [18]

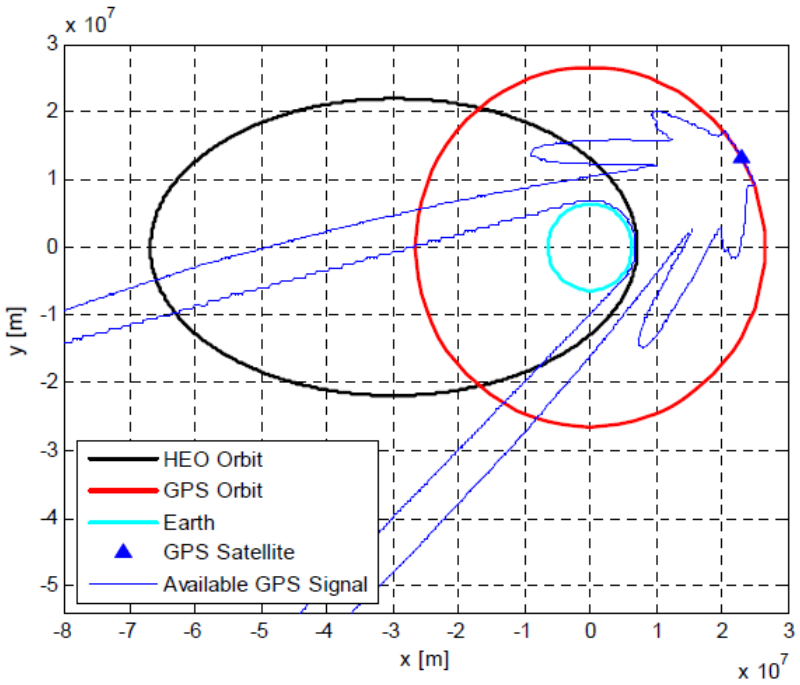

Figure 2.2. Potential GPS Beams Available at HEO [10]

2.3 GPS

Current GPS constellation consists of 31 operational SVs flying in MEO. GPS SVs fly in a nearly circular orbit with an altitude of approximately 20,200 km and an orbital period of approximately 12 hrs [14]. The satellites are divided into six orbits, each containing a minimum of four satellites. Every GPS satellite is three-axis stabilized, Earth pointing, with an inclination of 55°. The system is now mainly used for terrestrial applications but has recently been proven to work with receivers located in space. GPS receivers are being flight tested on-board certain SVs in LEO, e.g. [7].

2.4 GPS Error

Signals from GPS satellites that are near the Earth's horizon, though unobstructed by Earth, still have errors introduced from traversing through the ionosphere. The magnitude of errors from the ionosphere depends on the distance the signal travels

through the ionosphere before reaching a receiver. A good illustration of this is from [18] and is shown in Figure 2.3.

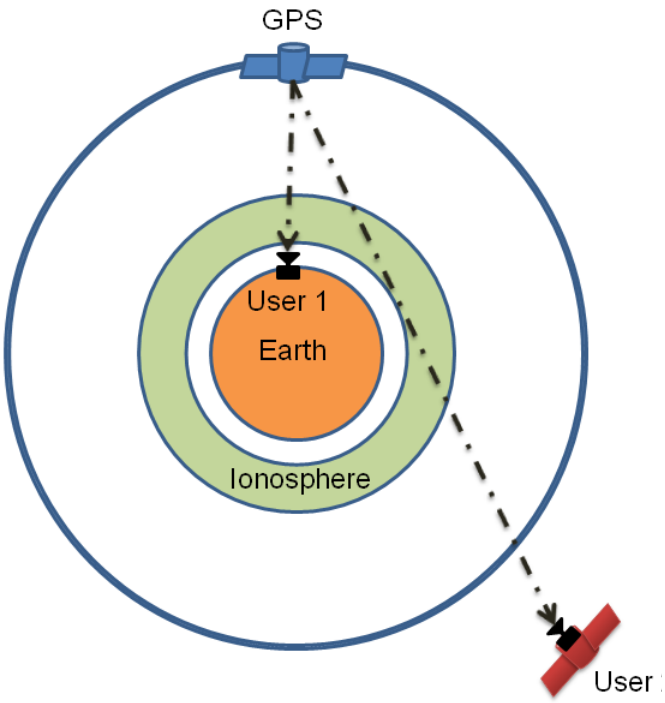

Figure 2.3. Ionosphere Layer Illustration (not drawn to scale)

Ionosphere Effects.

The ionosphere refers to a region of ionized gases which is also a dispersive medium for radio waves. The ionosphere extends from around 50 km to 1000 km above the Earth [14]. When the GPS signal passes through the ionosphere, the code and modulating signal propagate at different speeds. This results in the code phase being delayed and the carrier phase being advanced by the same magnitude [14]. This effect can be negated by using a dual frequency receiver that processes both GPS L1 and L2 frequencies.

For the purposes of determining GPS tracking capability above LEO, many of the current research makes the assumption that the ionosphere completely obstructs GPS signals similar to the Earth. This research assumes the use of a dual frequency

receiver so ionospheric effects are minimized. More information on the method can be found in [14].

Signal Degradation.

As a signal travels through a space, there is inherent power loss. The amount of power loss is directly related to the distance traveled. Received signal strength (RSS), the amount of signal power at the receiver, from the ith transmitter can be represented as follows [21]:

$$\underline{A}_i(d_i) = A_0 - 10n_p \log_{10}\frac{R_i}{R_0} + \underline{V}_i \tag{2.1}$$

where $\underline{A}_i(d_i)$ is the estimate of received power in Decibels (dB) at a distance of R_i, R_0 is the reference distance, A_0 is the known power in dB at the reference distance, n_p is the path loss exponent, and $\underline{V}_i$ is a zero-mean Gaussian random variable in dB [21]. GPS uses a relatively low power signal, with a minimum received strength for a 3 dB polarized antenna on Earth between -160 dBW and -153 dBW for the L1 signal [19]. In [18], one of the underlying assumptions made to consider an unobstructed GPS signal available to the simulated GPS receiver at GEO is for the power received to be higher than -185 dBW. GPS signal strength is referred in terms of the Signal to Noise Ratio (SNR) or more commonly Carrier Power to Noise Density Ratio (C/N0) (in units of dBHz). Comparing the signal strength to the background noise is important when determining if the signal is strong enough to be acquired by a receiver. For a simulation study in [13], a usable GPS signal required the C/N0 at the receiver to remain above the user defined minimum long enough to decode the navigation message. Another example is an actual flight test in [4] where the GPS receiver is equipped on a satellite named Equator-S. The receiver had an acquisition threshold of 37 dBHz but did not directly measure and output SNR, so a relation between its

signal strength parameter and SNR value was used to determine relative physical SNR values. This helps portray the importance of keeping track of SNR and selecting a receiver with an appropriate threshold.

2.5 Position Determination

Navigation data in the GPS signal contains a variety of information including signal transmission times, clock error corrections, ephemeris data for that specific GPS SV, almanac information for the entire GPS constellation, satellite state of health, etc. Signal transmission time, clock error corrections, and ephemeris data are used to calculate the location of each GPS SV in view as well as approximate ranges from the SVs to the user.

Approximate range measurements derived from the difference between GPS signal transmit time and time of arrival at the receiver are called pseudoranges. A pseudorange is an approximate range from the user's current position to the GPS SV's position. By using the pseudoranges from multiple SVs together with knowledge of SV location, a receiver can estimate its position.

Multiple algorithms are openly available that use pseudoranges to estimate a user's position. One position determination algorithm in particular, generally referred to as the Newton-Raphson method, requires a minimum of four GPS SVs in view. The Newton-Raphson method is implemented in this research and a summary of this method is given in the next section based on a more in-depth description in [14].

Newton Raphson - Least Squares Algorithm.

The Newton-Raphson method is based around solving the range equation. The process of estimating user position involves calculating range to each GPS SV based on a nominal initial guess of the current user's position. The calculated range is

compared with the measured pseudorange to produce an error. Afterwards, the first order Taylor series expansion of the range equation in Equation (2.2) is used to show sensitivities to a user's position. The last step combines the sensitivity information with at least four of the calculated errors to solve for a minimum least squares position error.

The Newton-Raphson method requires a minimum of four satellites because it involves solving a linearized form of the ranging equation:

$$\rho_u^{[s]} = \sqrt{(x^{[s]} - x_u)^2 + (y^{[s]} - y_u)^2 + (z^{[s]} - z_u)^2} + c * t_u \tag{2.2}$$

about an approximate user's position and receiver clock error. In Equation (2.2) the superscript (s) represents the GPS SV, the subscript u refers to the user, ρ is the range, x, y, z are position axes and $c * t_u$ is the receiver clock error t_u being multiplied by the speed of light c to convert it into units of length. After the range equation is linearized, it is iteratively solved for the four unknowns (user's three dimensions of position and receiver clock error) [14].

An initial estimate of user position $[x_u, y_u, z_u]$ and receiver clock error t_u are required for the Newton-Raphson method and will be denoted in equations with a subscript of 0. In the updated range equation:

$$\rho_0^{[s]} = \sqrt{(x^{[s]} - x_0)^2 + (y^{[s]} - y_0)^2 + (z^{[s]} - z_0)^2} + c * t_0 \tag{2.3}$$

$\rho_0^{[s]}$ represents the range from the s^{th} GPS SV to the initial estimated user position at $[x_0, y_0, z_0]$ affected by an estimated receiver clock error of t_0. Relating the estimated values to the truth is accomplished by using the variables $\delta\mathbf{x}$ and δt to represent the difference between truth and estimation. Expressing the true position on each axis as $x_u = x_0 + \delta x$, $y_u = y_0 + \delta y$, $z_u = z_0 + \delta z$ and true receiver clock error as $t_u = t_0 + \delta t$

allows Equation (2.3) to be rewritten in terms the error δt and $\delta \mathbf{x}$ as shown below:

$$\rho_u^{[s]} = \sqrt{(x^{[s]} - x_0 - \delta x)^2 + (y^{[s]} - y_0 - \delta y)^2 + (z^{[s]} - z_0 - \delta z)^2} + c(t_0 + \delta t) \quad (2.4)$$

The next step is to linearize Equation (2.4) by taking the Taylor series expansion of it and only using the first order terms. The resulting form is shown in Equation (2.5) below:

$$\rho_u^{[s]} = \rho_0^{[s]} - \frac{x^{[s]} - x_0}{\rho_0^{[s]}}\Delta x - \frac{y^{[s]} - y_0}{\rho_0^{[s]}}\Delta y - \frac{z^{[s]} - z_0}{\rho_0^{[s]}}\Delta z + c\Delta t \quad (2.5)$$

where $\Delta x, \Delta y, \Delta z$, and Δt represent the approximated difference between the initial estimated user position and the truth. Expressing the range of all GPS SVs in view in the form of Equation (2.5) allows the relationship to be expressed in the form of a matrix operation with some rearranging. The resulting matrix operation is shown in Equation (2.6) and an expanded form is shown in Equation (2.7) [20].

$$\mathbf{\Delta}\rho = \mathbf{H}\mathbf{\Delta x} \quad (2.6)$$

$$\begin{bmatrix} \Delta\rho^{[1]} \\ \Delta\rho^{[2]} \\ \vdots \\ \Delta\rho^{[N]} \end{bmatrix} = \begin{bmatrix} a_x^{[1]} & a_y^{[1]} & a_z^{[1]} & -1 \\ a_x^{[2]} & a_y^{[2]} & a_z^{[2]} & -1 \\ & \vdots & & \\ a_x^{[N]} & a_y^{[N]} & a_z^{[N]} & -1 \end{bmatrix} \begin{bmatrix} \Delta x \\ \Delta y \\ \Delta z \\ c\Delta t \end{bmatrix} \quad (2.7)$$

$\mathbf{\Delta}\rho$ is a vector containing the differences between estimated ranges and the true ranges $\rho_0^{[s]} - \rho_u^{[s]}$, $\mathbf{H}$ is a matrix made up of the Taylor series expansion for each GPS SV, $\mathbf{\Delta x}$ is a vector representing the difference between the true user position and the estimated position, and N is the number of visible satellites. The Taylor series components represented in the $\mathbf{H}$ matrix are shown in Equation (2.8).

$$a_x^{[s]} = \frac{x^{[s]} - x_0}{\rho_0^{[s]}} \qquad a_y^{[s]} = \frac{y^{[s]} - y_0}{\rho_0^{[s]}} \qquad a_z^{[s]} = \frac{z^{[s]} - z_0}{\rho_0^{[s]}} \tag{2.8}$$

Since $\Delta\mathbf{x}$ is the difference between the true user position and the estimated position, it can be solved for and used to correct the initial position estimate using Equations (2.9) and (2.10):

$$\mathbf{\Delta x} = (\mathbf{H}^T\mathbf{H})^{-1}\mathbf{H}^T\mathbf{\Delta}\rho \tag{2.9}$$

$$\hat{\mathbf{x}} = \mathbf{x}_0 + \mathbf{\Delta x} \tag{2.10}$$

where $\hat{\mathbf{x}}$ is the new estimate. Simple matrix operations such as this can be applied due to the use of linearized estimates and neglected higher order terms. The whole process is now required to be iterated for those same reasons. The iterative process involves using an initial position estimate, solving for $\mathbf{\Delta x}$, updating the position estimate $\hat{\mathbf{x}}$, using the new estimate to start the process over again, and repeating until the least squares of $\mathbf{\Delta x}$ is under a set threshold.

2.6 Geometry Errors

Precision of the Least Squares method is not only dependent on the number of available GPS SVs but also the geometrical orientation of those SVs relative to the user. A position and time solution cannot be calculated if less than four GPS SVs are available. Even with four or more GPS SVs present, position precision can be degraded due to poor geometry if all the SVs are in the same relative direction. A two dimensional example of this is presented in Figure 2.4. DOP is a metric that takes into account the effect of user-satellite geometry on errors. The more favorable the user-satellite geometry is, the lower the DOP value [14].

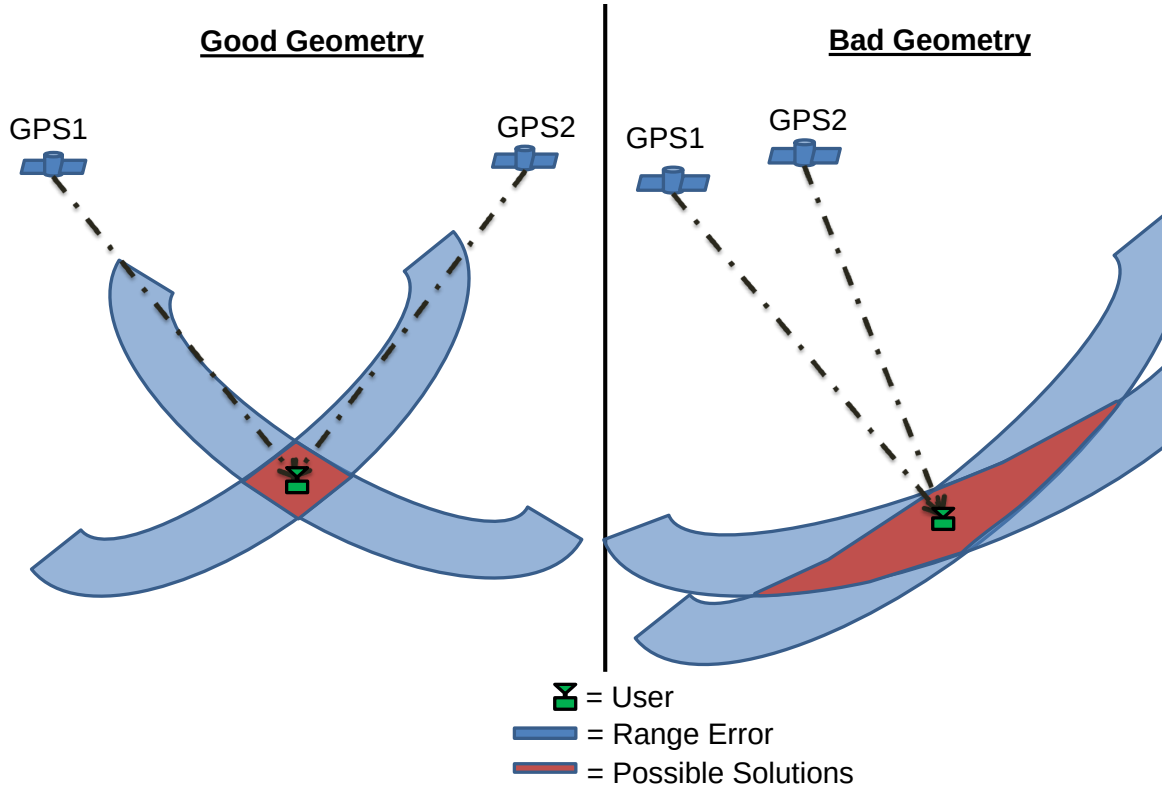

Figure 2.4. Illustration of the effect of geometry on position error

Dilution of Precision.

DOP is a unitless measurement that directly relates sensitivity of range measurement errors to user position errors. Range measurements in this context refer to the pseudoranges from user to GPS SVs. The relation between range and position errors takes into account the geometry of the GPS SVs relative to the user's position. DOP measurement favors relatively large angles of separation between GPS SVs visible to the user. DOP originates as a 4x4 covariance matrix relating to the four dimensions of position (including time). This matrix is calculated in the process of solving for $\mathbf{\Delta x}$ in the Newton Raphson iterative process. In Equation (2.9), the $(\mathbf{H}^T\mathbf{H})^{-1}$ calculation produces the DOP matrix as shown in Equation (2.11).

$$\text{DOP Matrix} = (\mathbf{H}^T\mathbf{H})^{-1} = \begin{bmatrix} D_{xx} & D_{xy} & D_{xz} & D_{xt} \\ D_{yx} & D_{yy} & D_{yz} & D_{yt} \\ D_{zx} & D_{zy} & D_{zz} & D_{zt} \\ D_{tx} & D_{ty} & D_{tz} & D_{tt} \end{bmatrix} \tag{2.11}$$

Each diagonal represents the variance of one axis, $D_{xx} = \sigma_x^2$, $D_{yy} = \sigma_y^2$, etc. It is not practical to refer to the DOP matrix as a whole so DOP is normally referred to with a scalar value. The scalar value is derived from a combination of diagonal values in the 4x4 matrix. Two common combinations are Geometric Dilution of Precision (GDOP), which includes all four dimensions; and Position Dilution of Precision (PDOP), which includes all but time. The equations for the different types of DOP are [20]:

$$\begin{aligned} \text{Geometric DOP} &= \sqrt{D_{xx} + D_{yy} + D_{zz} + D_{tt}} \\ \text{Position DOP} &= \sqrt{D_{xx} + D_{yy} + D_{zz}} \\ \text{Horizontal DOP} &= \sqrt{D_{xx} + D_{yy}} \\ \text{Vertical DOP} &= \sqrt{D_{zz}} \\ \text{Time DOP} &= \sqrt{D_{tt}} \end{aligned} \tag{2.12}$$

As a note, the Horizontal and Vertical DOP is only applicable when using the East-North-Up (ENU) or a similar coordinate system. The lower the DOP value the better the positional precision, with a DOP of 1.0 being ideal. DOP should be viewed as a multiplier for the potential user position error. For example if the user had a range error of 5 m then a GDOP of 5 would indicate the potential for up to 25 m error in the user's position.

2.7 Previous Research Incorporating an On-Board GPS Receiver

A GPS receiver was installed on-board the Highly Elliptical Orbit (HEO) satellite Equator-S and launched in December 1998 into a Geostationary Transfer Orbit (GTO) [4]. The main goal of the experiment was to determine if reception of GPS signal was possible above the GPS constellation. Despite various configuration issues that arose, the research proved that tracking GPS at altitudes above the GPS constellation and near GEO is possible [4]. The research also proved that reception of signals originating from the side lobes of the GPS transmit antenna is also possible [4].

The US Air Force Academy sponsored an experiment called "Falcon Gold" to measure GPS signals at high orbital altitudes using the NAVSYS TIDGET sensor [16]. Falcon Gold was flown in November 1997, mounted to the side of the Centaur upper stage. Once the Centaur upper stage separated from the payload in GTO, the Falcon Gold sensor started collecting 40 ms of sampled data every 5 minutes. The data was not processed onboard. This experiment confirmed that a low cost sensor can be used to detect GPS signals in GTO, including those signals from the GPS antenna side lobes. The research also provides the C/N0 values observed at various altitudes in the GTO orbit.

There are other research that use a GPS receiver on-board a satellite as part of a bigger experiment. The "Navigation and Occultation eXperiment" uses a GPS receiver on a small satellite "TET-1" to prove that low cost commercial-off-the-shelf hardware can be used in space-borne applications with only minor changes to the receiver's firmware [7]. While the GPS receivers on the "Constellation Observing System for Meteorology, Ionosphere and Climate (COSMIC)" satellites are used for precise orbit determination and surveying the environment through radio occultation [12].

2.8 Tools Used in Research

A combination of three different tools are used for this research. These tools include Systems Tool Kit (STK), used for orbit propagation; MATLAB, for numerical computation and object oriented programming; and the SPIRENT GSS8000, for Radio Frequency (RF) signal generation. Each of these systems are described in more detail below.

STK.

STK is a modeling and simulation program from Analytical Graphics Incorporated (AGI), located in Exton PA, that deals with aircraft, satellite, ground vehicles, sensors, as well as communication elements. STK is known for its ability to model orbit propagations. The program offers a variety of different orbit propagators that differ in fidelity and complexity of included orbital perturbations. Using STK allows for study of orbit models and parameter sensitivity. Loading a satellite, the GPS constellation, or an antenna into STK can be done from an external file or STK's default repository. There are also options for calculating connection times, dilution of precision, navigation accuracy, as well as setting various constraints. Since these functions are used in industry for terrestrial scenarios involving GPS, STK will be used to validate the software developed for this research using similar terrestrial scenarios.

MATLAB.

MATLAB is a high level language and numerical computing environment. MATLAB does not have a built in orbit propagator but it does have the ability to integrate with STK. STK and MATLAB can be integrated through file interoperability, plug-ins, and through Microsoft's COM library which allows MATLAB to operate STK's functions using object-oriented programming commands. For this research, MAT-

LAB is used to automate the scenario creation in STK, load and propagate the user and GPS orbits at the desired time step, attach transmit and receive sensors to each satellite, and finally export data back into MATLAB for processing. This level of automation to do the systematic sweeps needed for parameter studies allows this study to be feasible based on available resources.

MATLAB GUI.

Using MATLAB to connect to STK with connect commands involves a moderate learning curve, partly due to the complexity in deciphering errors and the translation of examples given in C# into MATLAB's COM syntax. AFIT Summer 2014 interns Arnett, Wagner, and Dieterle created a Graphic User Interface (GUI) to handle the MATLAB to STK transactions. Figure 2.5 shows the top level interface for the GUI.

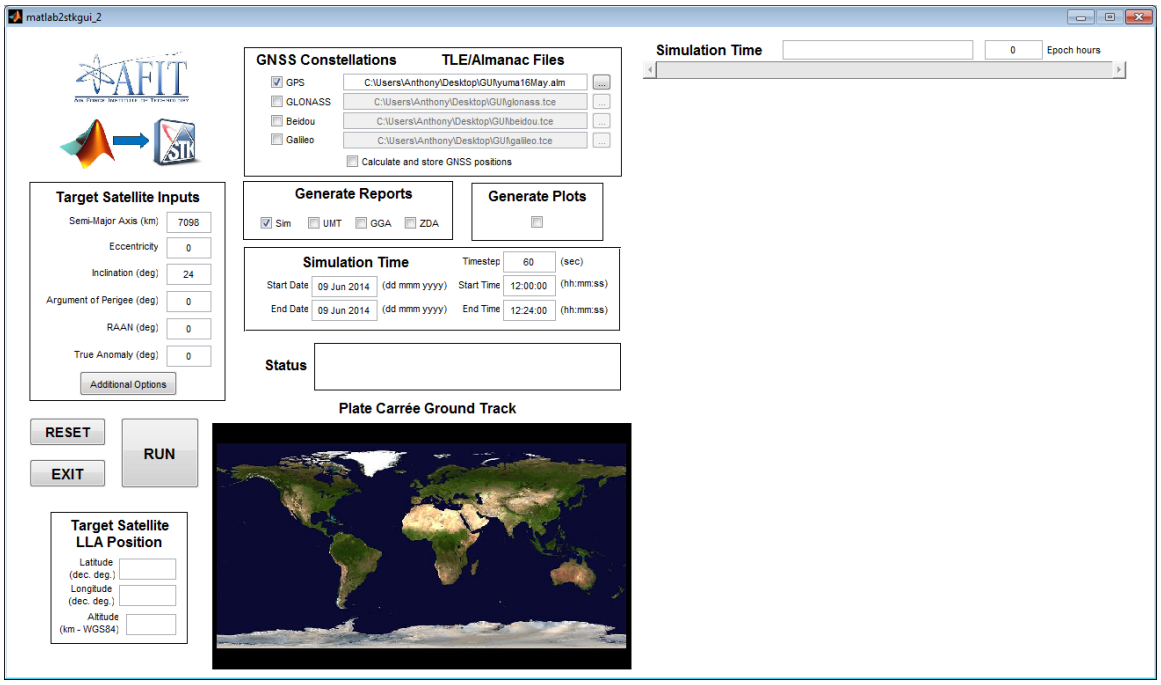

Figure 2.5. MATLAB to STK GUI

The GUI requires the user to input the satellite's six classical orbital elements, simulation time and time step, GPS almanac location or other Global Navigation

Satellite System (GNSS) Two-Line Element (TLE) file locations, and to select which reports are to be generated. Some of the default parameters that can be changed in the GUI include the receiver antenna's pattern, receiver antenna orientation and offset, C/N0 constraint, and orbit propagator preference.

SPIRENT GSS8000.

SPIRENT GSS8000 is a RF constellation simulator that supports GPS, Galileo, Global'naya Navigatsionnaya Sputnikovaya Sistema (GLONASS), and Quasi-Zenith Satellite System GNSSs. It is designed as a platform for the development and testing of GNSS enabled devices as well as the GNSS technology itself. Spirent Communications has developed different models of GNSS signal simulators, each with different levels of functionality. Utilization of SPIRENT's RF generator, as well as various models included in the SPIRENT software package, is found in different research efforts such as in [5] and [6]. The simulator is able to produce the GNSS RF signal expected to be received at the user's location by taking into account variables such as: user position and velocity, antenna patterns, obscuration effects, signal propagation, and various error models (including multipath). The RF signal is generated in real time and transmitted via antenna or cable to a GNSS receiver for processing. A GNSS enabled device can process the signal in real time as the signal is being transmitted. The signal can also be recorded and downsampled with an RF front end for eventual post-processing using a Software Defined Radio (SDR). The simulator's real time signal generation requires the time step for the user motion input to be in one second increments or less. If using one second increments, an option can be set to allow the simulator to interpolate the user's position in the time spans between the one second increments.

GPS Antenna Model.

SPIRENT specializes in RF signal simulator so the simulator includes a higher fidelity model of the GPS transmit antenna beams. Unlike STK, which only models the main beam of the GPS antenna, SPIRENT's model includes the antenna sidelobes as well. STK's antenna model is included by default with their GPS transmitter model, as shown in Figure 2.6.

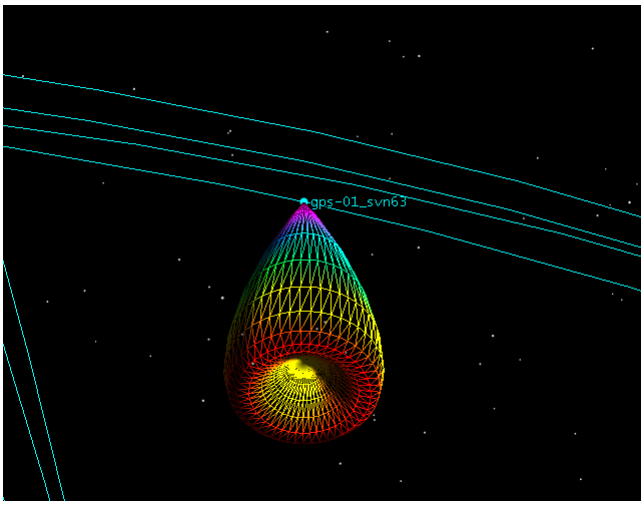

Figure 2.6. STK's GPS Transmit Antenna Beam Model

SPIRENT's antenna model offers a more detailed version of the GPS transmit beam with a variety of attenuation values. Figure 2.7 shows a visualization of the GPS transmit antenna's attenuation model used in SPIRENT. The model is also exportable as a table of attenuation values by azimuth and elevation which is more useful for increasing simulation fidelity. For the purposes of this research, SPIRENTs antenna model is imported into MATLAB and used to calculate the GPS signal power expected at the receiver. The antenna pattern output from SPIRENT's model resembles the GPS signal model shown in Figure 2.2.

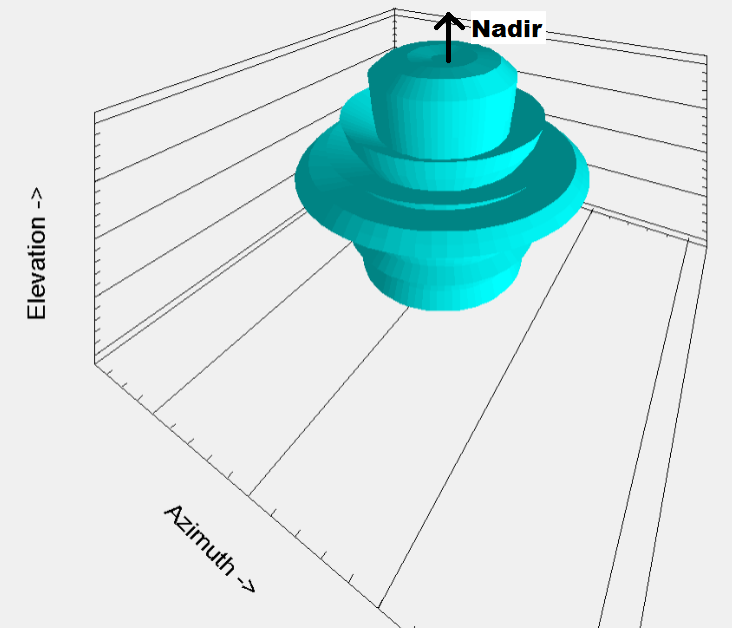

Figure 2.7. SPIRENT's GPS Transmit Antenna Beam Model

2.9 Summary

The chapter finished with the tools that will be used to simulate the GPS - user interactions that will result in evaluating the position estimation errors. Various position estimators are currently available in the PNT community and a few common techniques were mentioned. This research chose to implement the Newton-Raphson position estimation algorithm in order to evaluate both position errors and the applicability of the DOP metric. DOP is a metric that evaluates position precision errors based on the geometry of GPS SVs relative to the user. Space based errors affecting the GPS signal were also discussed along with a brief description of the orbits in space of interest to this research.

III. Methodology

3.1 Introduction

Before position can be calculated, it is necessary to determine the number of GPS SVs the receiver is able to detect. To be detectable, the signal from the GPS to the receiver must not be obstructed by Earth, fall within the receiver's Doppler band limits, and be at a sufficient power level at time of reception. This chapter will discuss the initial setup in STK, line of sight vector calculation, Doppler and power calculation, and finally position calculations.

3.2 Work Flow

Figure 3.1 shows the flow of this research from start to finish. The scenario specific data is inputted into the MATLAB to STK GUI. This GUI is responsible for setting up and running the scenario in STK. STK is a closed source commercial product so the source code is not released to the public. As a result, this research only uses STK to 1) propagate the orbits of the user and GPS satellites, and 2) return the Earth Centered Earth Fixed (ECEF) or Earth Centered Inertial (ECI) position and velocities for each time step. Next, the GUI takes the outputs from STK, formats them in MATLAB, and then saves off two separate data files. The *position and velocity* file is used for analysis in MATLAB as described in Section 3.5, while the *user motion trajectory* file is used for physical simulation of the RF signal with the GNSS simulator in Section 3.8. Both options result in pseudoranges to be used in the Newton-Raphson least squares position calculation algorithm. To determine position error, the results of the position calculation algorithm is compared with the true user position from STK.

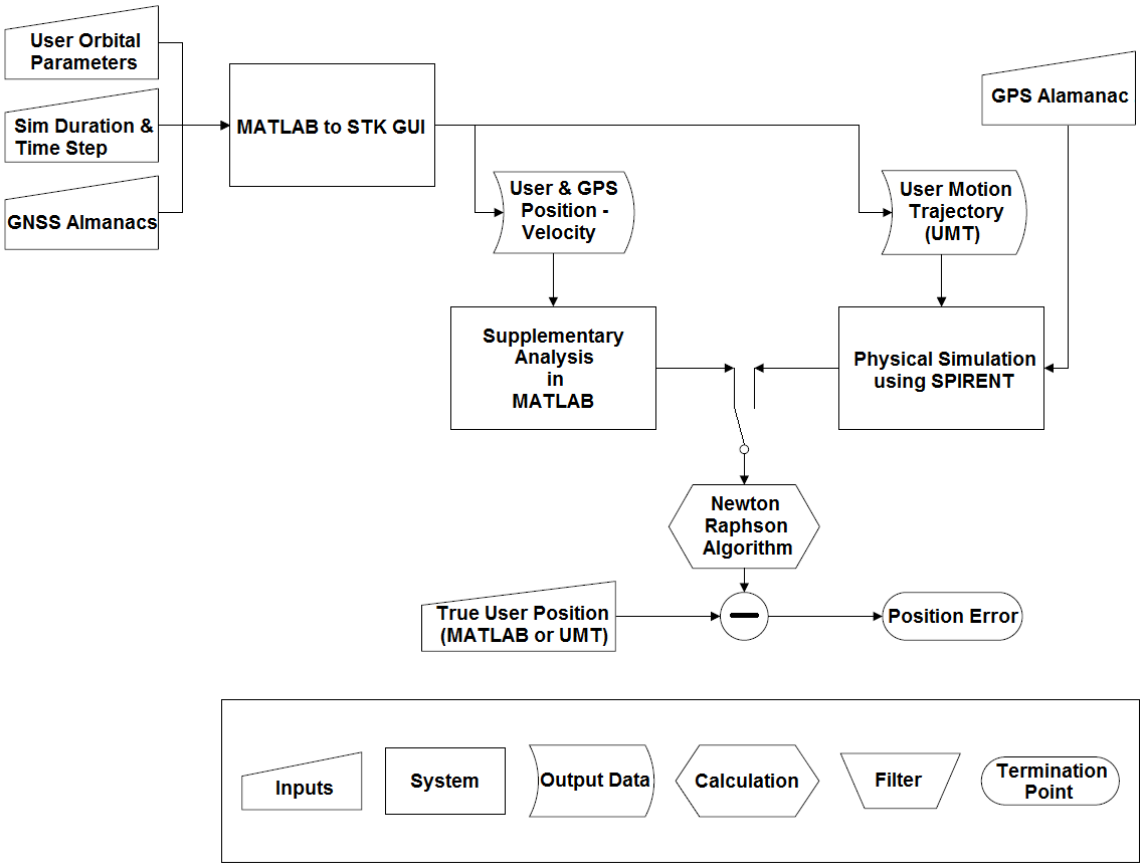

Figure 3.1. Research Work Flow

3.3 Assumptions

A few assumptions are made when building the scenarios to narrow the scope of the research or to ensure realistic values are achieved for noise and equipment settings. Below is a list of the assumptions.

1. The receiver antenna is isotropic, thus able to receive signals from 360°.

2. Range measurements are not affected by multipath errors.

3. Dual frequency (L1 and L2 bands) measurements are used in the receiver to implement ionosphere free measurements. Outside of ionosphere free measurements, the receiver will only process the L1 civilian frequency.

4. The Earth's radius will include the height of the troposphere.

5. A third order Phase Lock Loop (PLL) is used to accommodate the high dynamics of a elliptical orbit.

3.4 Code Validation

Coding for this research takes place in MATLAB in order to provide a clear view of all calculations taking place. All calculations are manually coded from known equations in GNSS open literature, such as Line of Sight (LOS), DOP, and Doppler. Confidence in the MATLAB code working as expected was gained by comparing results with STK for a scenario involving terrestrial based receiver and no consideration for GPS antenna side lobes. Even though STK is only being used for the position and velocity information, it is capable of providing information on DOP, C/N0, navigation accuracy, and transmitter to receiver connection time. Different analyses on the data can be run in STK by using the Reports & Graph manager. These values can then be compared with the results from MATLAB to verify similarity of both processes.

The following sections provide more detail about what happens during the supplementary analysis phase and the physical simulation phase. A detailed flow chart of the supplementary analysis is shown in Figure 3.2.

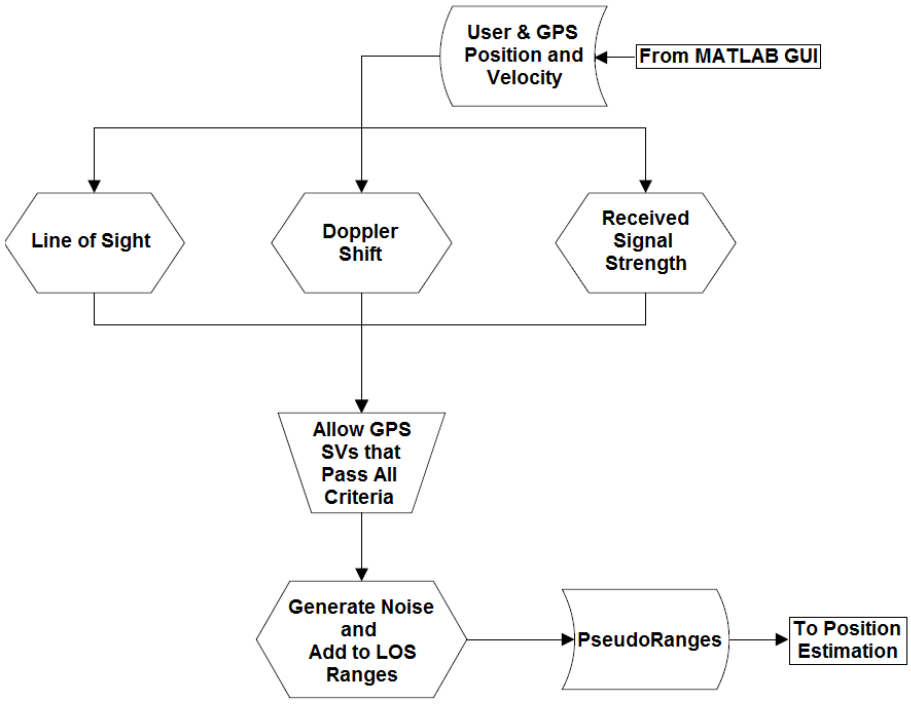

Figure 3.2. Detailed Supplementary Analysis

3.5 Supplementary Analysis

Supplementary analysis occurs in MATLAB and handles all of the calculations, criteria comparison, position estimation, and finally data analysis involved in this research. Required inputs are position and velocity vectors from STK, GPS antenna model, and the GPS almanac file associated with the scenario time frame. The first portion of the supplementary analysis is to determine the GPS satellites to which the user connects. A connection is considered established if the user has LOS to the GPS SV, a Doppler shift magnitude under a predefined threshold, and received signal strength above a predefined level.

Line of Sight.

For two objects to have a Line of Sight connection in this research the vector connecting both objects is required to be unobstructed by Earth. The connecting LOS vector $\mathbf{P_{LOS}}$ is obtained by subtracting the user's position vector $\mathbf{P_U}$ from the selected GPS SV's vector $\mathbf{P_{GPS}}$. Figure 3.3 illustrates this operation: $\mathbf{P_{LOS}} = \mathbf{P_U} - \mathbf{P_{GPS}}$.

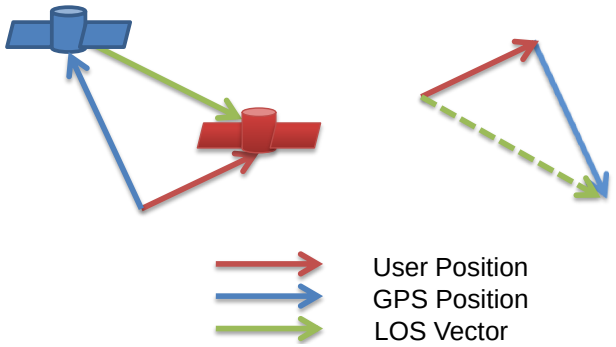

Figure 3.3. LOS Vector Calculation

Next, the range of the shortest distance vector from Earth to the LOS vector is examined. The shortest distance vector is found by first calculating the projection of the user position vector onto the LOS unit vector $\vec{\mathbf{P}}_{LOS}$ using the dot product. Afterwards, that projection vector is subtracted from the original user position vector to obtain the shortest distance vector. The range is found by taking the norm of the shortest distance vector. An illustration of this mathematical operation, $R_{E_{arth}2S_{ignal}} = \|\mathbf{P}_U - ((\vec{\mathbf{P}}_{LOS} \cdot \mathbf{P}_U)\vec{\mathbf{P}}_{LOS})\|$, is shown in Figure 3.4.

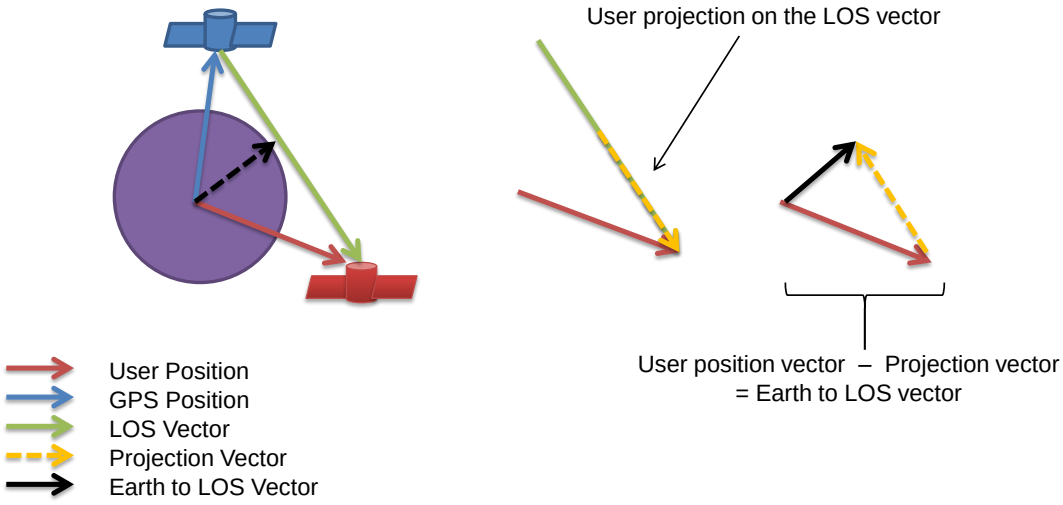

Figure 3.4. Earth to LOS Vector Calculation

Normally the projection vector is calculated with a dot product. However, for this research the dot product to find the user-to-LOS projection is limited to account for two outlier cases, when the dot product is negative or the magnitude is greater than the LOS magnitude.

A negative dot product means the projection of the LOS vector onto the user position vector is pointing towards the Earth. This happens when the LOS vector's origin, i.e. GPS SV's position, is at a higher altitude relative to Earth than the user. If the GPS SV is above the user, relative to Earth, then obstruction from Earth cannot occur. Thus the first limitation is to set a lower bound of zero on the dot product by taking the maximum value between zero and the calculated dot product to ensure non-negative values. In other words, the zero lower bound prevents the calculated nearest point on the LOS vector from being beyond the user satellite.

The second limitation involves setting an upper bound for the projection vector. This upper bound prevents the nearest point on the LOS vector from being beyond the GPS SV. If the magnitude of the LOS vector is smaller than the magnitude of the user's position vector, then the possibility exists for the projection vector to

be greater than the LOS vector. This in turn causes problems when calculating the shortest distance vector from Earth to the LOS vector. Figure 3.5 illustrates a simple example of the reason for the projection vector upper bound. In this example, Earth, the GPS SV, and the user are all inline with the user being above the GPS SV.

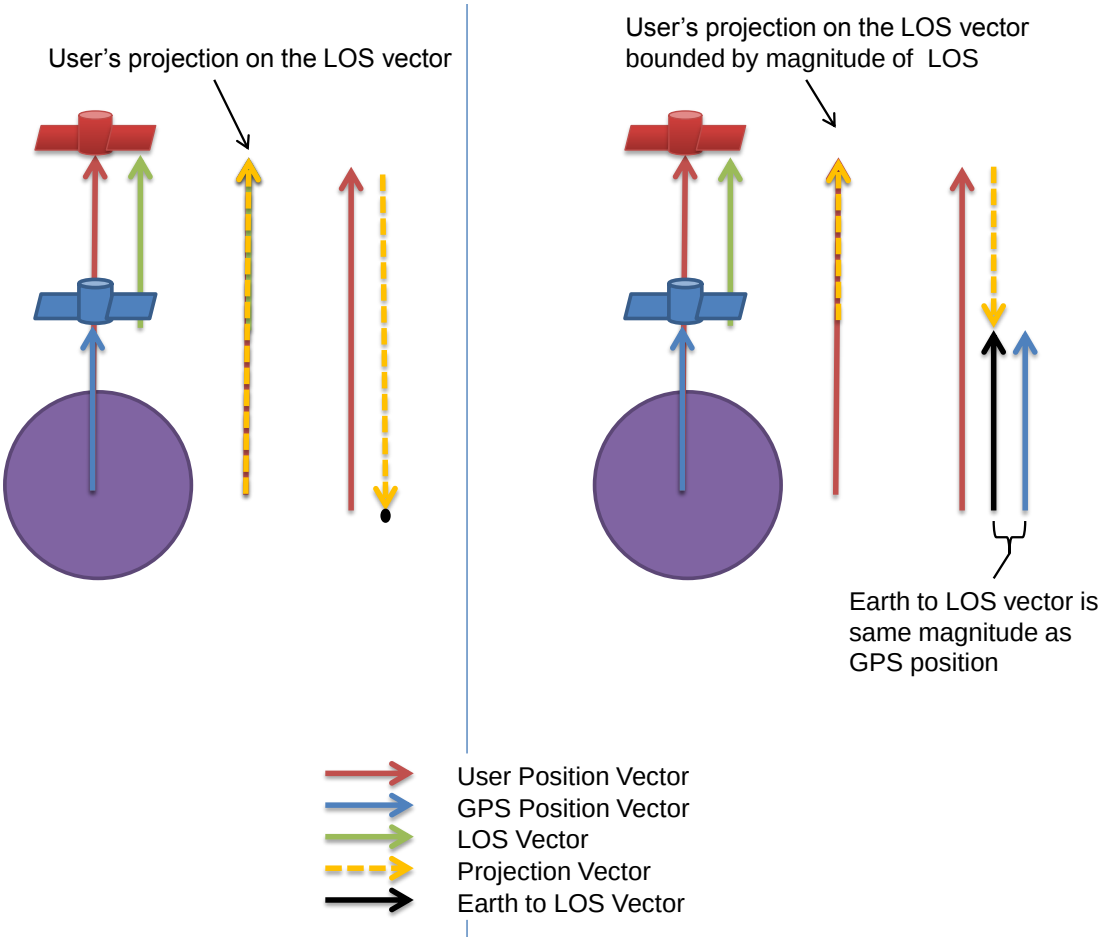

Figure 3.5. Unbounded vs Bounded projection comparison

In this situation the magnitude of the user position vector is greater than that of the LOS vector. When the user position-to-LOS projection is found and subtracted from the user position vector, the resulting Earth to LOS vector will point to a location outside of the bounds of the LOS end points. Once the Earth-to-LOS vector is found, the magnitude is used to determine if a GPS SV is considered in view to the user. This will be discussed in more detail in Section 3.6.

Doppler Shift.

The receiver's incoming GPS RF signal is a combined signal comprised of transmissions from multiple GPS SVs. To determine which GPS signals are present, the receiver produces a reference signal for each GPS SV to correlate with the incoming RF signal. The receiver has to account for the change in frequency due to Doppler effects from the relative speed, so the reference signal's frequency is varied over a range of potential Doppler values. If the incoming signal has a Doppler shift outside of range searched, then the signal is not recognized by the receiver. Thus for this research, the Doppler effect caused by relative velocity is calculated for each GPS SV.

Doppler shift depends on the velocity at which two objects are approaching or departing one another. This value is the same as the velocity along the LOS vector. First, the relative velocity for both the user and GPS SV is calculated by subtracting the velocity vectors. The relative velocity vector is then projected onto the LOS vector to determine the magnitude of approach or separation.

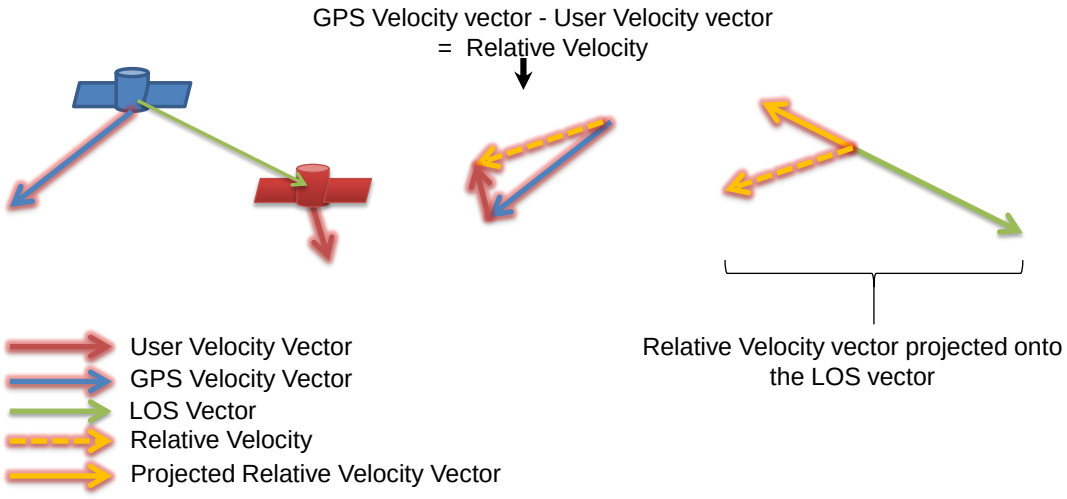

Figure 3.6. Relative Velocity Calculation

Doppler shift is calculated as follows:

$$\text{Doppler} = \frac{\|\mathbf{V}_{LOS}\| * f_{L1}}{c} \tag{3.1}$$

where $\mathbf{V}_{LOS}$ is the projected velocity on the LOS vector, f_{L1} is the frequency of the L1 band: 1575.42 MHz, and c is the speed of light. The Doppler shift value is then compared against a set criteria to determine if the receiver is able to process the signal from the GPS SV. More details on this process can be found in Section 3.6.

Received Signal Strength.

Another case where a GPS signal is not seen by the receiver is due to low signal strength. If the received GPS signal strength is too low then it will be indistinguishable from the background noise even after signal processing. Adequate signal strength in this research is determined in two different ways, depending on whether the GPS antenna sidelobes are being considered, or only the main beam.

No Sidelobes.

The simplest case considered is when only the main beam is used (so no sidelobes). In these scenarios, the received GPS signal is considered strong enough to be processed if the user is located within the main beam path of that GPS SV. Equation (3.2) shows the calculation of the GPS to user angle.

$$\theta_{G2U} = \cos^{-1}(-\vec{\mathbf{P}}_{GPS} \cdot \vec{\mathbf{P}}_{LOS}) \tag{3.2}$$

The angle represents how far the user is from the GPS antenna's boresight, which can be compared to the main beam half cone angle listed in the GPS Interface Control Document (ICD) [19].

Sidelobes Considered.

Power in the sidelobes is reduced when compared to the output from the main beam but can still be strong enough for signal reception. When considering the effects of sidelobes, a different approach for determining adequate signal strength is required. Instead of having the boresight angle determine reception, the boresight angle determines the amount of gain/attenuation applied from the GPS antenna in dB. The gain values are generated by interpolating the GPS antenna attenuation table exported from SPIRENT. Normally the next step would be to input the antenna gain and signal transmission power into a free-space path loss equation to determine signal strength at reception. Unfortunately, the GPS ICD does not mention specifics on the GPS signal transmission power, only the lowest guaranteed power at reception on Earth [19]. Thus a modified path loss equation from SPIRENT [1] is implemented to determine the signal power at reception, shown in Equation (3.3).

$$\mathrm{SP}_{rcvr} = \mathrm{SP}_{ICD} + O_g + 20 * \log_{10}(\frac{R_0}{R_{LOS}}) + G_{Tx} + G_{rx} \tag{3.3}$$

In this equation, SP_{rcvr} is the power at the receiver in dBm, SP_{ICD} is the lowest guaranteed GPS power at reception mentioned in the GPS ICD, O_g is a global offset constant used in SPIRENT, R_0 is the range of a GPS SV at the furthest point away from a terrestrial user, R_{LOS} is the actual range from the GPS SV to the user, G_{Tx} is the gain from the transmission antenna, and G_{rx} is the receiver antenna gain [1].

SP_{ICD} value is listed as $-128.5\,\mathrm{dBm}$ [19], the O_g default value in SPIRENT is 10 dB [1], R_{LOS} is the magnitude of P_{LOS}, G_{Tx} is the value from comparing GPS boresight angle with the antenna model interpolation, and the receiver is assumed to be isotropic resulting in G_{rx} being set to 0 dB. When calculating R_0 it is important to note that the farthest visible GPS SVs to the user will be on the horizon. Equation (3.4) shows how R_0 is derived, with α being the semi-major axis of the GPS SV pulled

from the current almanac used in the scenario, and r_E the radius of Earth.

$$R_0 = \sqrt{\alpha^2 - r_E^2} \tag{3.4}$$

Received power by itself gives little information unless compared to the background noise, i.e. in some signal to noise ratio. For GPS applications, C/N0 is the ratio commonly used because it refers to the ratio of the carrier power and the noise power per unit, as opposed to SNR which refers to the ratio in a given bandwidth [9]. If the background noise temperature is specified, then the GPS signal power at the receiver can be converted to C/N0 using Equation (3.5).

$$C/N0 = \mathrm{SP}_{rcvr} - 30 - 10\log_{10}(K * T_n) \tag{3.5}$$

Receiver power is first converted from dBm to dBW by subtracting 30 dB, K is the Boltzman's constant, and T_n is the background thermal noise set at 270 Kelvin for this research. Once the C/N0 is calculated, it is compared with a preset criteria to determine if the signal strength is strong enough to be discerned by the receiver.

3.6 Criteria for GPS in View

The main purpose of the LOS, Doppler, and C/N0 calculations is to determine which GPS Pseudo-Random Noises (PRNs) the user has access to. A connection is considered established if all three values of LOS, Doppler shift magnitude, and C/N0 meet the preset criteria. For LOS criteria, the Earth to Signal range is required to be greater than the Earth's radius plus troposphere height. Troposphere is included into the Earth's radius to avoid the issue of errors induced from traveling through multiple troposphere regions. Doppler shift criteria is purely receiver based, but terrestrial receivers have a height and velocity restriction in place. Special firmware can be

obtained to remove the restrictions and even increase the Doppler search window up to 45 kHz as in [7]. For this research, the Doppler criteria is therefore set to 45 kHz. Finally, the C/N0 threshold will be varied but kept between $30-35$ dBHz. This range was decided based on previous research where a GPS receiver in a Geosynchronous Transfer Orbit observed C/N0 values ranging from $30.41 - 42.72$ dBHz [16]. Once the GPS PRNs meeting all three thresholds are determined, the positions and LOS ranges are stored off to be used in a position determination algorithm.

3.7 Range Noise

Noise is added to the perfect LOS ranges, i.e. GPS to user range, to simulate a realistic environment. Normally distributed random numbers are generated to use as errors for range measurements in meters. The standard deviation for the noise is derived from range measurement errors a GPS user commonly experiences. These range measurement errors are referred to as UERE. UERE errors are considered to be normally distributed with zero mean. A standard deviation value of approximately 5.36 m was chosen as the UERE in this research and is described more in the subsection below.

User Range Error.

Range measurement errors, referred to as UERE, are the effective accuracy of pseudorange measurements from a GPS satellite to the user. UERE for a satellite is a combination of each error source for that satellite and is normally described as a one sigma error in meters. Each satellite's error sources are assumed to be independent but the UERE can be modified to accommodate correlated error between satellites [11]. UERE error sources can be grouped into two categories: Space and User. Space errors are those that originate from the GPS satellite itself. The space

error sources consist of ephemeris error, information about the position of the GPS SV, and satellite clock error. User error sources consist of troposphere, ionosphere, receiver, and multipath error. Table 3.1 lists the current error values from the National Oceanic and Atmospheric Administration as of April 2014 [8].

Table 3.1. The GPS Error Budget

ERROR	VALUE (in meters)
Ionosphere	4.0
Ephemeris	2.1
Clock	2.1
Troposphere	0.7
Receiver	0.5
Multipath	1.0
TOTAL	10.4
UNCORRELATED ERROR (UERE)	5.15 (rss of errors)

This research uses a larger UERE value, 5.36 m, than the value of 5.15 m listed in Table 3.1. Ionosphere and troposphere errors are reduced due to assumptions made about use of ionosphere-free measurements and the increased radius of Earth. The receiver error is increased to account for unmodeled error and the variety of available GPS receivers. For this research, the UERE value is not scaled to account for variable path loss among signals from multiple SVs; the UERE also does not increase due to the GPS signal originating from the GPS antenna sidelobes.

Thermal Noise Error.

Additional noise is added to each range measurement based on the respective C/N0 values for each GPS signal. Thermal noise is the main contributor to carrier

tracking error in the receiver's PLL [11]. Carrier tracking error affects range error and is directly related with C/N0:

$$\sigma_{pll} = \frac{c}{f_{L1}} \frac{1}{2\pi} \sqrt{\frac{B_n}{C_{N0}} \left(1 + \frac{1}{2 * \text{PIT} * C_{N0}}\right)} \tag{3.6}$$

c is the speed of light, f_{L1} is the frequency of the L1 band, B_n is the PLL noise bandwidth, C_{N0} is the Carrier Power to Noise Density Ratio, and PIT is the receiver's Predetection Integration Time (PIT). Before selecting values for B_n and PIT (which are receiver dependent), an assumption must be made about the type of PLL model to be used. Note this research bases the noise calculation off of the L1 frequency due to the assumption that the L1 band is the only frequency processed by the receiver. This research effort assumes a third order PLL is used for stability in a high dynamic environment. For a third order PLL to be stable, B_n must be less than or equal to 18 Hz, so this was the value chosen. PIT values are normally set between 1 ms and 20 ms. Lower PIT times are chosen in situations where high responsiveness is desired, whereas higher PIT times are selected for system robustness against errors stemming from noise. A PIT value of 20 ms is chosen due to the user's six classical orbital elements being known a priori allowing the orbit to be predictable.

The ranges with the noise added are considered pseudoranges and are input to the position determination algorithm.

3.8 Physical Simulation

A second step to this research is data comparison with position determined from a replicated GPS signal. The signal replication will be handled by the SPIRENT GSS800 which produces a RF signal that takes into account propagation loss as well as the GPS transmit antenna's sidelobes.

The SPIRENT GSS8000 is configured with the same scenario information that

was input into the MATLAB GUI to include start time, end time, and relevant GPS almanac. User position is generated from the User Motion Trajectory file produced by the MATLAB GUI. Once the scenario is started, the SPIRENT simulator generates the RF signal expected to be received at the user's location in real time. The generated signal is recorded for approximately 36 seconds to ensure one full frame of navigation data, 30 seconds, is present. This process is done for different sections in the user's orbit. Afterwards, the recorded data is processed with an SDR to calculate pseudoranges for each timestep.

Software Defined Receiver.

The SDR used for this research is also located within MATLAB. An RF front end is used to record and downsample the transmitted signal from the SPIRENT GSS8000. Individual GPS signals are found by correlating the PRN modulated on the carrier wave with a locally generated PRN for each GPS satellite. Doppler along with the carrier wave are then removed from each signal, leaving the navigation data remaining. GPS transmission time, in units of GPS week seconds, can be determined from the navigation message. Transmit time is then subtracted from the time the receiver first observed the signal, also in GPS week seconds. The difference is multiplied by the speed of light to generate pseudoranges. This process is well established and more information can be found in [14]. These pseudoranges are then put through the same position determination algorithm as the pseudoranges from the supplementary analysis.

3.9 Summary

This chapter provides an overview of the process involved in this research, the relevant assumptions made, and the steps taken to validate the code used in the

research. Afterwards, an in depth description of the supplementary analysis algorithm is reviewed, to include LOS calculation, Doppler shift calculation, received signal strength, and the process of selecting GPS SVs the user is capable of accessing. Finally, noise generation for the creation of pseudoranges and the SDR is described.

IV. Results and Analysis of GPS Based Position Solutions at Different Orbitial Altitudes

4.1 Introduction

A total of seven different orbits are simulated to determine the number of GPS SVs available to the user at various spots in its orbit. The magnitude of errors expected while using those GPS SVs to resolve position is also calculated. Each scenario simulation began on January 26, 2015, and ran for exactly 24 hours with one minute increments, terminating on January 27th, 2015. A 24 hour period is chosen for the simulation length, ensuring two orbital periods of GPS are present.

The orbits chosen represent various altitudes above Earth, to include those in LEO, MEO, and one in GEO. For each scenario, a breakdown of the number of GPS SVs meeting and failing the specified criteria is reviewed first. Afterwards, the DOP and position error standard deviations are compared against the user's range as well as each other. Eigenvalues of the errors and DOP are reviewed to check for consistency.

With the exception of the GEO scenario, the other orbits have orbital periods that are shorter than the 24 hour scenario duration. This allows all but one scenario to contain more than one revolution of the user's orbit present in the simulation. This research takes advantage of the user's multiple revolutions by representing some information with respect to the orbital period, "time since start of user's orbital period", as opposed to "time since start of scenario". All figures that are plotted using a time span less than 1440 minutes (24 hours) to be in reference to the orbital period.

4.2 General Parameters

The parameters listed in Table 4.1 remain constant for all the scenarios presented in this research unless otherwise stated.

Table 4.1. General Parameters

Parameter	Value	Notes
Earth's Radius	6478.1 km	Includes a troposphere height of 100 km
Noise Temperature	230 Kelvin	
Doppler Threshold	45 kHz	Improved Doppler search window from [7]
C/N0 Threshold	33 dBHz	Observed values of $30.41 - 42.91$ in GTO[16]
GPS Frequency	L1: 1575.42 MHz	
PIT	20 ms	
PLL Noise Bandwidth	18 Hz	3rd order PLL
Range Noise sigma	5.357 m	Derived from UERE

Creation of the different orbital altitudes is accomplished by varying the Semi-Major axis, causing the orbital parameters to be similar (with the exception of the GEO orbit). As the orbits are circular, perigee does not exist thus the argument of perigee is not defined. Circular orbits also have no eccentricity, so eccentricity is set to 0. The right ascension of the ascending node is set to 0° and the true anomaly also starts at 0° for each scenario. These four values will not be listed in the tables to follow.

4.3 Low Earth Orbit

Three altitudes were chosen for the LEO scenario group: 400 km, 500 km, and 600 km. Each of the resulting orbits have a nominal orbital period of 92 min. The classical orbital parameters used to described the orbit are listed in Table 4.2.

Table 4.2. LEO Scenarios: Orbital Parameters

Altitude	Semi-Major Axis	Inclination	Period
400 km	6,778.137 km	45°	92 min
500 km	6,878.137 km	45°	94 min
600 km	6,978.137 km	45°	96 min

Doppler at 400km Altitude.

The velocity required to maintain orbit results in the Doppler between the user and GPS SVs to values higher than that experienced on Earth. Orbital speed increases as the altitude decreases. A user at 400 km altitude will have Doppler shifts greater than the other orbits chosen for this research due to the higher orbital velocity. Figure 4.1 shows that the maximum value the Doppler can reach during the 400 km simulation is around 40 kHz.

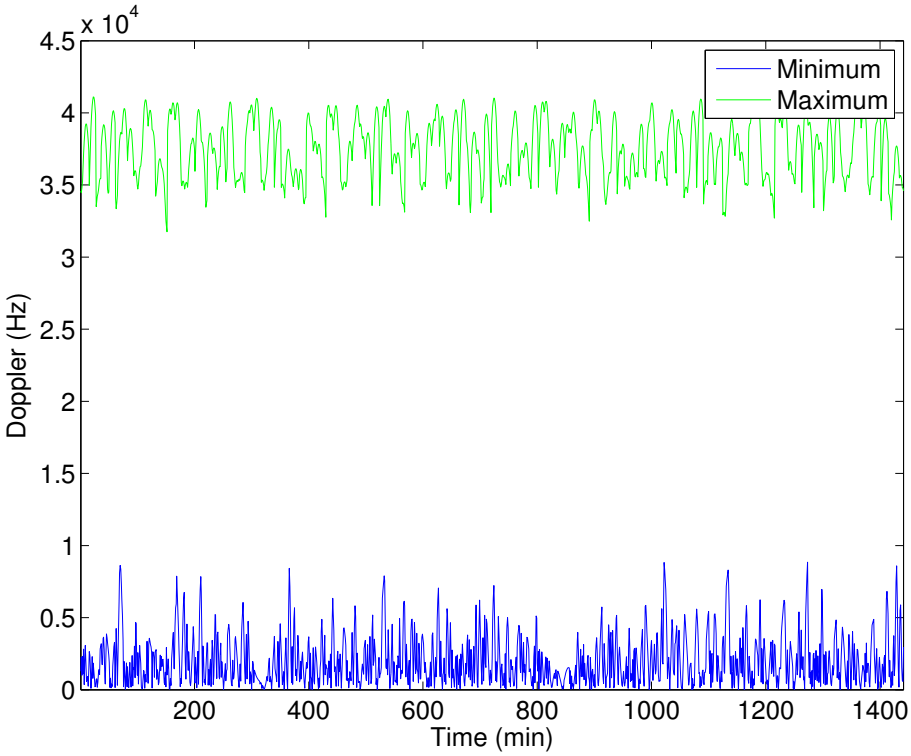

Figure 4.1. Maximum and minimum Doppler by time at 400km

The Doppler search window for this research is assumed to be expanded to 45 kHz based on data found in [16]. The increased Doppler search window causes the velocity experienced at LEO to no longer be a limiting factor to the number of GPS SVs in view. A relative speed of 8.563 km/s is required between the GPS and user to fail a Doppler threshold of 45 kHz. Failure due to Doppler shift does not appear in any of the criteria breakdown figures, such as Figure 4.2.

GPS Connection Overview.

Figure 4.2 shows the number of GPS SVs that either passed or failed the criteria for connection during the 400 km simulation.

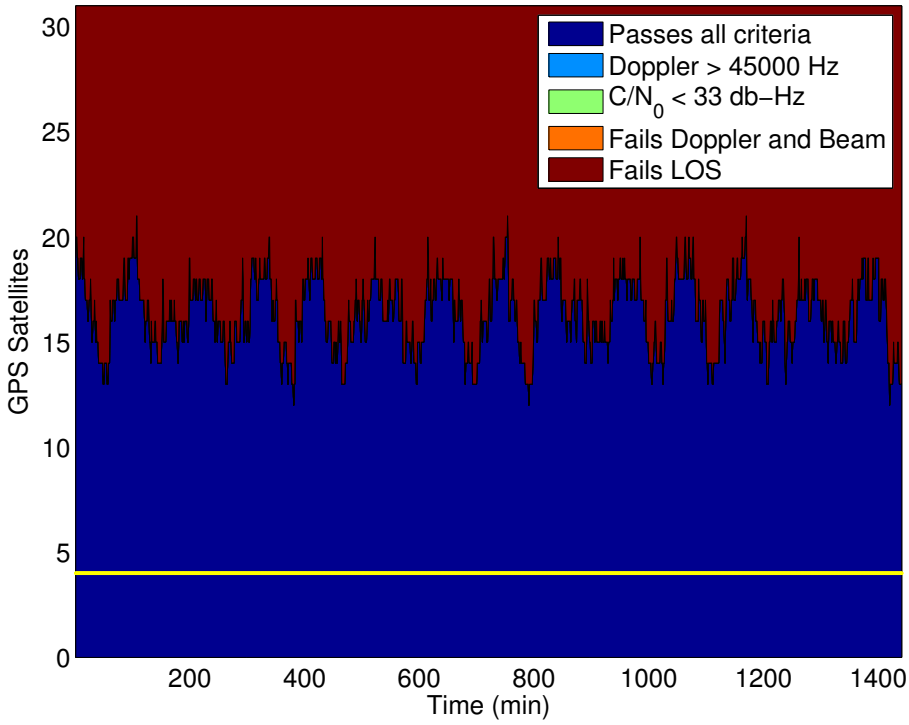

Figure 4.2. GPS Satellite Connection at 400km

For the entire 24 hour (1440 min) duration of the 400 km scenario, a minimum of 13 GPS SVs passes all the criteria necessary to be considered usable, as indicated in blue. GPS SVs that failed to meet the connection criteria did so because of obstruction from Earth, and are shown in red. The yellow horizontal line indicates access to at least four GPS SVs for that particular time instance. The times with access to less than four GPS SVs are indicated by red instead of yellow on the horizontal line.

The results for the other LEO scenarios, chosen at altitudes 500 km and 600 km, are similar to the 400 km case.

Figures 4.3a and 4.3b both show the 500 km and 600 km scenarios having a minimum of 13 GPS SVs in view for the entire scenario duration. Failing the LOS criteria, being obstructed by Earth, is the only criteria for failure of any of the GPS SVs.

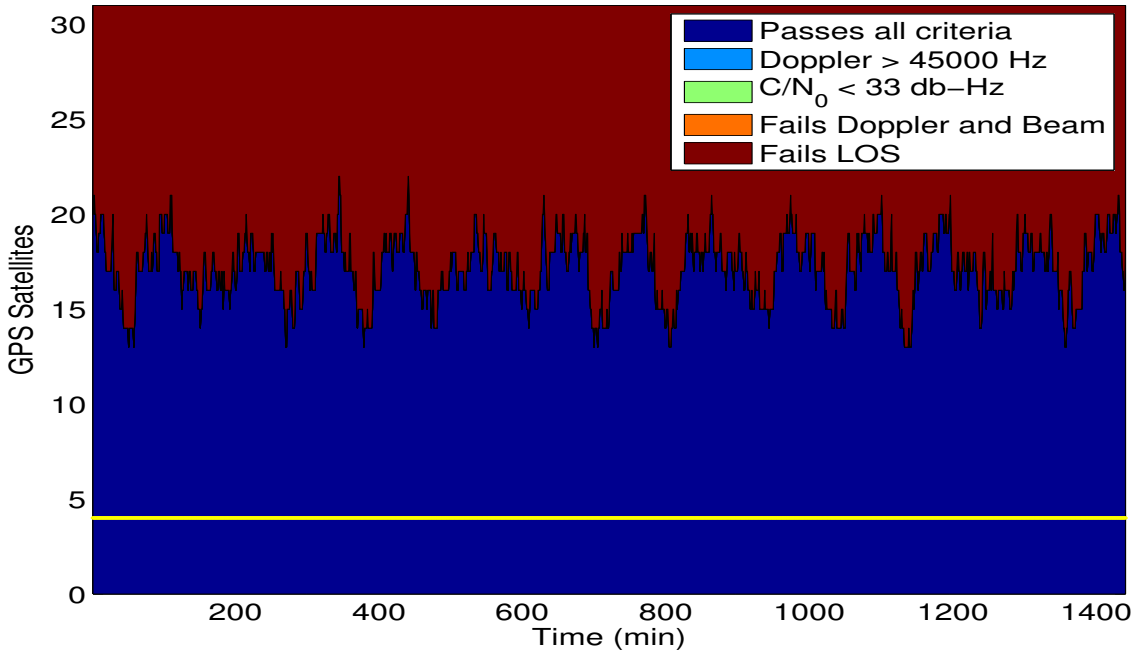

(a) GPS Satellite Connection at 500km

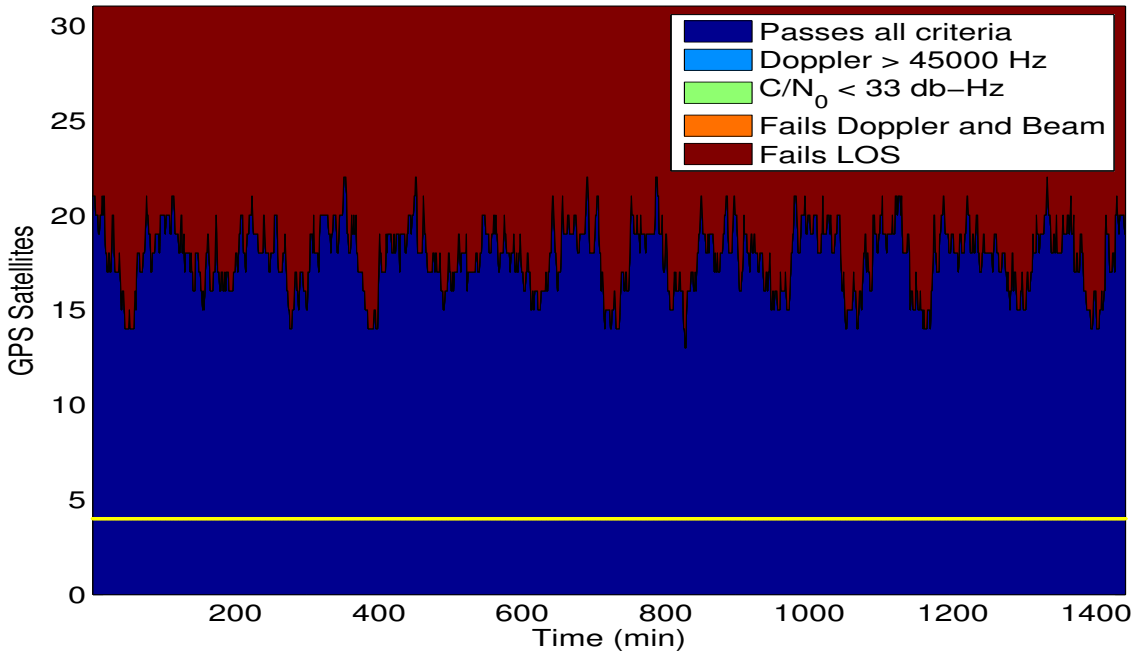

(b) GPS Satellite Connection at 600km

Figure 4.3. GPS Satellite Connection for LEO Scenarios

DOP.

Being positioned beneath the GPS orbit, along with the large number of GPS SVs in view, benefited the user. It increased the chances for a high angle of separation existing between GPSs SVs, relative to the user. High angle of separation directly contributes to a lower DOP. DOP is calculated based on the true position of the user and the positions of the GPS SVs meeting all three access criteria. GDOP experienced by the user in the 400 km altitude scenario remained under two for the entire duration. GDOP and PDOP for the 24 hour scenario are shown in Figure 4.4 as a function the user's orbital period.

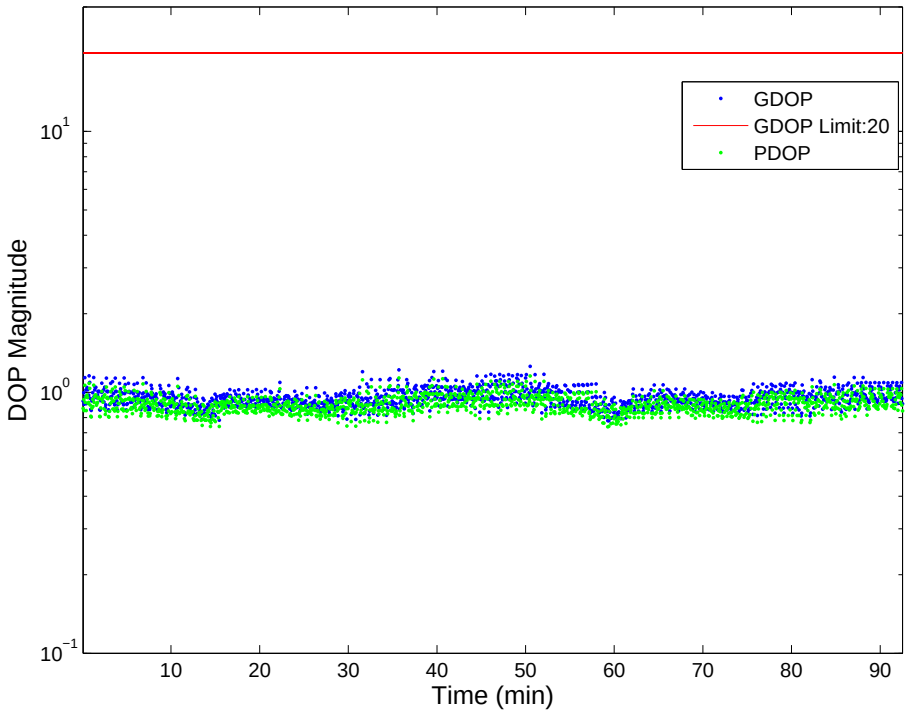

Figure 4.4. Comparison of the GDOP and PDOP vs time at 400km

In Figure 4.4, GDOP is greater in magnitude but follows the same trend as PDOP. Due to the similarities, GDOP is the DOP metric this research uses to since the others will only have improved values relative to GDOP. The red line in Figure 4.4 is a visual representation of a DOP threshold of 20. Any DOP value above the threshold

is considered to be poor and unusable for a terrestrial user based on [15]. The GDOP values for this scenario are well below this threshold.

Similar to the 400 km scenario, both 500 km and 600 km GDOP values also remain well under two for the entirety of the simulation duration. GDOP for all three LEO altitudes is shown in Figure 4.5. This shows that in addition to no significant loss in the number of SVs available, there is no significant change in geometry over this altitude range.

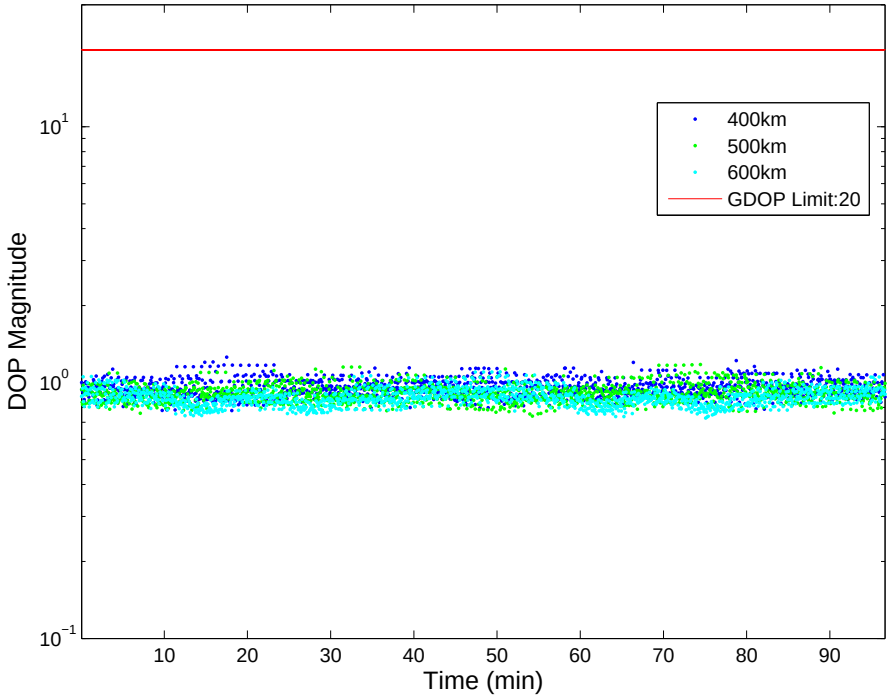

Figure 4.5. GDOP vs Time at LEO

Position Errors.

Position errors presented in this chapter refer to the distances between true user positions and the results of the Newton-Raphson least squares calculations over time. Errors in position estimates for the user at 400 km altitude are similar to those experienced by terrestrial GPS users. The overall errors are below 10 meters for a majority of the user's orbit, with the exception of a few instances where the error rises above

10 meters. Figure 4.6 shows a trace of the user's orbit for one Monte Carlo instance for the entire scenario duration. The color of the dots represent the magnitude of the position estimation error, true user position compared against the position calculated from the Newton-Raphson algorithm. The percentages represented in the legend are calculated based on the current Monte Carlo run represented.

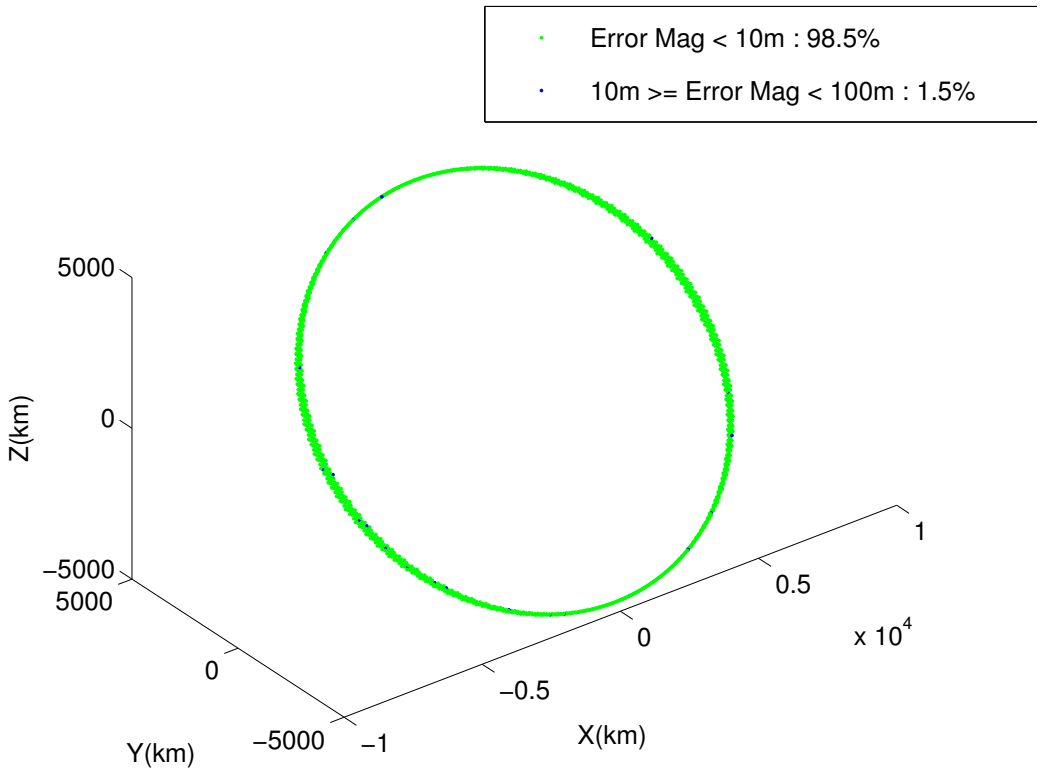

Figure 4.6. RMS Error at 400km

Figure 4.7 shows the standard deviation of the overall position error by orbital period for all of the LEO scenarios. For the duration of the user's orbital period, the rms error standard deviation remains under 3 meters for all three LEO scenarios.

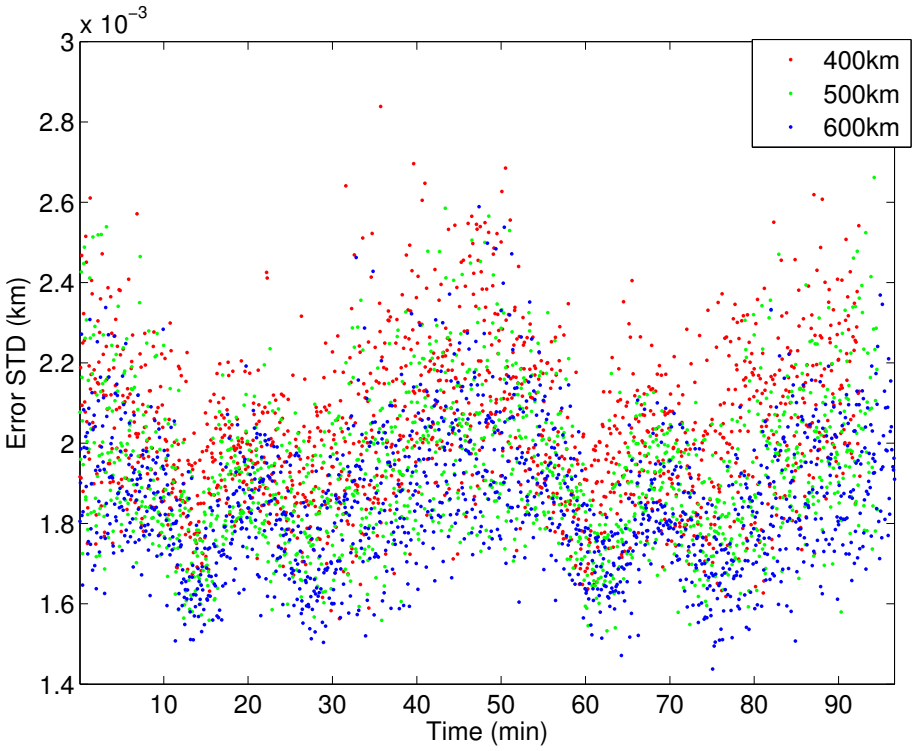

Figure 4.7. RMS Error STD for LEO scenarios

A breakdown of the position error standard deviation for each axis in the 400 km scenario is shown in Figure 4.8. Over 1000 Monte Carlo trials, the error standard deviation for all three axes each remain under six meters.

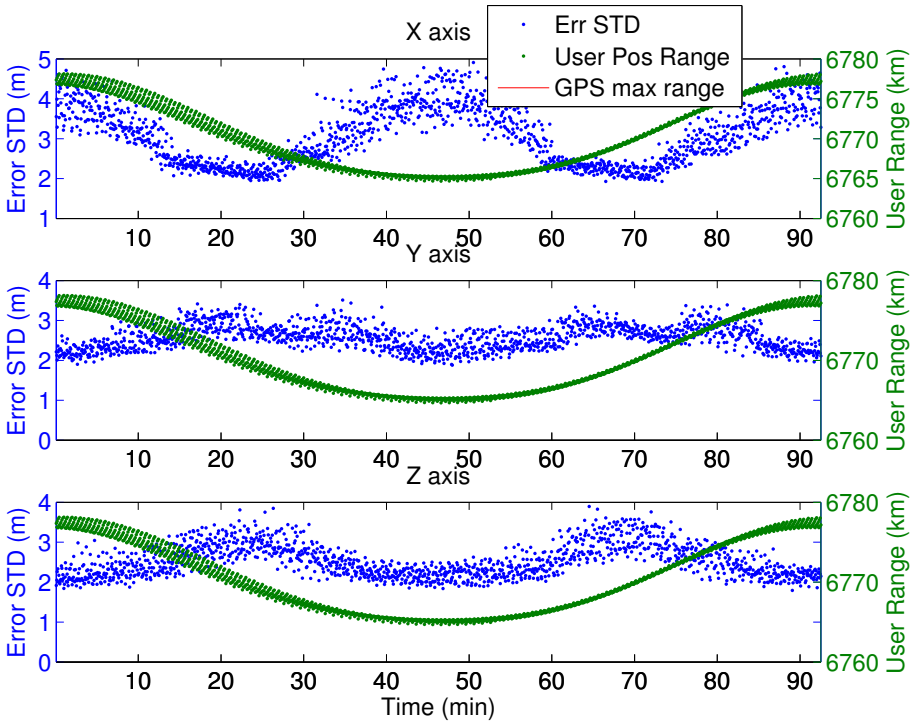

Figure 4.8. Error STD by axis vs User Range at 400km

Similar to the 400 km scenario, position errors for the 500 km and 600 km altitude scenarios also remain under 10 m with standard deviations remaining under 3 m. Figures 4.9a and 4.9b display the position error over the orbit.

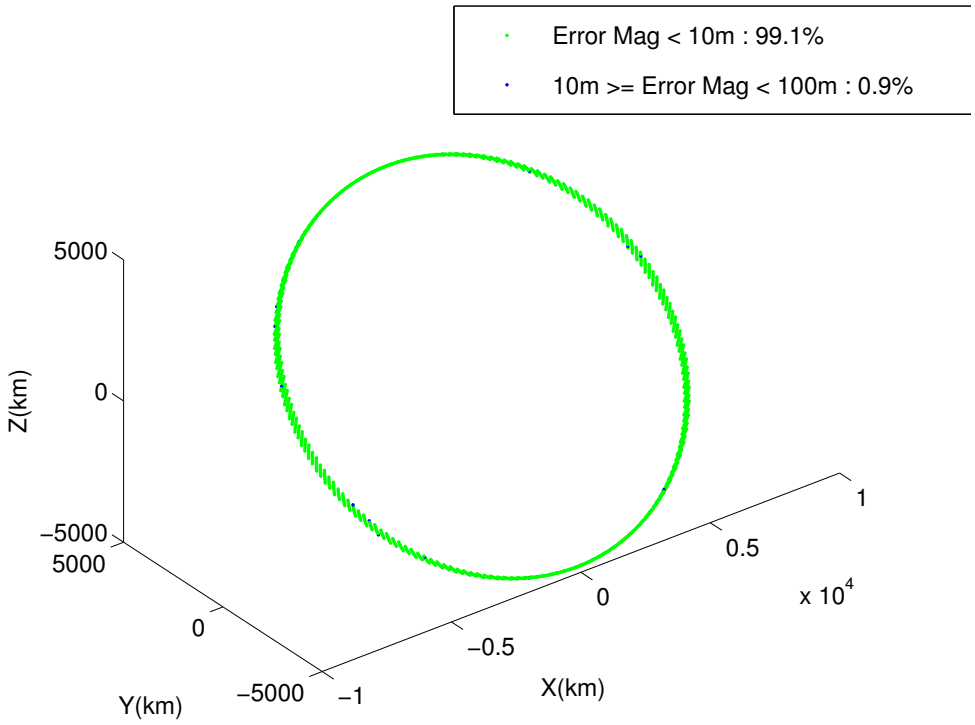

(a) 3D RMS Error at 500km

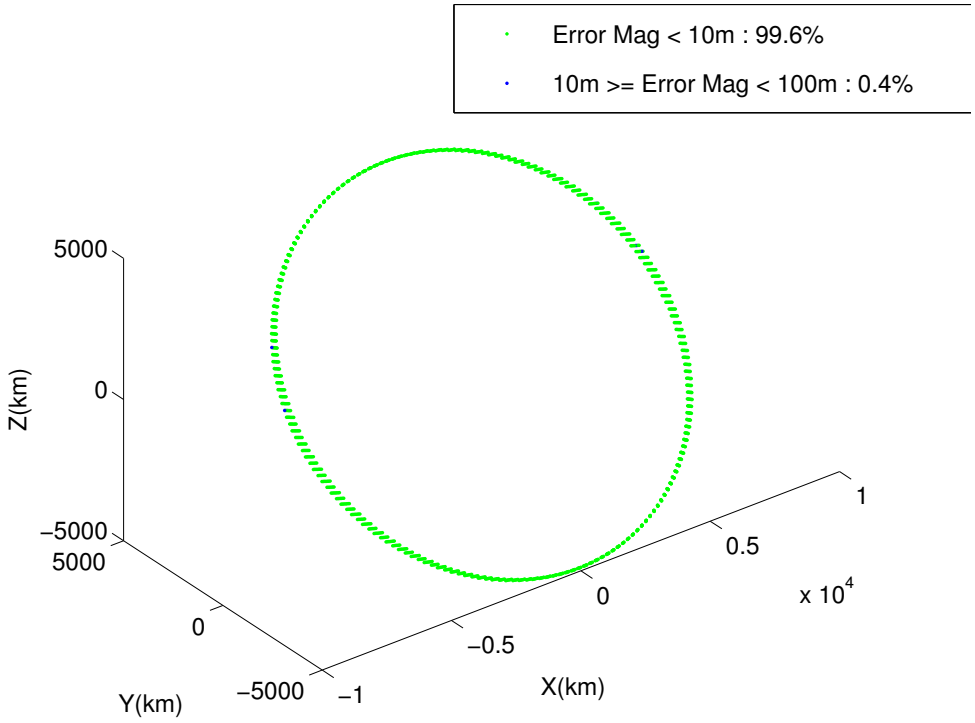

(b) 3D RMS Error at 600km

Figure 4.9. Position Error Over Orbital Trajectory for LEO Scenarios

Applicability of DOP.

Another goal of this research is to determine if DOP is applicable for predicting precision for non-terrestrial users of GPS. For the LEO scenarios, the magnitude of both DOP and position errors are consistent with those of a terrestrial user. To determine consistency between DOP and position error, it is necessary to compare two results against each other. In order to do so DOP had to be weighted with the range errors expected for each GPS SV in view. Weighting was accomplished by multiplying the UERE with DOP to obtain predicted position sensitivity. The comparison of the 400 km scenario's DOP and position error are shown in Figure 4.10.

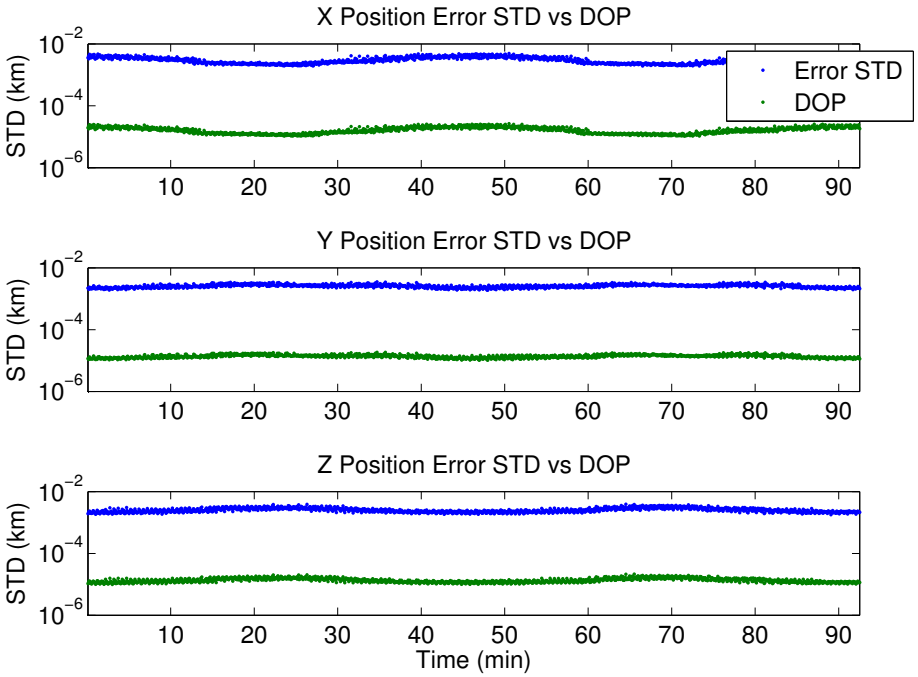

Figure 4.10. Position Error STD by axis vs DOP at 400km

Plotting the position error standard deviation against each axis's DOP helps determine if the linear relationship between position error, DOP, and range error exists. Figure 4.11a shows the standard deviation of position error plotted again the respec-

tive DOP values for each axis. Figure 4.11b shows the DOP vs position error STD broken up into the three axes.

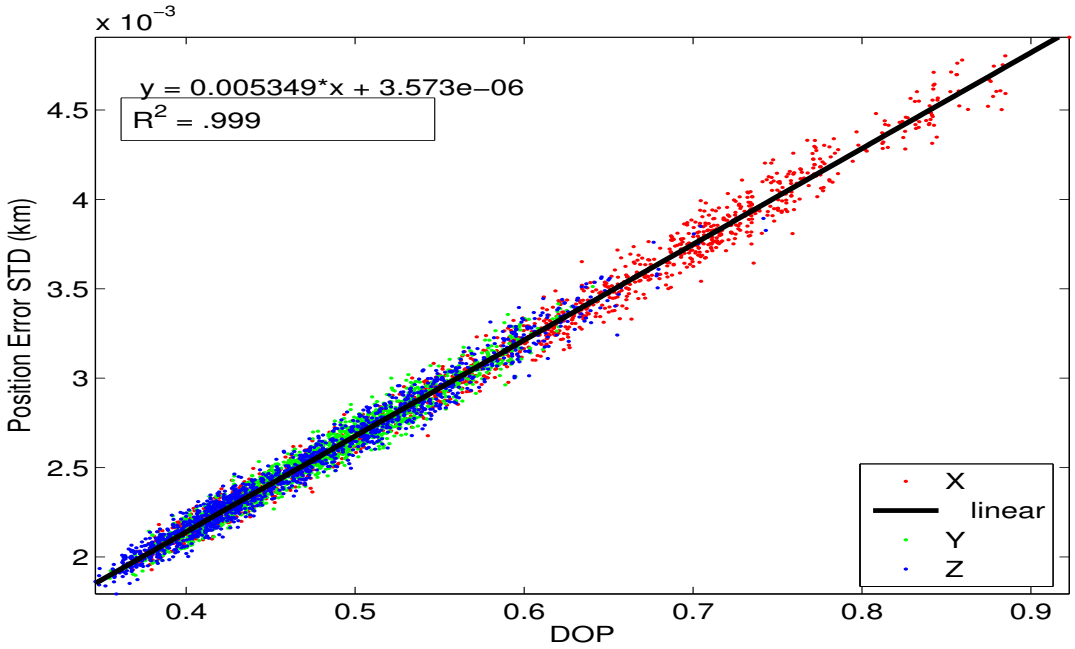

(a) DOP vs Combined Position Error STD at 400km

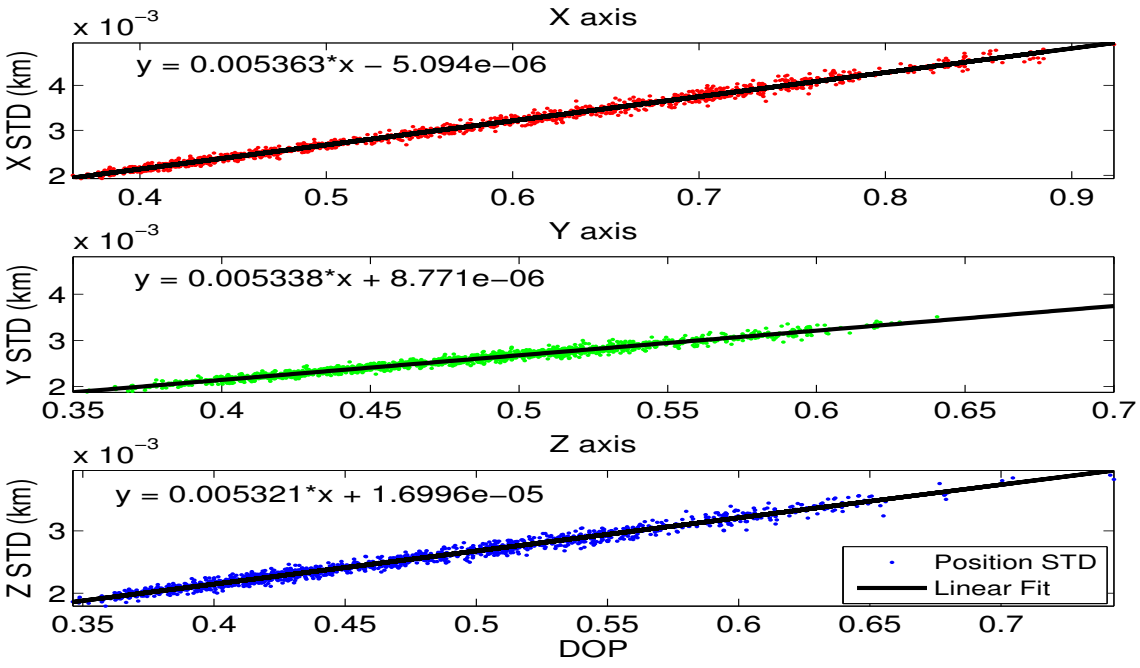

(b) DOP vs Position Error STD for each Axis at 400km

Figure 4.11. DOP vs Position Error STD at 400km

A table of the linear fit values for all scenarios can be found after the GEO section in Table 4.5. Applying a linear fit to the combined data points produces a line with a slope of .00535 km and a offset of approximately 0. Each axis also shares a similar STD to DOP linear fit equation, where the slope is around .0053 km. This value is consistent with the previously set range noise sigma of $5.357m$ derived from the UERE, proving that the linear relationship still exists.

The linear relationship also holds true for the remaining LEO simulations as seen in Figures 4.12a and 4.12b.

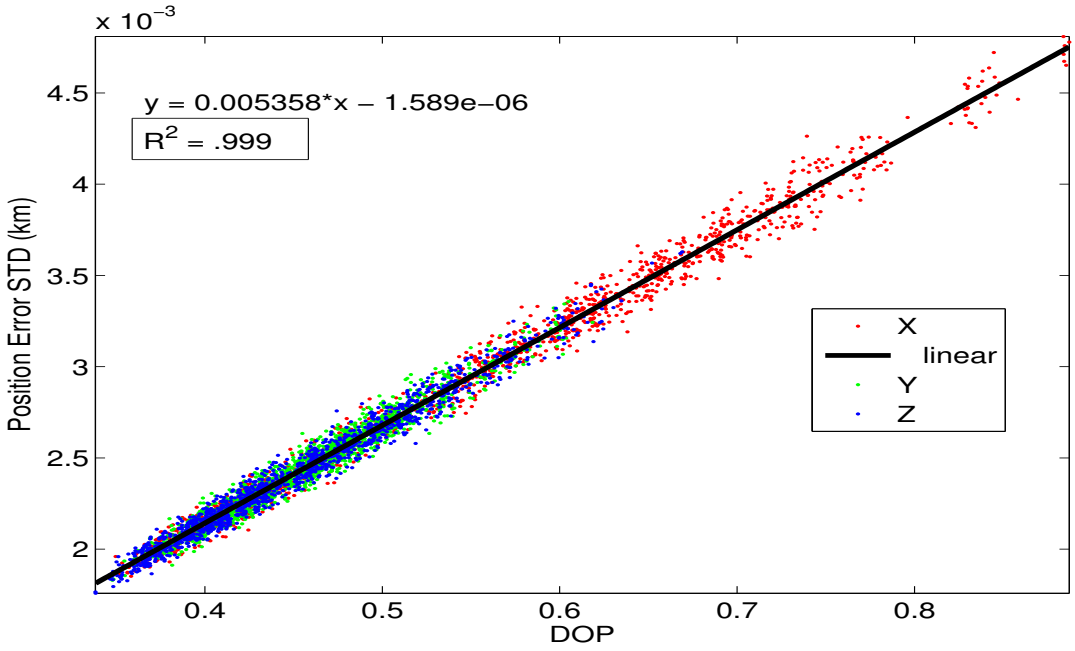

(a) DOP vs Position Error STD at 500km

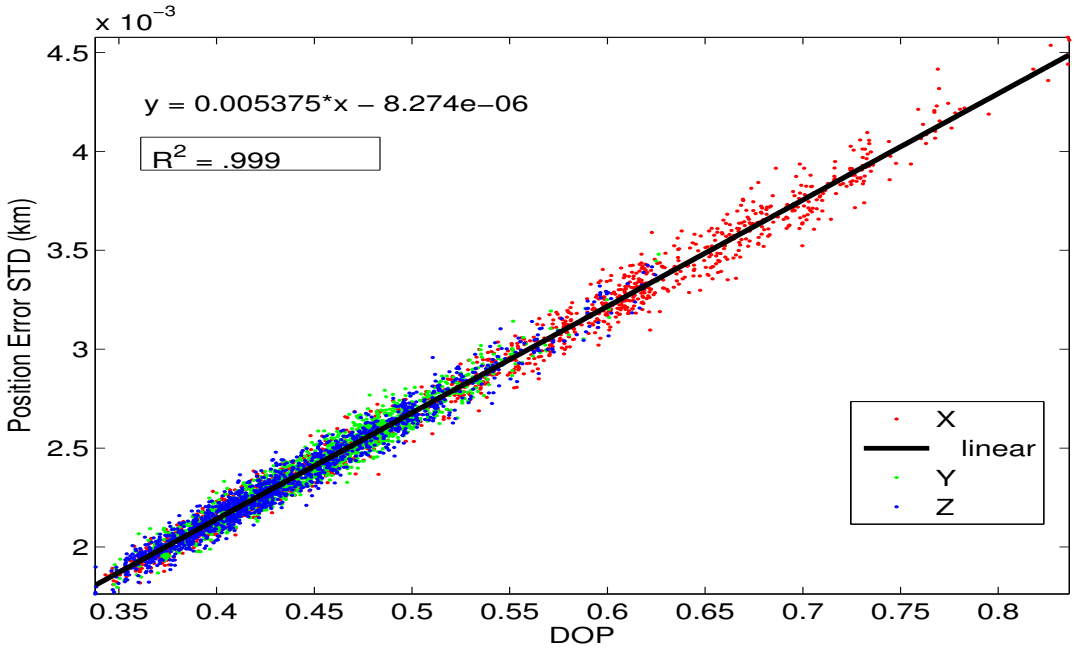

(b) DOP vs Position Error STD at 600km

Figure 4.12. DOP vs Position Error STD for LEO Scenarios

To see if the DOP and position errors are aligned within the same space, the Eigenvalues for position error and DOP are compared. Figure 4.13 compares the Eigenvalues between GDOP and the error RMS standard deviation, while Figure 4.14 shows the comparison for each axis over the scenario duration.

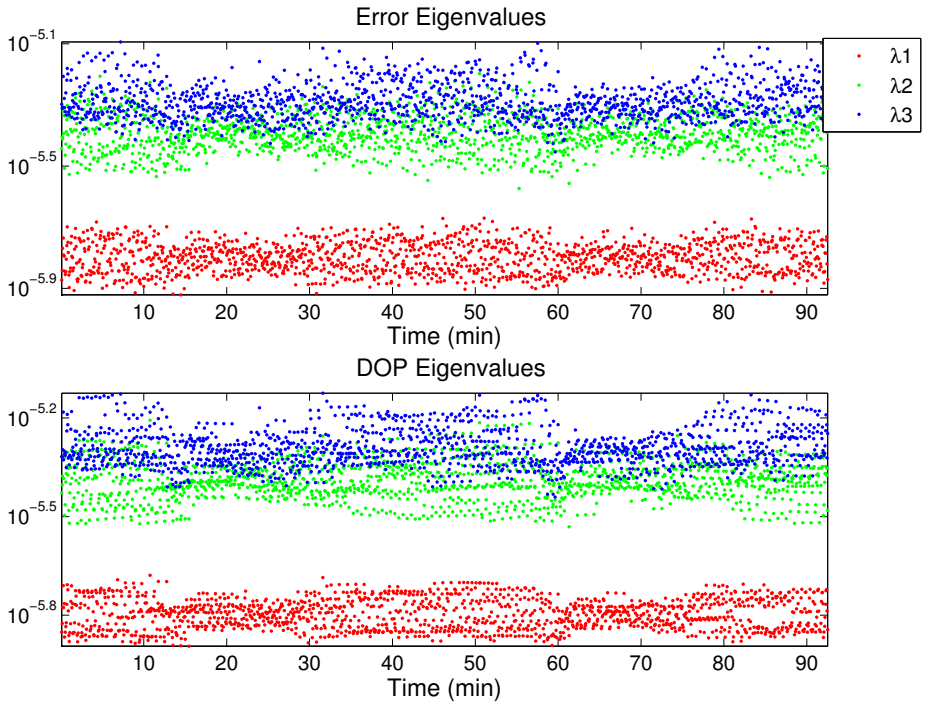

Figure 4.13. Error vs DOP Eigenvalue Comparison at 400km

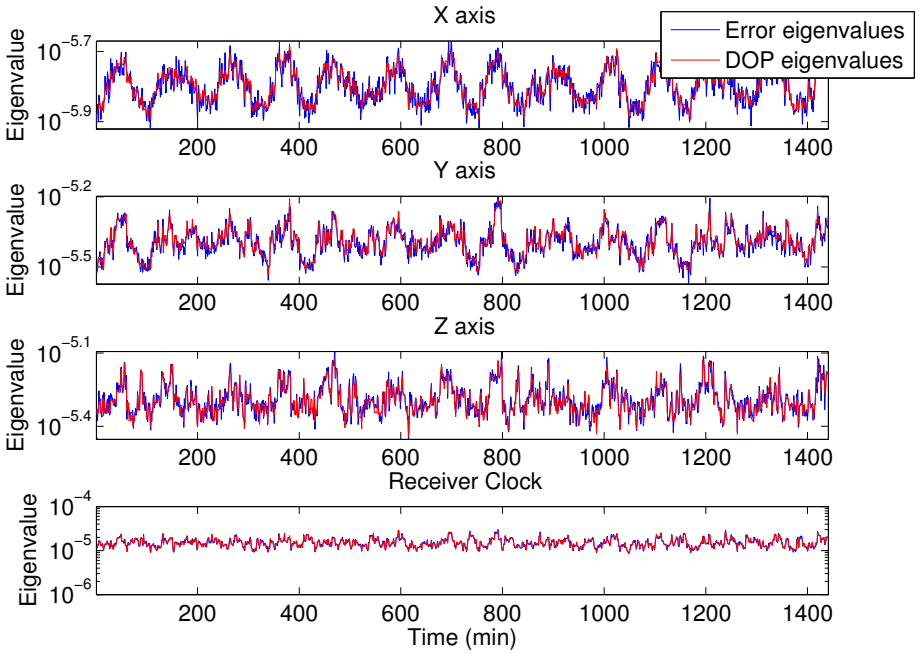

Figure 4.14. Eigenvalue Comparison by axis at 400km

Both plots shows that the position errors still follow the respective axis's DOP. Similar results are seen with the 500 km and 600 km scenarios in Figures 4.15 and 4.16.

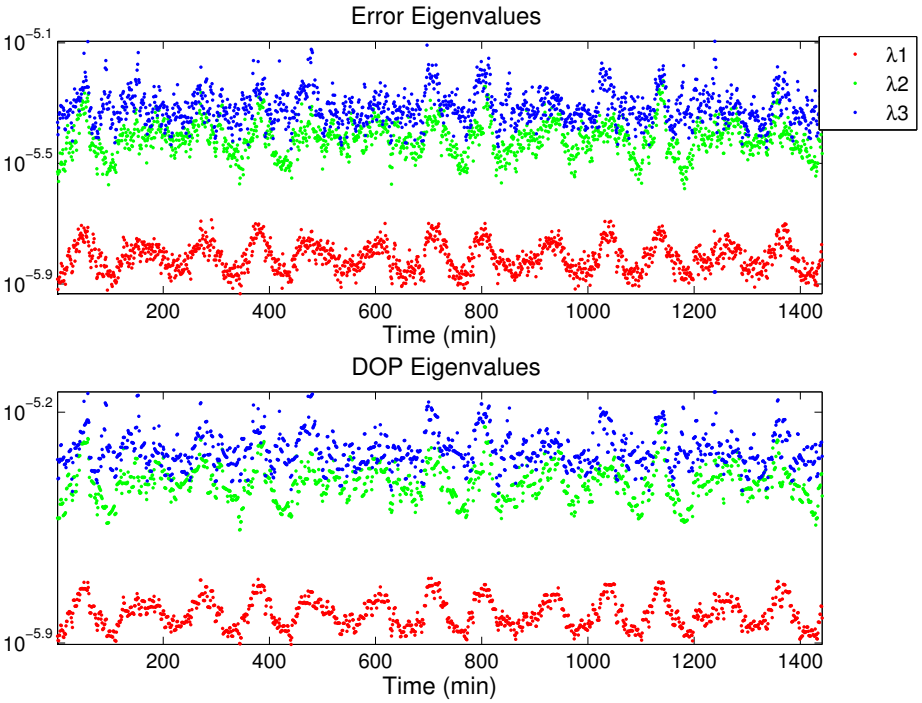

Figure 4.15. Error vs DOP Eigenvalue Comparison at 500km

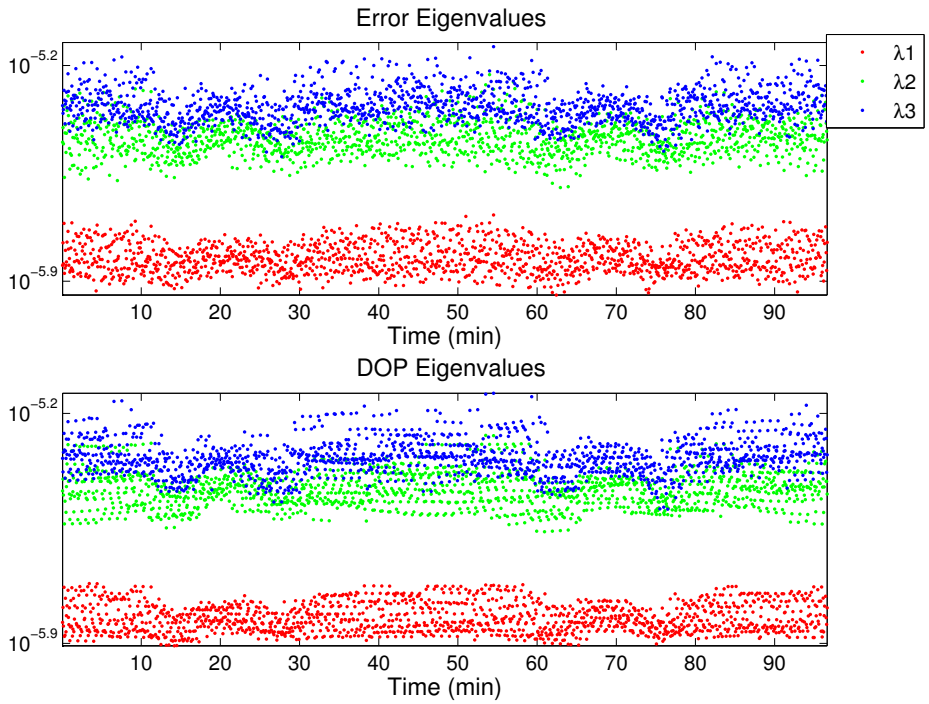

Figure 4.16. Error vs DOP Eigenvalue Comparison at 600km

Based on the result of these three LEO altitudes, DOP is still a valid metric for predicting position error sensitivity based on GPS SV geometry for a user in LEO. In addition, the software is validated to perform the expected calculations according to the sensitivity analysis/measurement theory.

4.4 Medium Earth Orbit

Three altitudes were chosen for the MEO scenario group: 10100 km, 15150 km, and 25000 km. These altitudes were chosen relative to the GPS constellations altitude. The orbits are at $\frac{1}{2}$ GPS altitude, $\frac{3}{4}$ GPS altitude, and slightly above the GPS constellation altitude. The classical orbital parameters for these orbits are listed in Table 4.3.

Table 4.3. MEO Scenarios: Orbital Parameters

Altitude	Semi-Major Axis	Inclination	Period
10,100 km	16,478.137 km	45°	351 min
15,150 km	21,528.137 km	45°	524 min
25,000 km	31,378.137 km	45°	922 min

Comparing the number of GPS SVs in view for the LEO and 10100 km scenario brings about an unexpected result. Figure 4.17 indicates that a receiver at 10100 km will have double the available GPS SVs than those available at LEO.

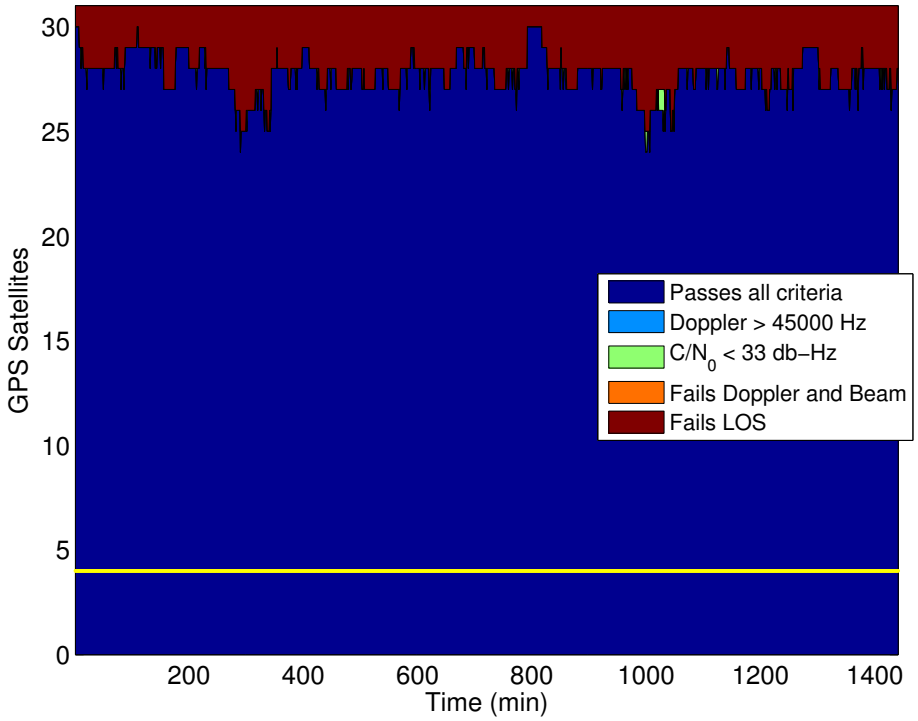

Figure 4.17. GPS Satellite Connection at 10100km

Earth becomes less of an obstruction the further away the user is. However, this also increases the likelihood of being outside of the GPS transmit antenna's main beam area. The large number of GPS SVs available to a user at an orbital altitude of 10100 km is due the effect of GPS antenna's side lobes. Figure 4.18 shows the result of running the same scenario again but only considering effects from the main beam of the GPS antenna.

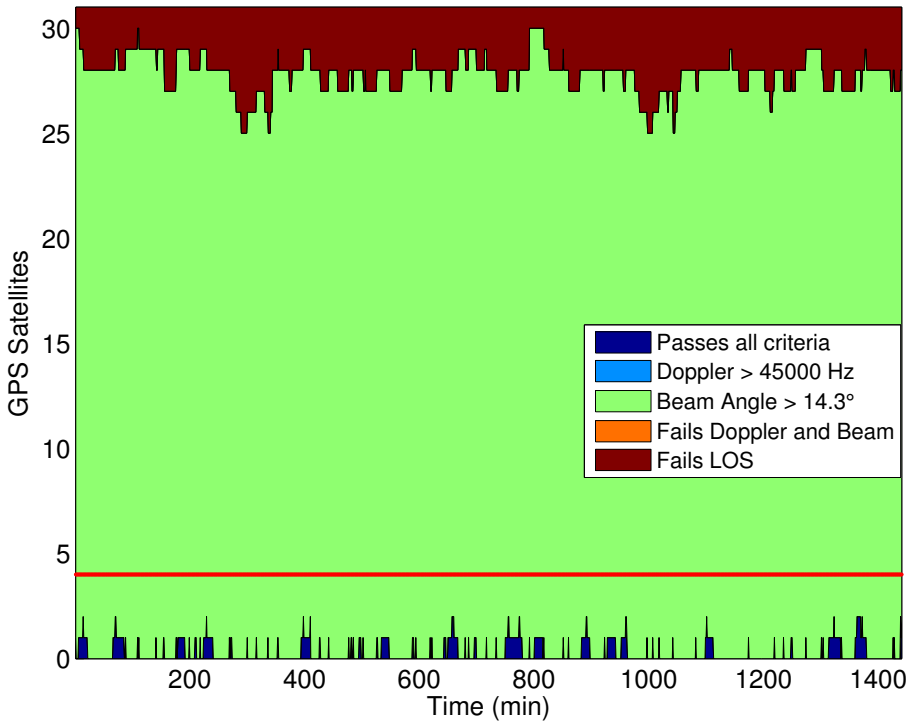

Figure 4.18. Satellites in View only considering GPS's main beam at 10,100km

In this variation of the scenario, the user was not in the main beam path of four or more GPS SVs at any point in the 24 hour simulation duration. The remainder of this research will only consider the cases that use both the GPS antenna main beam and side lobes.

The number of GPS SVs in view drops as the orbital altitude of the user increases due to lower signal strength. This is seen when looking at Figures 4.19 and 4.20.

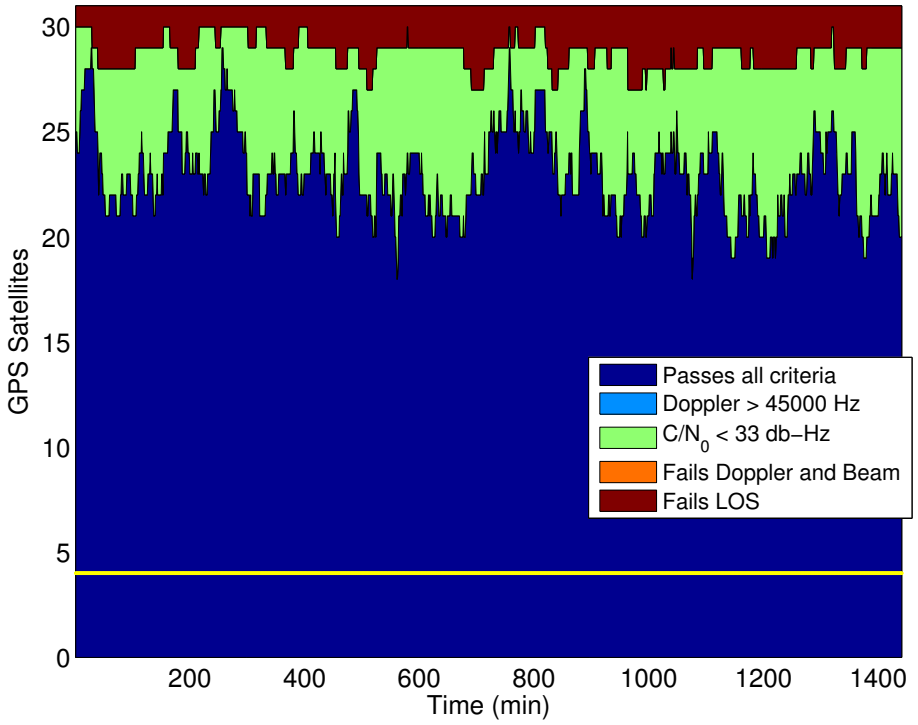

Figure 4.19. GPS Satellite Connection at 15,150km

Unlike the LEO altitude scenarios, the majority of connection failures is not from Earth obstruction. Rather the predominate criteria failures originate from low signal strength, when C/N0 is less than the receiver threshold. This is more pronounced in Figure 4.20.

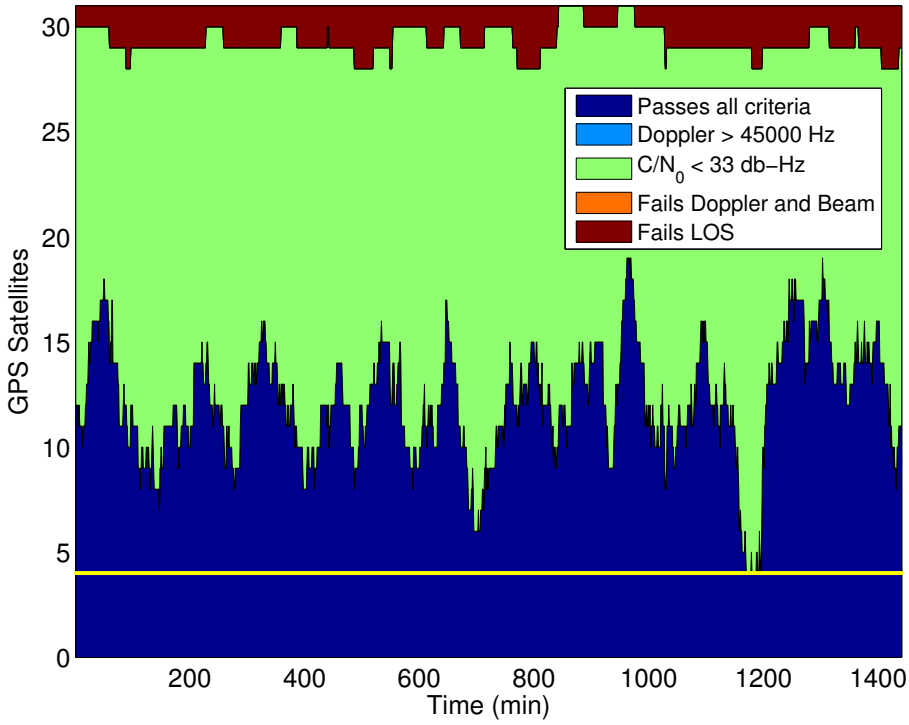

Figure 4.20. GPS Satellite Connection at 25,000km

There is even a point in time where the user at 25000 km altitude is "in view" of only four GPS SVs. Even though more SVs have line of sight to the user, the distances are greater. The increased distance causes the signals originating from GPS side lobes, which started with low gain, to fall under the receiver's C/N0 threshold at time of reception.

DOP.

DOP for the 10100 km and 15150 km altitude scenarios are both around one. Different results are seen for the 25000 km orbital altitude scenario. Figure 4.21 displays all three scenario's GDOP for comparison.

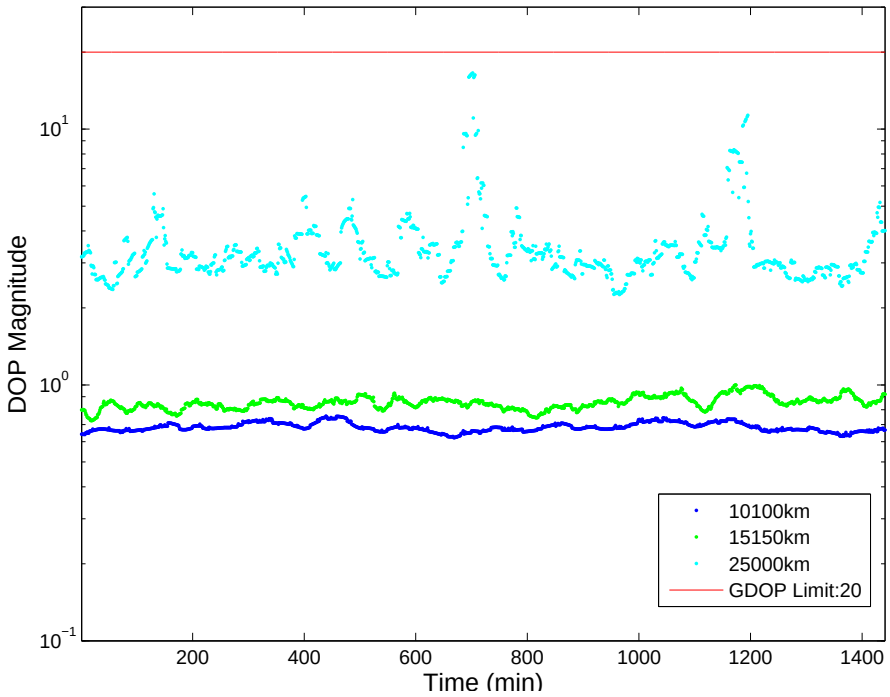

Figure 4.21. GDOP vs Time at MEO

Unlike the 10100 km and 15150 km altitudes, the 25000 km scenario is above the GPS constellation. The location of available signals is changed when the user's altitude surpasses that of the GPS constellation, thus affecting the GDOP. The values of the 25000 km scenario's GDOP generally stay around two but does occasionally rise past 10.

Position Errors.

The effect the number and location of available GPS SVs has on position can be viewed when comparing the position errors for altitudes 10100 km, 15150 km, and 25000 km. Figures 4.22, 4.23, and 4.24 present one realization of the position errors expected for the user's orbit for each MEO scenaro.

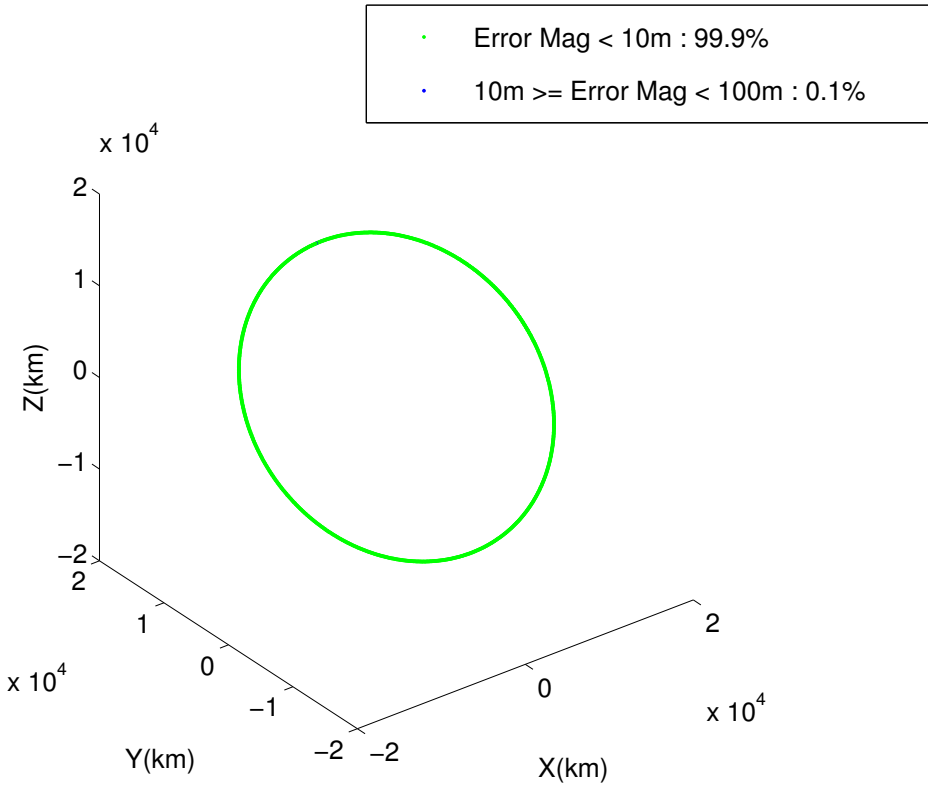

Figure 4.22. 3D Visualization of RMS Error at 10,100km

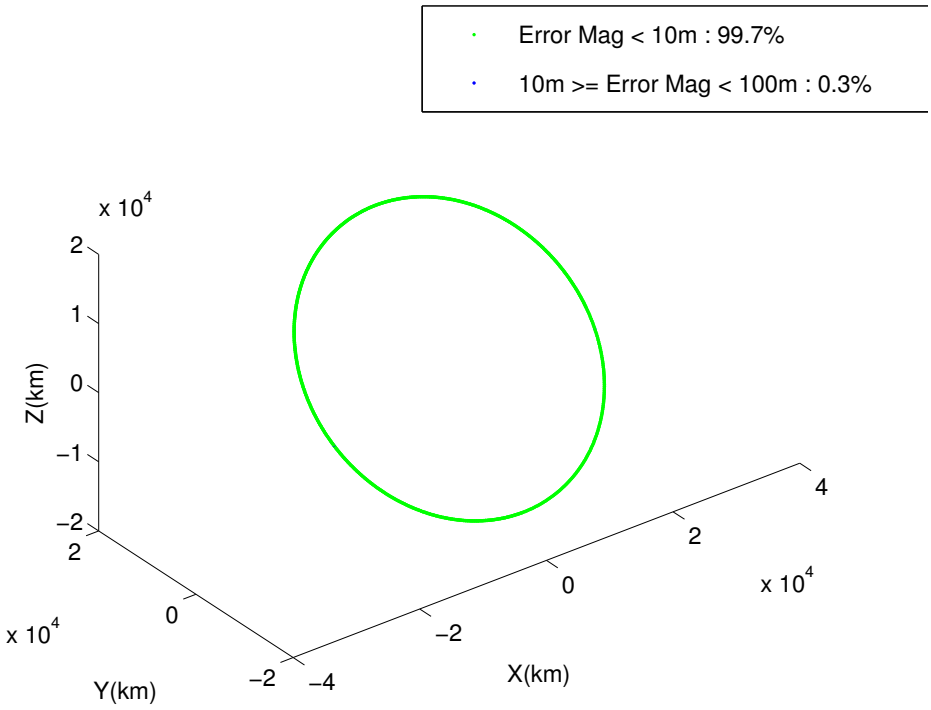

Figure 4.23. 3D Visualization of RMS Error at 15,150km

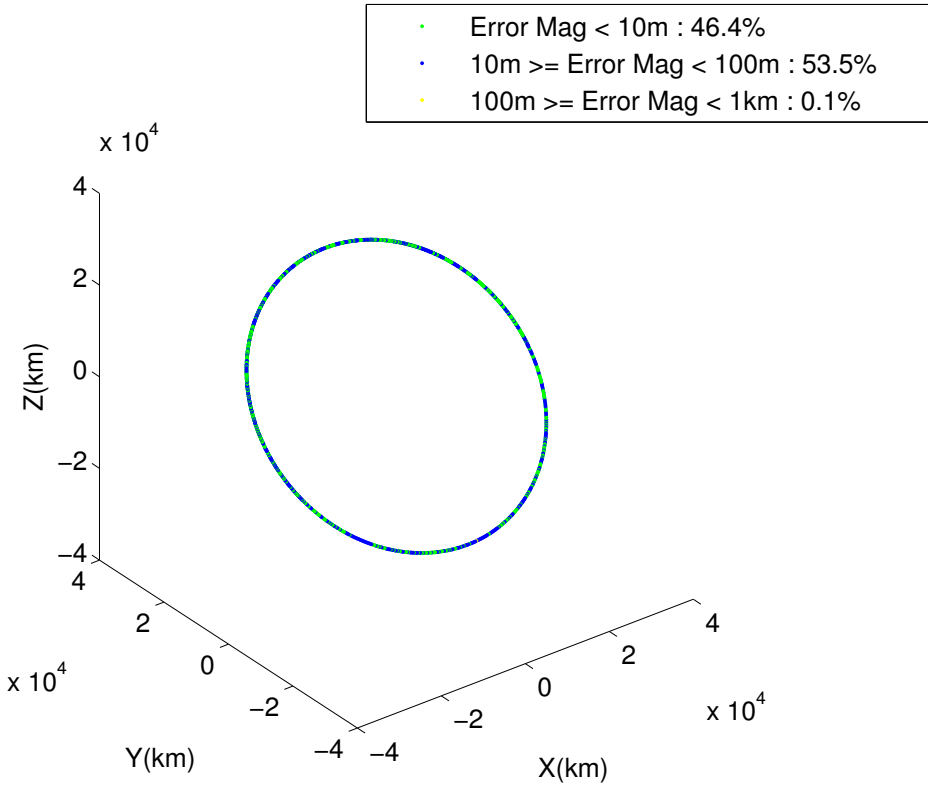

Figure 4.24. 3D Visualization of RMS Error at 25,000km

A majority of the position errors experienced at an altitude above the GPS constellation were between 10 m and 100 m, as opposed to under 10 m for the altitudes below the constellation. At altitudes above the GPS constellation, the user has to rely more on GPS signals originating from the opposite side of Earth. This not only decreases signal strength, it also decreases the relative angle between GPS SVs available to the user. The reliance on these signals with increasingly singular direction of origin causes the positional error to also be along that same direction as shown in Figure 4.25. The magnitudes of DOP and the position errors have been amplified by a factor of $4 * 10^4$ to provide a visual representation along the orbit's path.

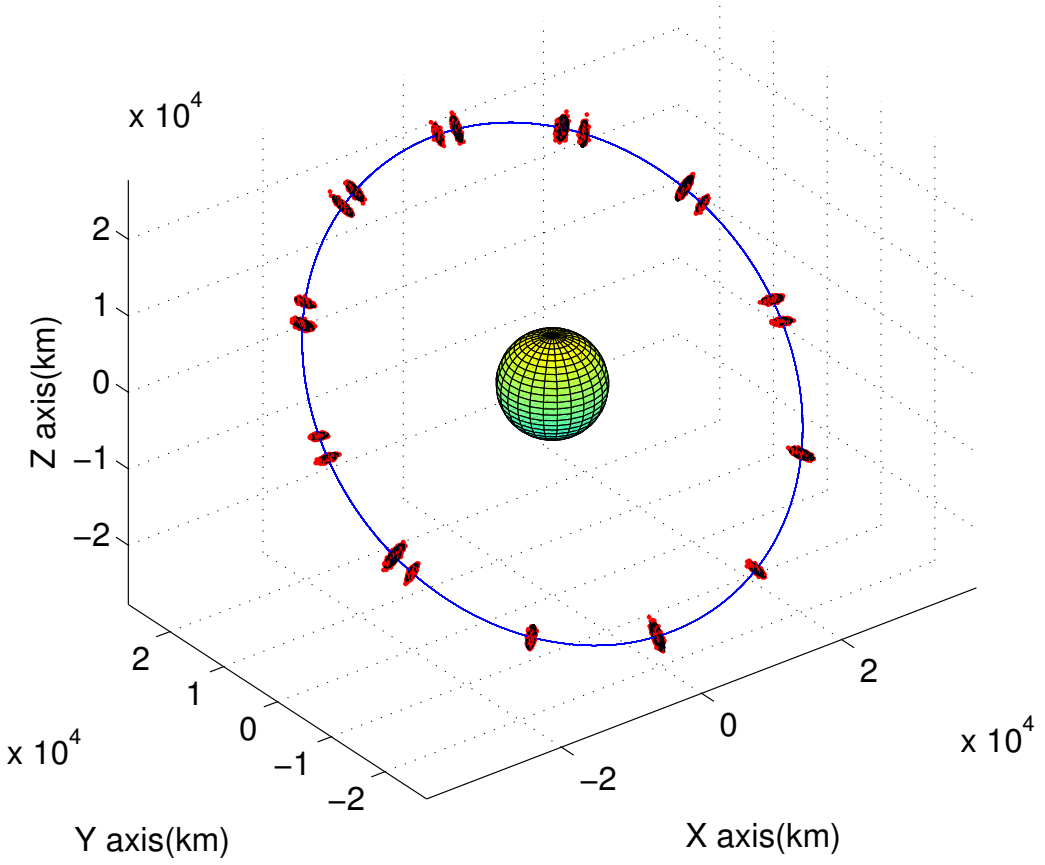

Figure 4.25. 3D Visualization of DOP and Error at 25,000km

The position error indicated by the red dots in Figure 4.25 are more elongated compared to those of the 10100 km case in Figure 4.26.

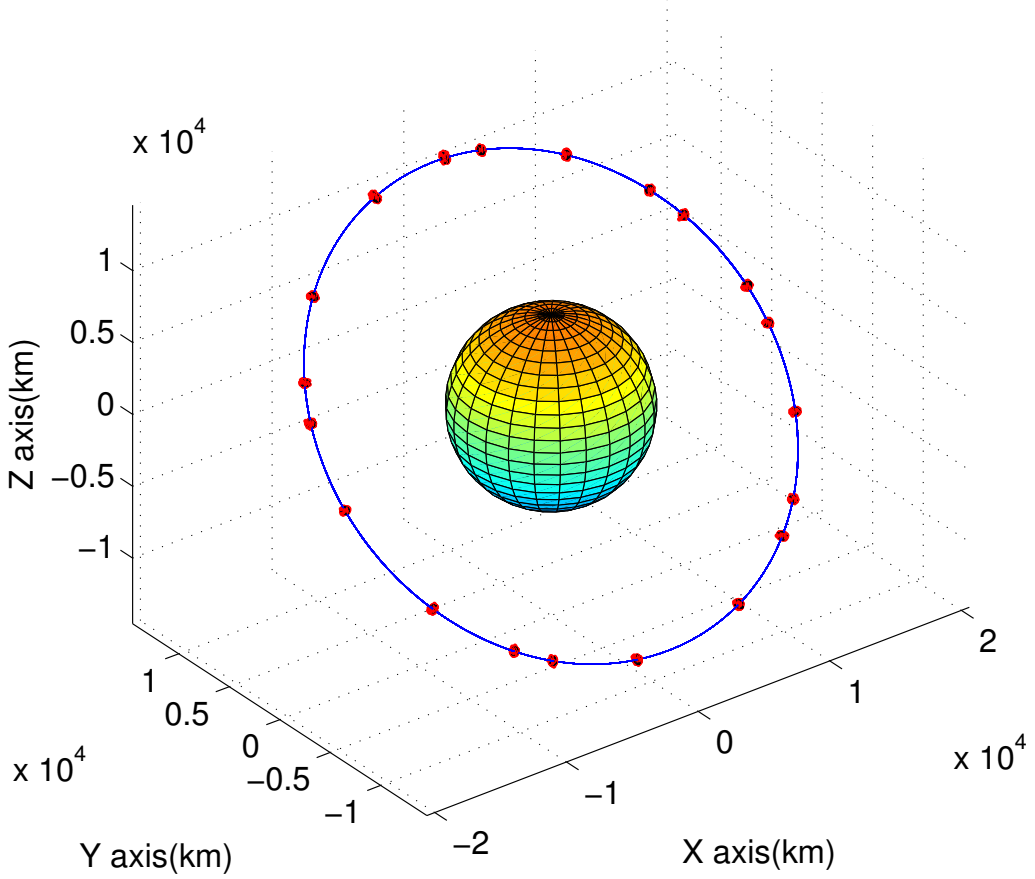

Figure 4.26. 3D Visualization of DOP and Error overlap at 10,100km

Figure 4.27 displays a 3σ representation of both 10100 km and 25000 km's weighted DOP at the very beginning of the simulation. Both positions are aligned over the same location on Earth at this time instance.

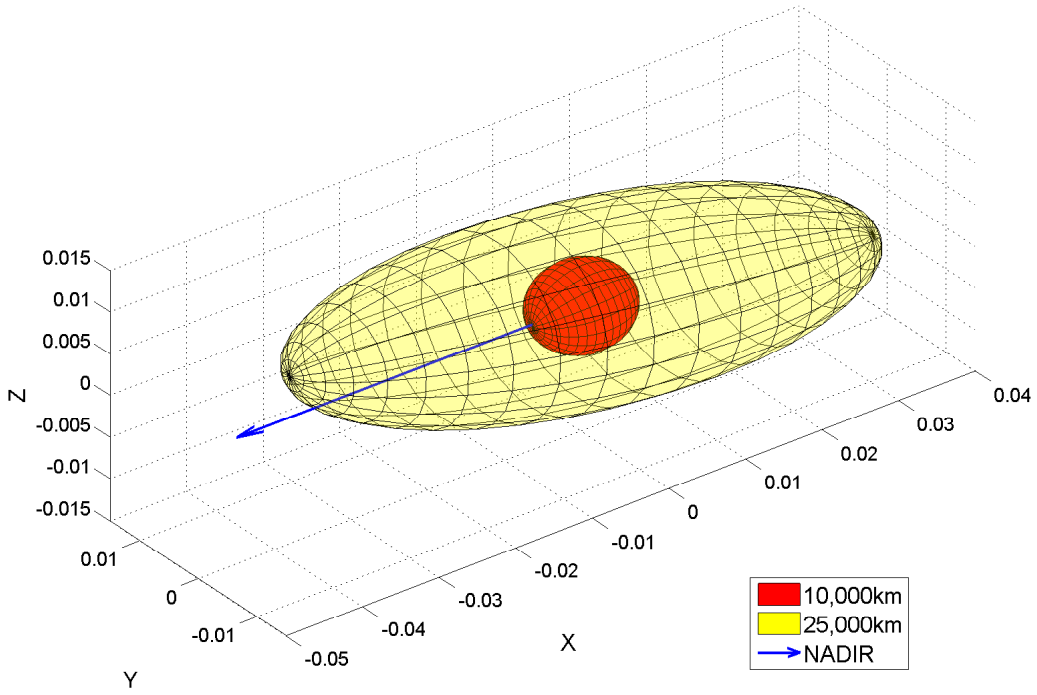

Figure 4.27. 3σ **DOP Comparison at Scenario Start**

Applicability of DOP.

The MEO scenarios above and below the GPS constellation exhibited the linear relationship between DOP and position error similar to the LEO scenarios. Altitudes 10100 km and 25000 km are shown in Figures 4.28 and 4.29 respectively.

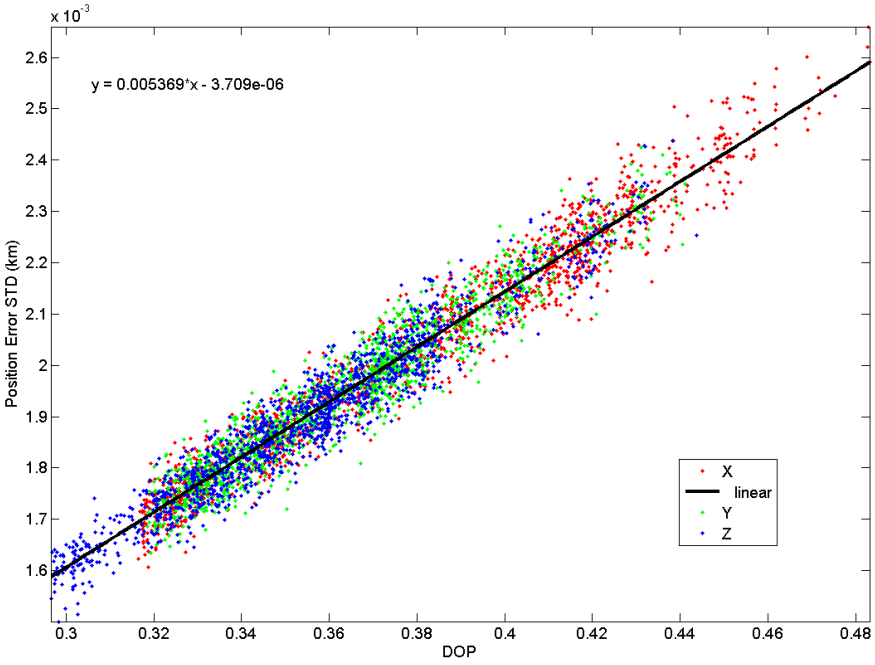

Figure 4.28. DOP vs Position Error STD at 10,100km

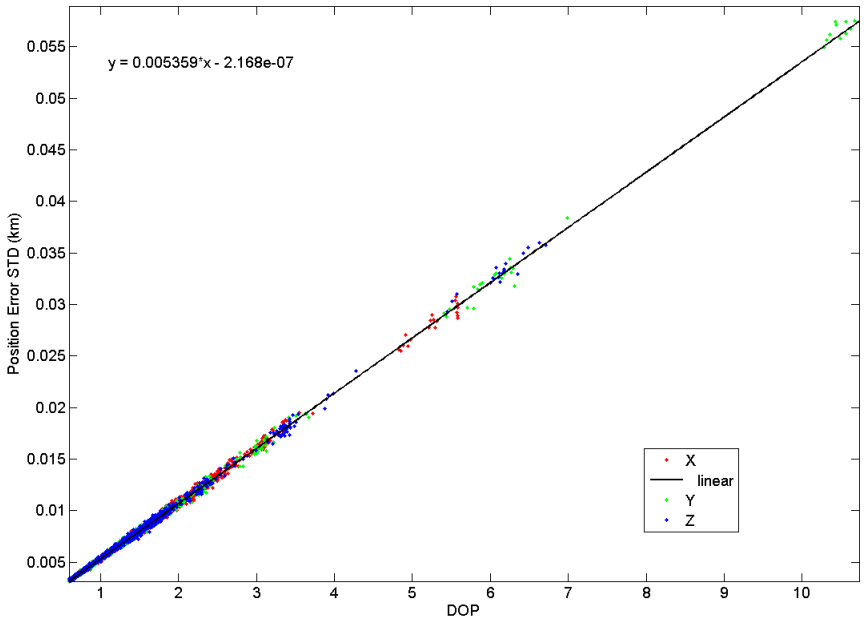

Figure 4.29. DOP vs Position Error STD at 25,000km

4.5 Geostationary Orbit

A Geostationary orbit with an altitude of 35788 km is chosen as the last scenario to test. The orbital parameters are listed in Table 4.4

Table 4.4. GEO Scenarios: Orbital Parameters

Altitude	Semi-Major Axis	Inclination	RAAN
35,788 km	16,478.137 km	45°	1436 min

At this distance obtaining an abundance of GPS SVs "in view" is difficult due to the distance from the GPS constellation. Similar to the 25000 km scenario, the limiting factor is low signal strength as seen in Figure 4.30. Since users at higher orbits depend on the low gain GPS antenna's side lobes, the increased distance causes the signals to fall below the receiver's signal strength threshold. Unlike the LEO and MEO altitudes, the number of GPS SVs in view for the GEO scenario never reaches 10. There are multiple instances where the minimum threshold, four GPS SVs present, is not met for position and DOP calculation.

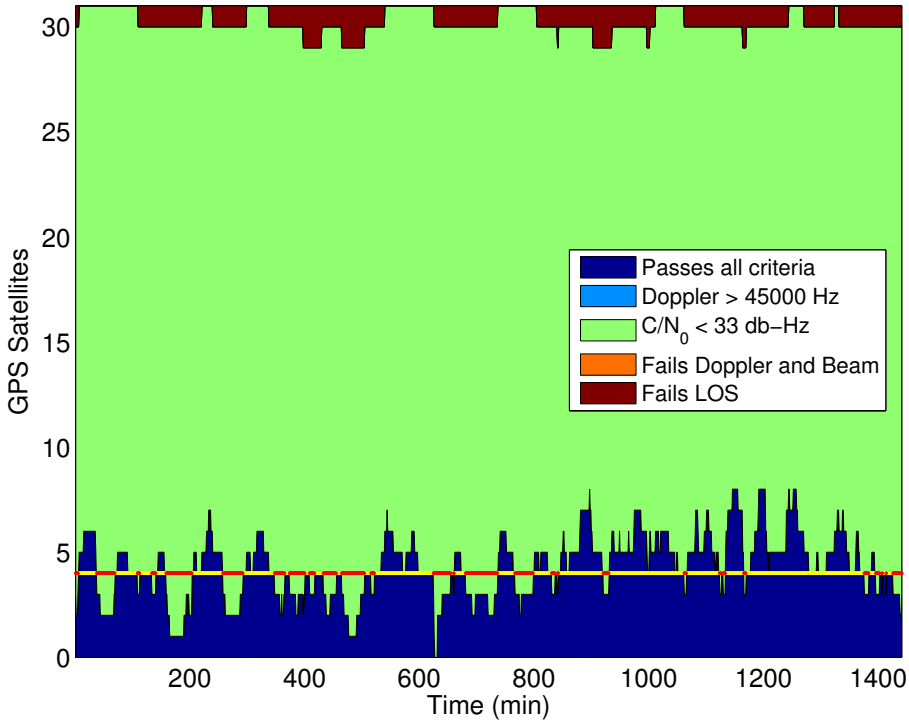

Figure 4.30. GPS Satellite Connection at GEO

DOP.

The few number of GPS SVs in view all originate from a similar general direction, causing the DOP to worsen. At no point during the scenario duration does the GDOP fall under the threshold of 20, shown in Figure 4.31.

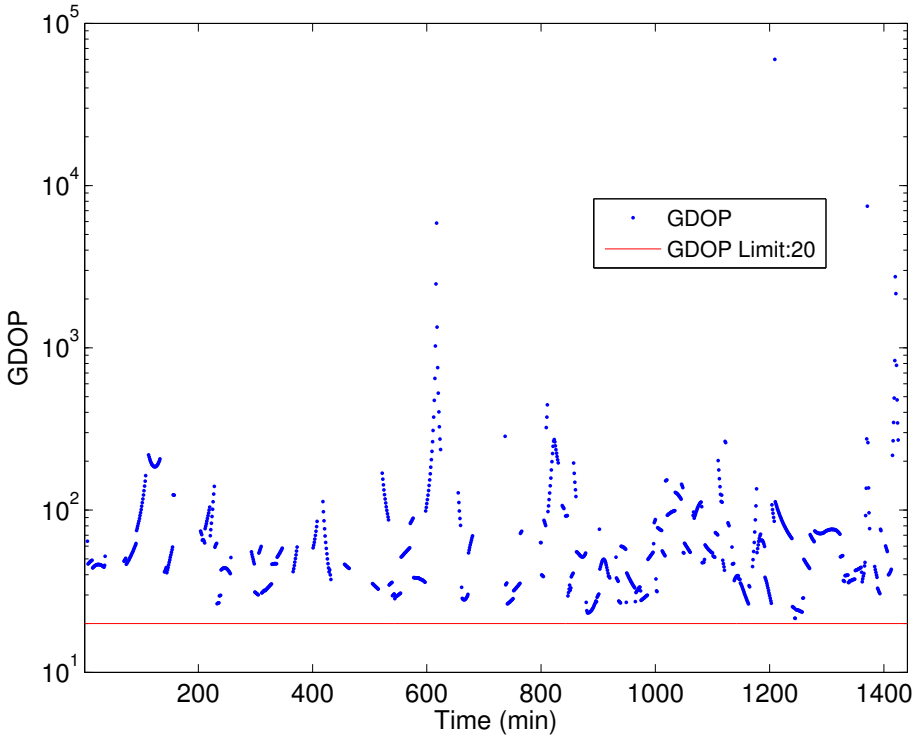

Figure 4.31. GDOP vs Time at GEO

If these GDOP values were received on Earth, they would be considered poor and possibly advised to be discarded [15].

Position Error.

Unlike the LEO and GEO scenarios, the position error for the GEO altitude is rarely below 10 m. When the GEO position is able to be calculated, the position error ranges anywhere from under 10 m to over 1 km as shown in Figure 4.32.

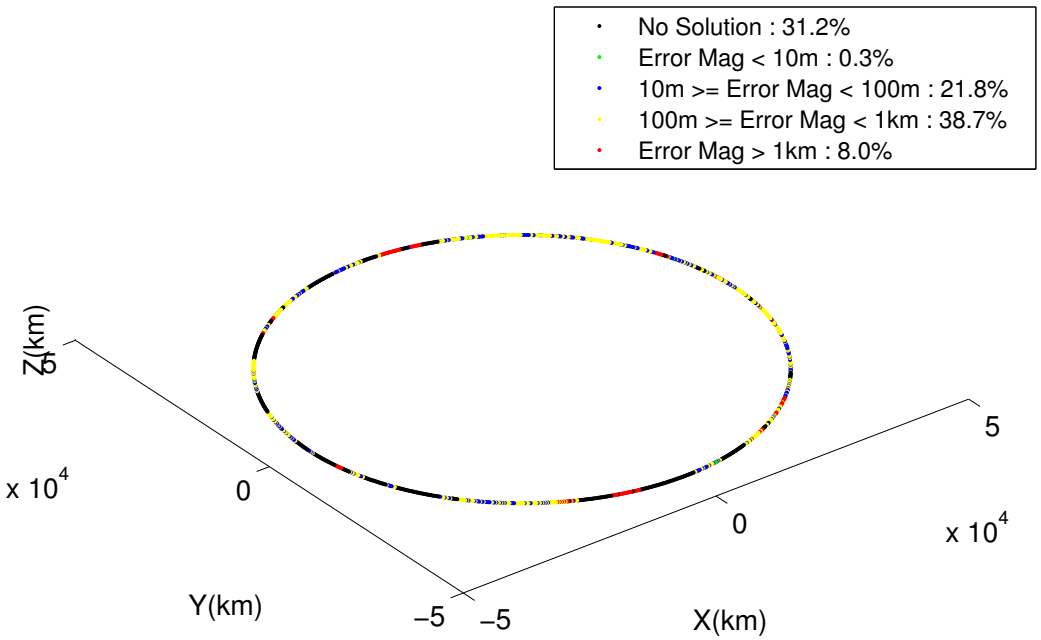

Figure 4.32. 3D Visualization of RMS Error at GEO

Applicability of DOP.

The linear relationship between DOP and the position error is still present for the GEO altitude even though the magnitude of the position errors have increased. Figure 4.33 displays this relationship. The linear fit values for each scenario can be found in Table 4.5.

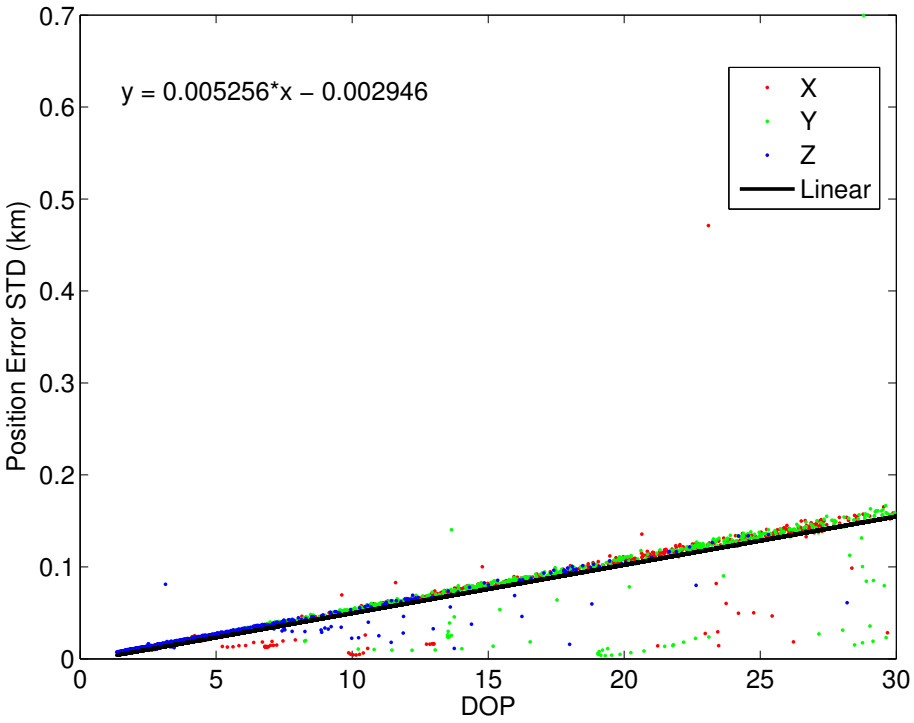

Figure 4.33. DOP vs Position Error STD at GEO

Table 4.5. Linear Fit Model for Error to DOP Relationship. Linear equations takes the form: Position Error STD = Linear Fit * DOP + Offset. The linear fit factor in the figures above are in units of km while the table converts it to units of m for comparison with the UERE

.

Scenario	Linear Fit	Offset	‖UERE - Fit‖	R^2
400 km	5.349	3.573e-06	0.0082	.999
500 km	5.358	-1.589e-06	0.0007	.999
600 km	5.375	-8.274e-06	0.0177	.999
10100 km	5.369	-3.709e-06	0.0117	.999
15150 km	5.371	-6.733e-06	0.0138	.999
25000 km	5.359	-2.168e-07	0.0018	.999
GEO	5.256	-0.0029	0.1012	.999

When overlaying the position errors and DOP values onto the user's orbit, it can be shown that the majority of the error is in the direction from which the GPS signals arrive. The errors in Figure 4.34 are more pronounced compared to the 25000 km scenario whose altitude is also above the GPS constellation. In Figure 4.34, the scaling factor applied for visualization purposes is $\frac{1}{4}$ of the value used for the MEO scenarios in Figures 4.25 and 4.26.

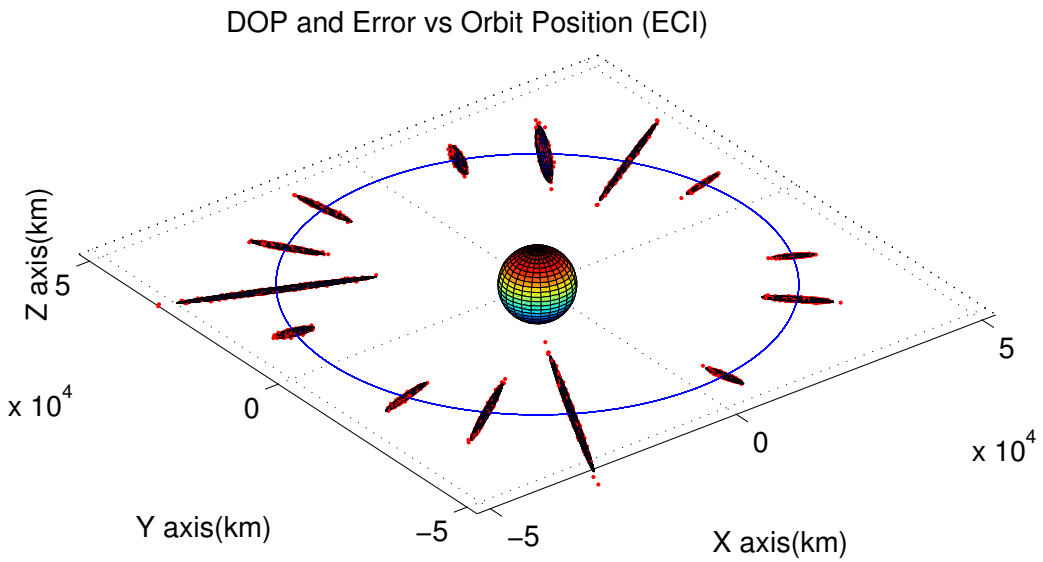

Figure 4.34. 3D Visualization of DOP and Error overlap at GEO

4.6 Visual Summary of GPS Connections

At the beginning of the LEO and MEO scenarios, each user's relative position over Earth is the same. The distance away from Earth is represented as different magnitudes along the ECI X axis. At the scenario start time, each GPS SV with a valid connection to the user is calculated and plotted for scenarios 500 km, 15150 km, and 25000 km. Figures 4.35 - 4.37 provide a visualization of how the connected GPS geometry changes with altitude. The GEO simulation does not start at the same relative position over Earth. However Figure 4.38 provides an example when four GPS SVs are in view.

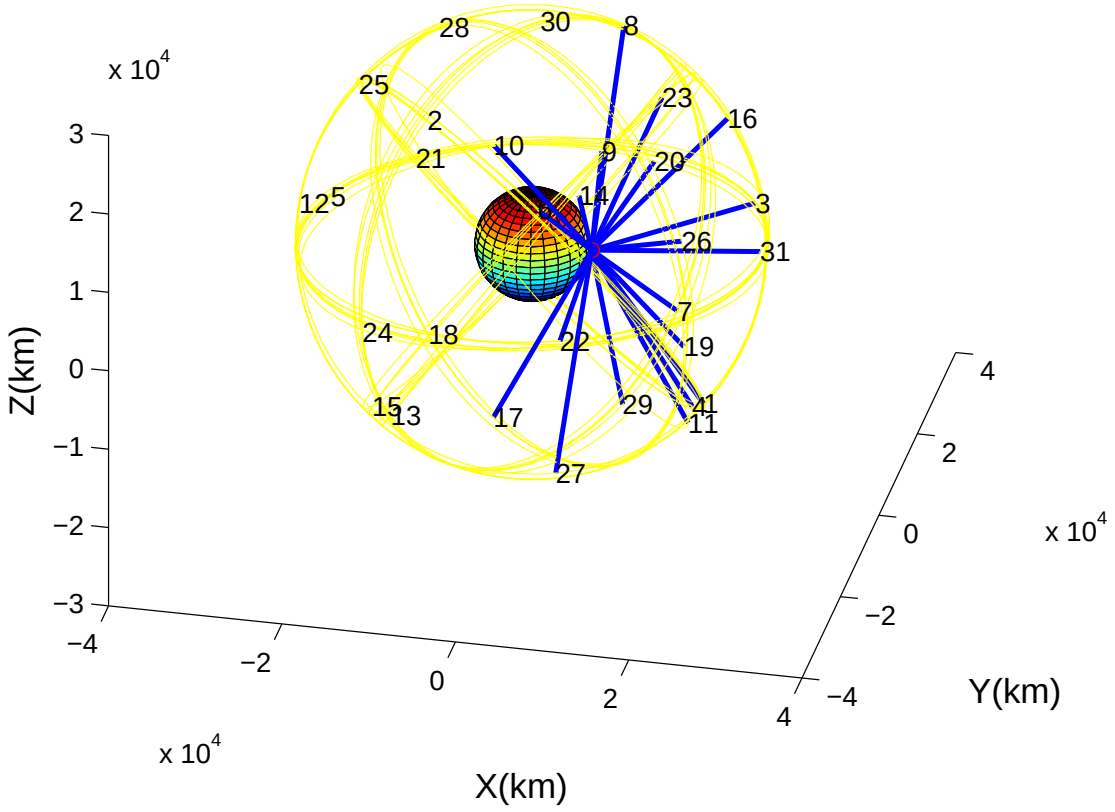

Figure 4.35. GPS in View at Scenario Start at 500km

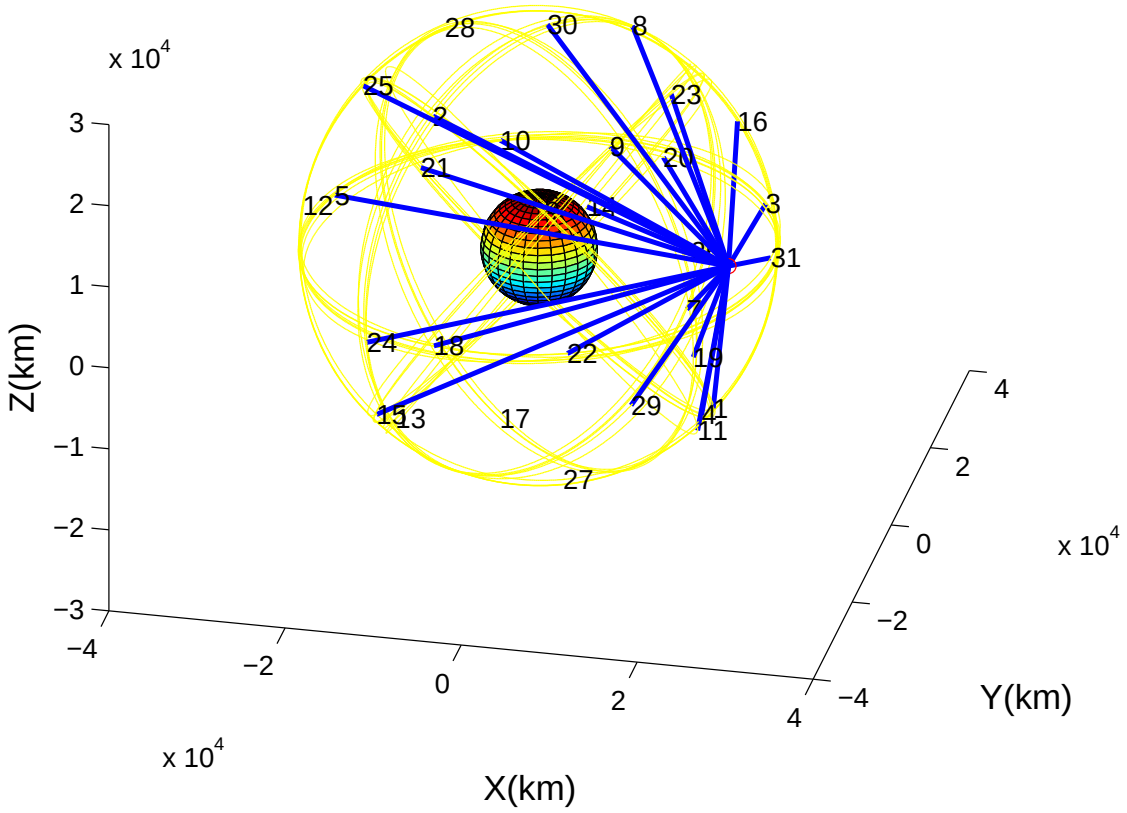

Figure 4.36. GPS in View at Scenario Start at 15,150km

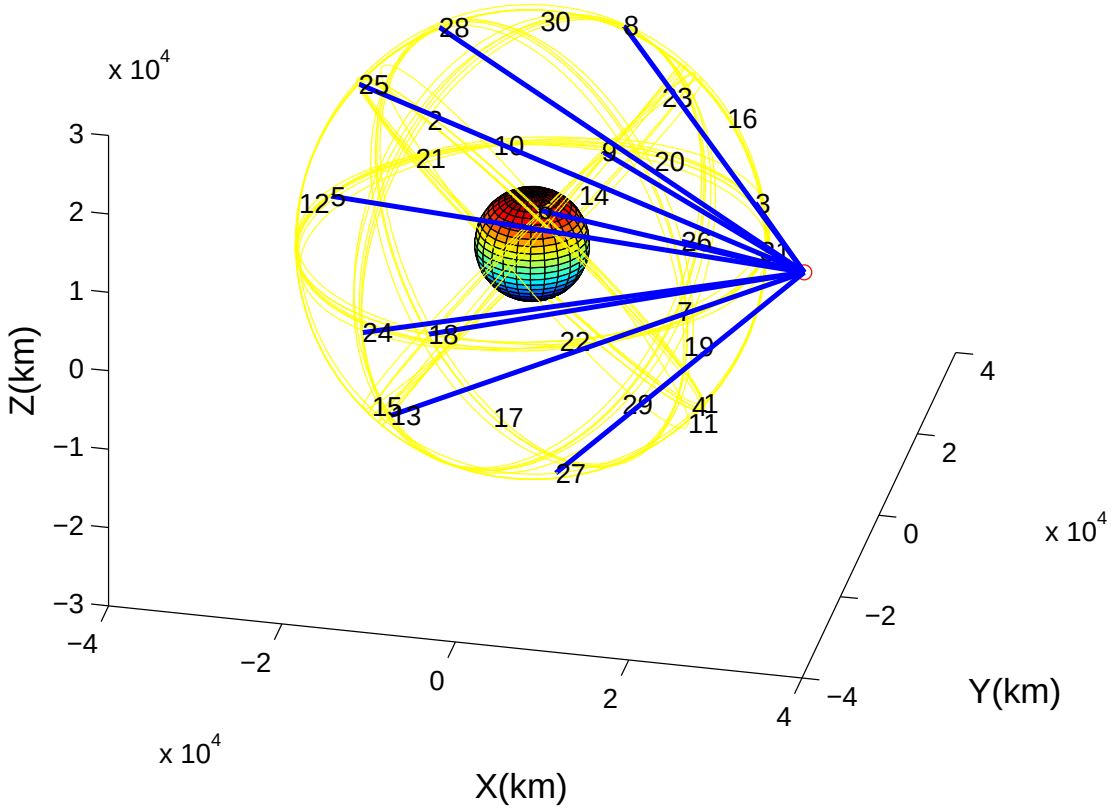

Figure 4.37. GPS in View at Scenario Start at 25,000km

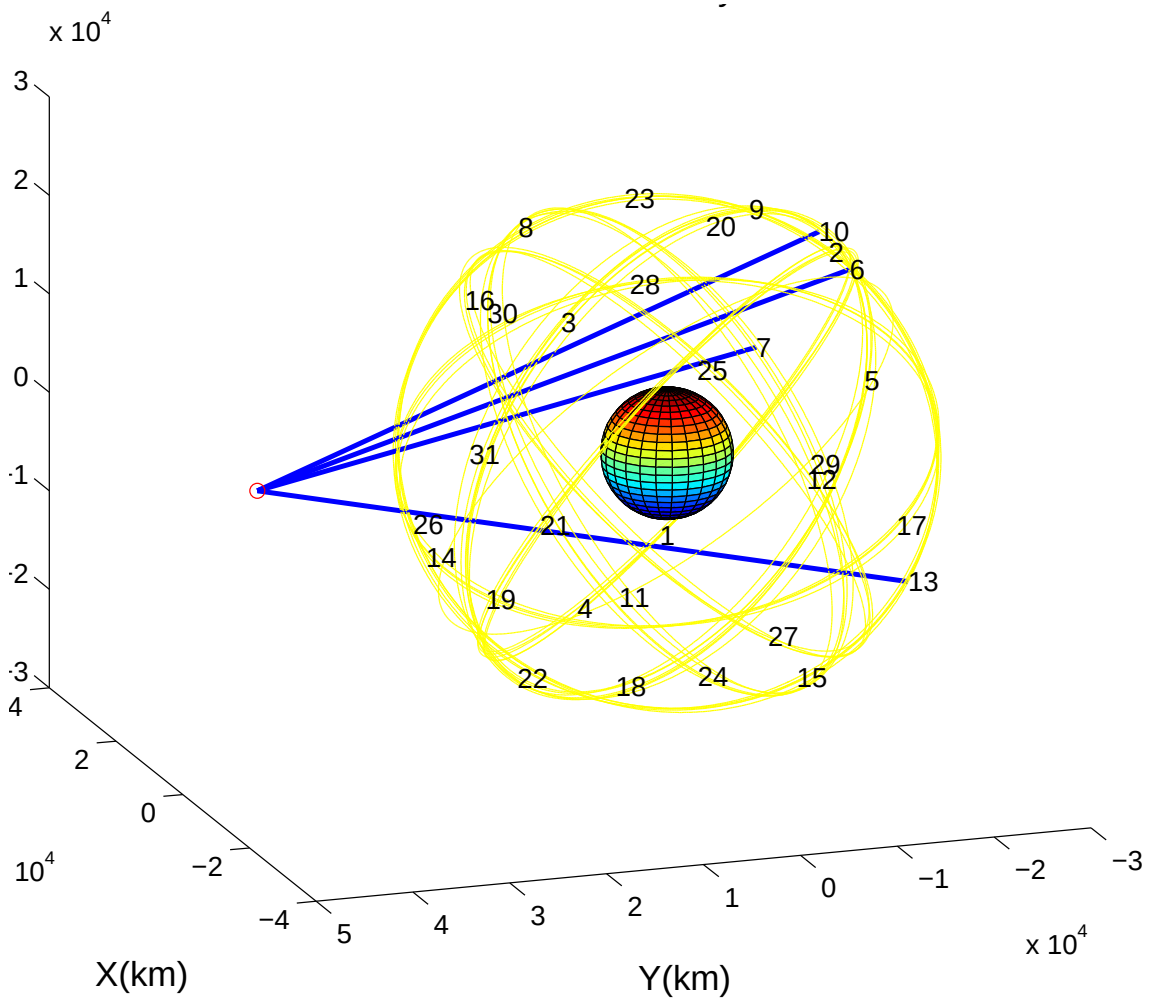

Figure 4.38. GPS in View at Scenario Start at GEO

4.7 RF Signal Generation

A GPS RF signal generator was operated in an attempt to validate the results of the MATLAB supplementary analysis. The four scenarios chosen to be loaded into the SPIRENT GSS8000 signal generator were the 400 km, 15150 km, 25000 km, and GEO scenarios. The resulting RF signal for each scenario was recorded for 37 second and then processed by a SDR.

GPS SV Acquisition.

After being recorded, the RF signal is processed to determine the number of GPS signals present. Simplistically speaking, the recorded signal is correlated against multiple versions of the reference signal (accounting for shifts in Doppler and PRN code). This correlation process is repeated for a preset number of PRN code iterations (civilian signal's PRN repeats every millisecond). The multiple versions of the reference signal that were correlated are converted to power and then analyzed by comparing the power against one another. A signal is considered present if the power of the strongest correlation compared to that of the 2nd strongest is above a certain threshold.

The ratio between the two strongest signals, known as the acquisition ratio, is a scale to determine the likelihood of a specific GPS SV being present. A GPS SV is considered present if its acquisition ratio is above the preset threshold of 3 for this research. An acquisition threshold of three requires the power of the highest correlation to be a minimum of three times greater than the next highest correlation. Figures 4.39 to 4.42 are the results of processing the recorded RF signal from the four scenarios.

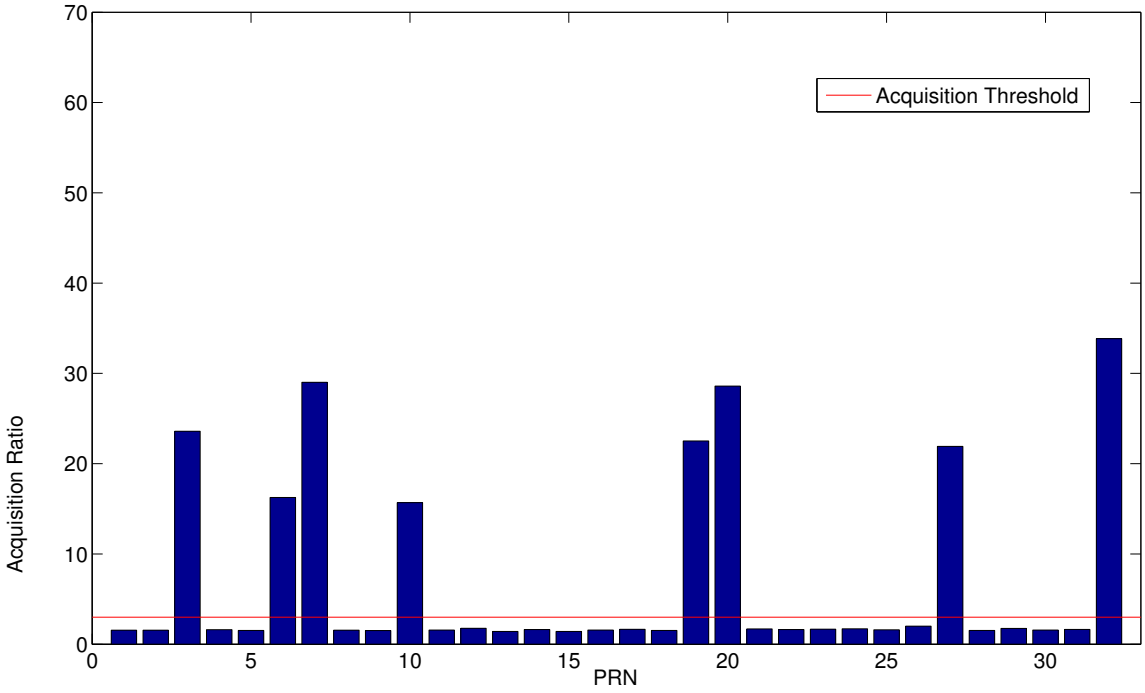

Figure 4.39. GPS Signal Acquisition Strength at 400km

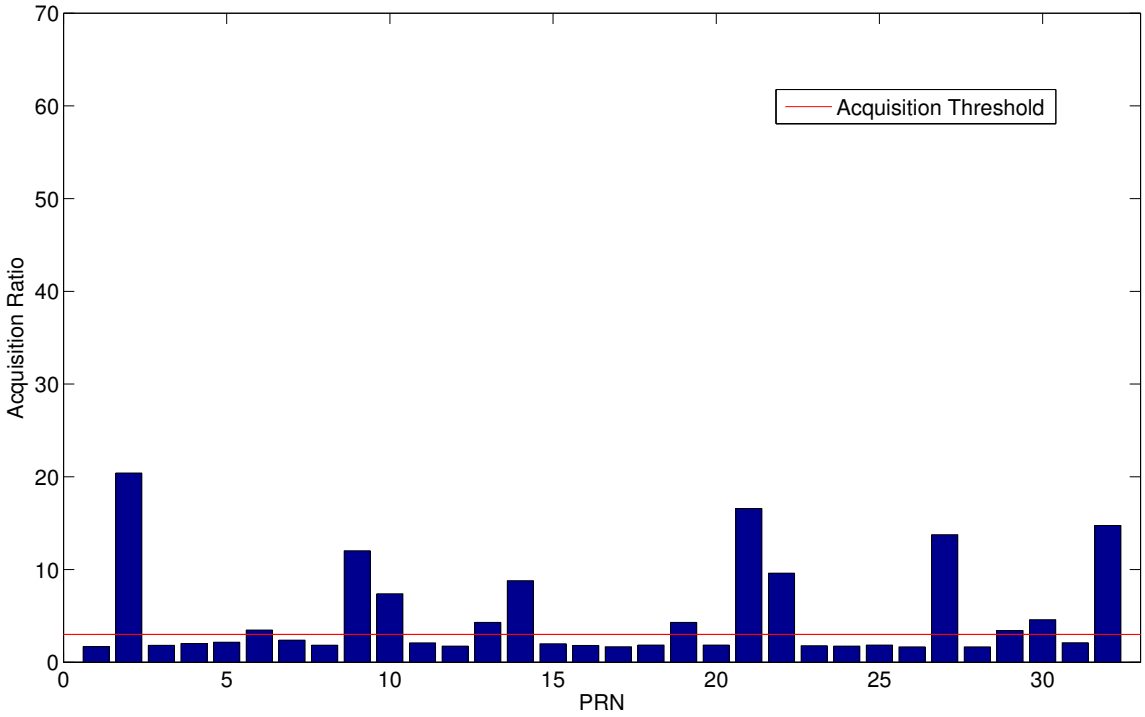

Figure 4.40. GPS Signal Acquisition Strength at 15,150km

At 400 km, Figure 4.39, eight GPS SVs are present and each have an Acquisition ratio of 15 or greater. The 15, 150 km scenario in Figure 4.40 has 13 GPS SVs present but only three are above an Acquisition ration of 15. Five of the signals are barely over the threshold, meaning the signal strength is so low as to be almost be indistinguishable from noise. Picking up signals that originate from the side lobes of the GPS antenna would produce these types of results.

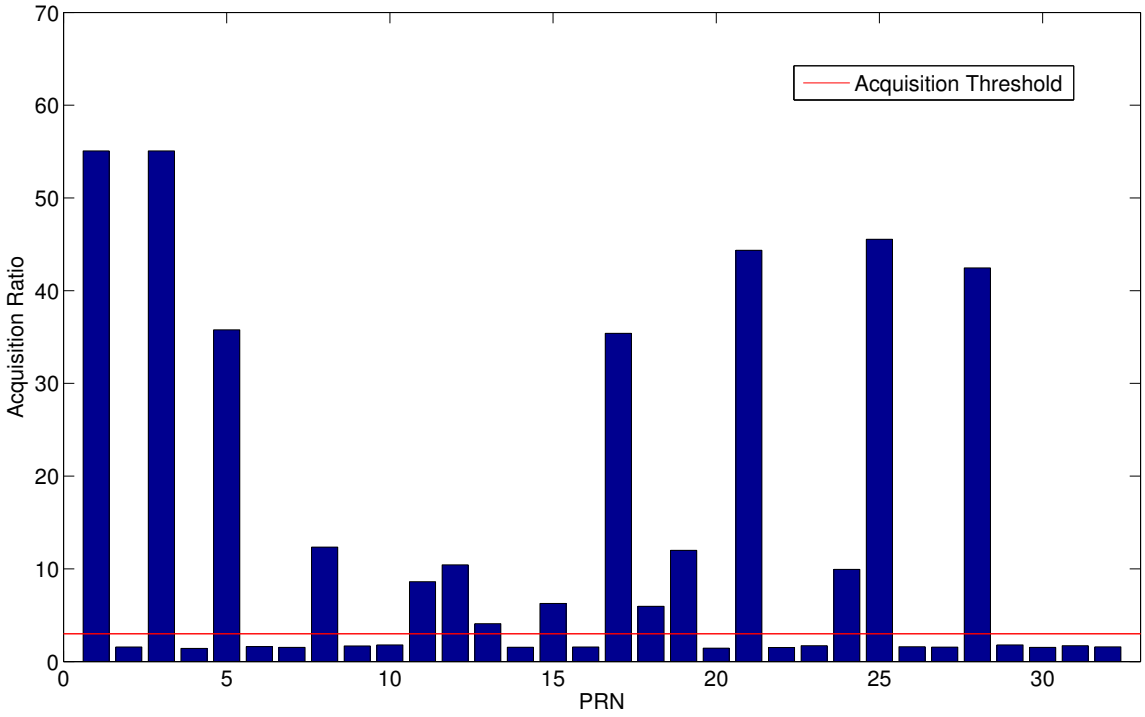

Figure 4.41. GPS Signal Acquisition Strength at 25,000km

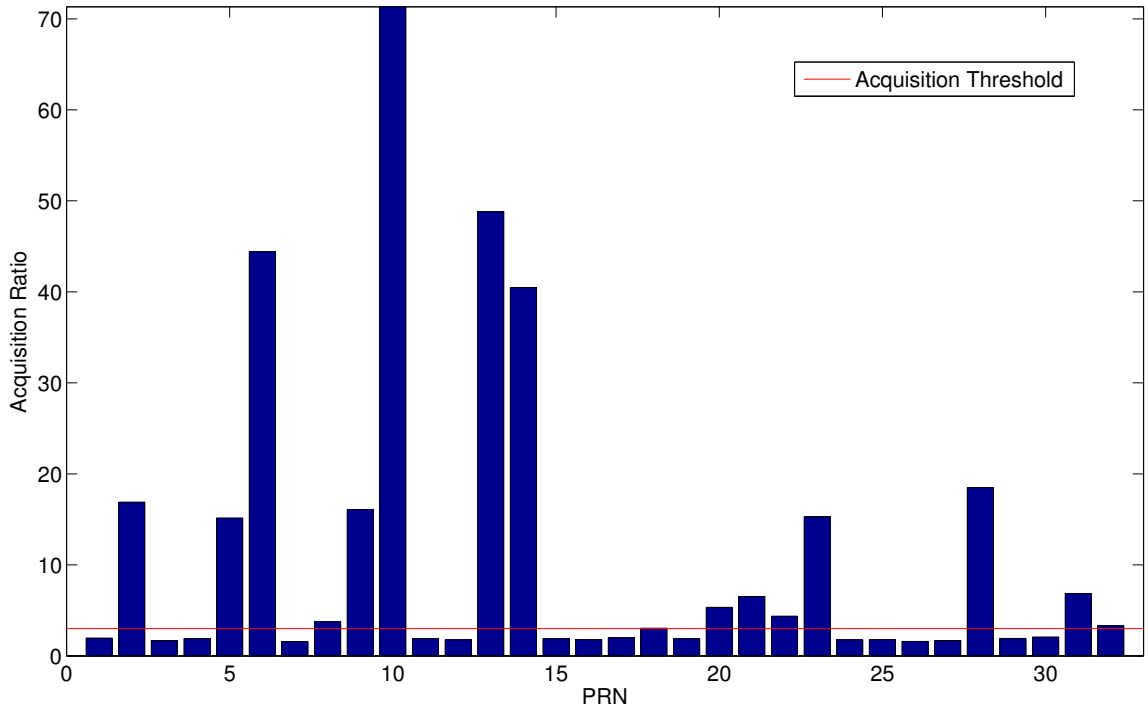

Figure 4.42. GPS Signal Acquisition Strength at GEO

The processed RF data is showing 14 GPS SVs in view for the 25,000 km scenario and 15 for the GEO scenario, Figures 4.41 and 4.42 respectively. The signals in the 25,000 km RF data have stronger Acquisition thresholds than the 15,150 km data. Results from the GEO scenario was vastly different than the MATLAB analysis, showing well over the predicted maximum of 10 SVs in view. Having four PRNs that distinctly standout compared to the rest was predicted for the GEO case, but the sheer number of GPS signals found was unexpected so there are some reservations about the RF results.

One method to validate the RF signal would be to run the same scenario multiple times and record the resulting position errors. Afterwards, analyze the position errors for a Gaussian trend that matches the expected error ellipse. The results of the RF signal can also be checked by analyzing the positions of the GPS SVs, whose PRN was observed in the RF signal, with the location of the receiver to ensure that signal

reception is possible.

Low Acquisition Ratio.

Choosing an appropriate acquisition threshold is important for limiting the amount of weak signals. If a signal is too weak, then it may be difficult to read the navigation data in the signal. Errors could also arise due to the noise's effect on the signal as well. To illustrate the difference in strength, PRNs 10 and 18 were from the GEO RF data were processed and the tracking results are shown with Figures 4.43 to 4.46.

Plotting the two outputs of the RF signal after it's been correlated and accumulated gives information on how well the signal is being tracked. If the receiver is not tracking the GPS signal or no signal is present, then all the data points will be at the center of the plot. If the signal is strong and the receiver is tracking both the GPS signal's frequency and phase, then the data points will be concentrated in two small circles far away from the center as shown in Figure 4.43 for PRN 10.

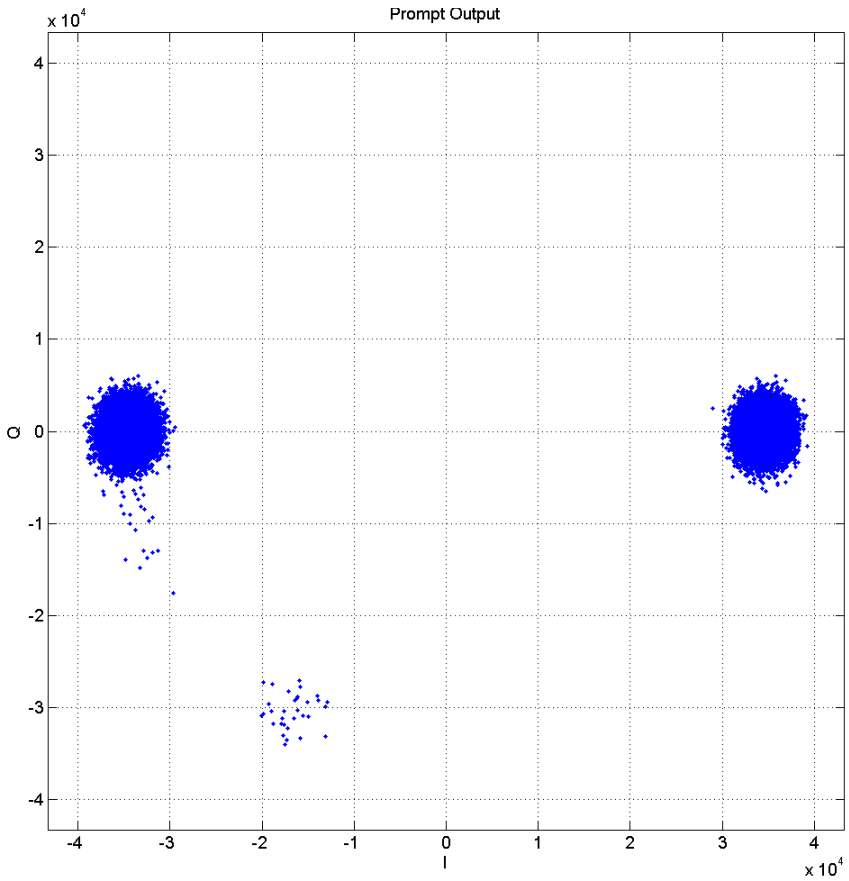

Figure 4.43. GEO Signal Tracking for PRN 10

Even while able to be tracked, PRN 18's signal strength is not as a strong so the data points will be closer to the center of the plot, as shown in Figure 4.44.

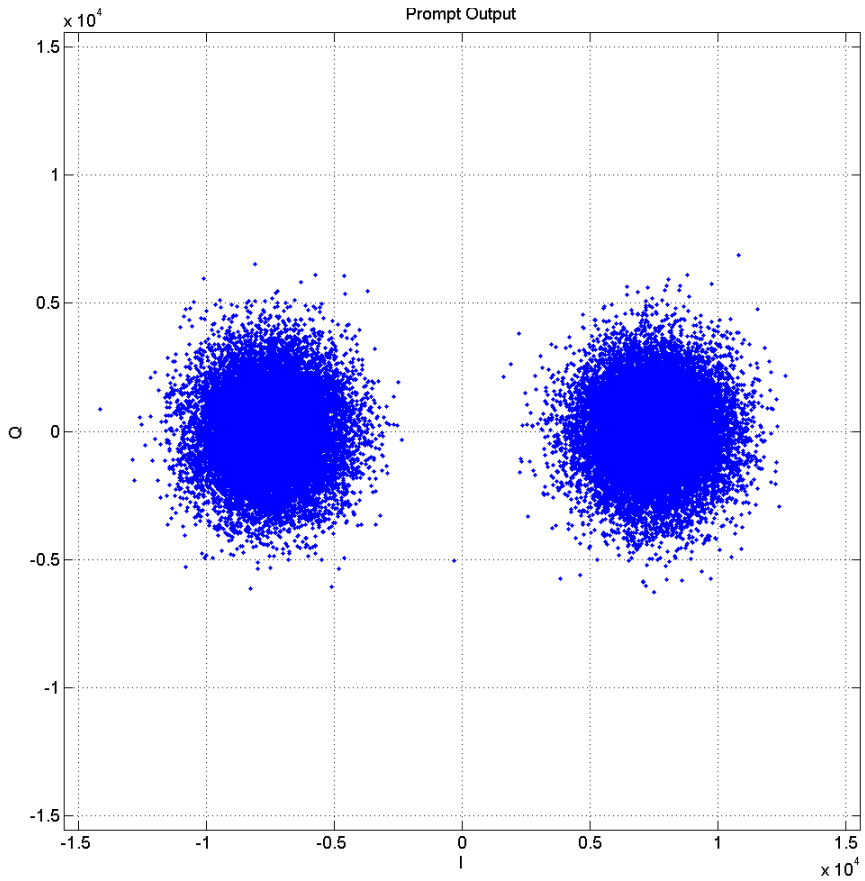

Figure 4.44. GEO Signal Tracking for PRN 18

If the same data is plotted against time, data bit transitions can be observed if the signal strength is strong enough. PRN 10 is plotted in Figure 4.45 as an example of a strong signal case while PRN 18 is plotted in Figure 4.46 is an example of the contrary.

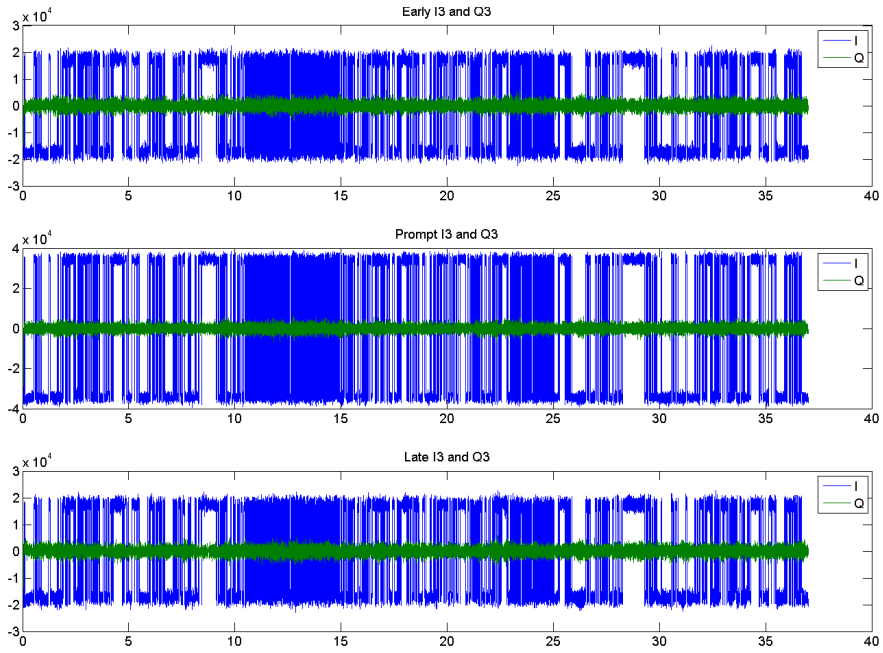

Figure 4.45. Tracked and Correlated Signal for PRN 10 at GEO

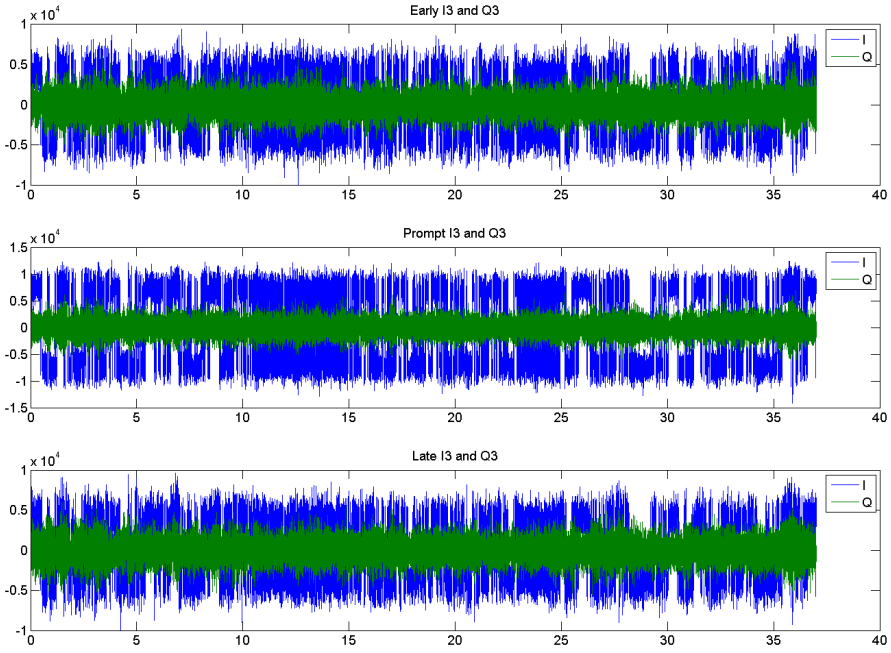

Figure 4.46. Tracked and Correlated Signal for PRN 18 at GEO

4.8 Summary

This chapter compared the position errors and resulting DOP for orbital altitudes that positioned the user from LEO to GEO. It is shown that the altitudes lower than the GPS constellation experienced position errors under 10 m when utilizing the GPS antenna sidelobes. As the orbital altitude increases from LEO until about $\frac{3}{4}$ of the GPS constellation, the number of GPS SVs in view also increased. Increasing the altitude from that location causes the number of available GPS to decrease due to lower signal strength received. Access to more than four GPS SVs while at GEO became difficult and the errors greatly increased. The errors accrued are in the same direction as the incoming GPS signals. The linear relationship between DOP and position errors existed for all the scenarios simulated in the research. This shows that DOP is still a valid metric for predicting precision levels in altitudes exceeding LEO.

Results from the RF signal processed by the SDR showed trends similar to the results of the MATLAB analysis. The signals uncovered in the 400 km LEO case are all distinctly above the noise floor (acquisition level of the non-present signals) and acquisition threshold. At 15150 km altitude, the processed RF contained more GPS SVs than the LEO signal, though a portion of these signals are close to the noise floor and barely passed the acquisition threshold. The scenarios above the GPS constellation showed an unexpected number of signals present. Based on this discrepancy, geometric analysis may be insufficient for analysis, especially at GEO.

V. Conclusion

5.1 Contributions

The research outlined in this thesis involved developing a process to evaluate expected GPS accuracy tailored to the concerns of satellite orbits. The process described in Chapter III involved modeling the orbits of the user and GPS constellation over a 24 hour period to obtain position and velocity information. This information is processed and compared against preset criteria thresholds on line of sight, Doppler shift magnitude, and received signal strength to determine which GPS SVs were accessible to the user. Pseudoranges are created for the accessible GPS SVs by calculating the true GPS to user range, then adding noise based on User Equivalent Range Error and the C/N0 for each signal. These pseudoranges are used to evaluate position estimation accuracy and the applicability of Dilution of Precision for users in the space environment.

Seven user orbits ranging from LEO up to GEO are simulated, with two of the orbits having an altitude above the GPS constellation. All the scenarios below the GPS constellation maintained access to a minimum of 13 GPS SVs throughout for the entire 24 hour simulation duration. The number of GPS PRNs steadily dropped as the altitude increased for the scenarios above the GPS constellation. The GEO scenario encountered multiple instances where 3 or less GPS PRNs are available.

The metrics discussed in this section are based off of a total of 1,000 Monte Carlo executions, with 1,441 time steps/data points for each Monte Carlo run. Each time instance is treated as a trial, resulting in $1,441,000$ samples of position rms error over the Monte Carlo runs for each scenario. Error percentages are calculated by finding the number of trials out of 1,441,000 data points that meet the desired criteria, e.g. under $10\,m$.

The results of 1,000 Monte Carlo simulation runs for position estimation are as follows: 99% the rms position errors stayed under $10\,m$ for the LEO scenarios. The position error for both MEO scenarios below the GPS constellation's altitude rose above $10\,m$ for 0.2% of the total trails. These results are specific to the scenarios where the GPS antenna's side lobes are modeled. Running a MEO scenario without the side lobe model resulted in less than four GPS SVs available for the entire simulation duration. As expected, the two orbits above the GPS constellation showed the worst results out of the group. In the MEO scenario with altitude of $25,000\,km$, 46% of position errors fell under $10\,m$ and 53.5% are between $10\,m$ and $100\,m$. The GEO scenario has the worst results: 31.2% are unable to calculate a solution, 0.4% of the errors are below $10\,m$, 23% are between $10\,m$ and $100\,m$, and 45.4% of the errors are greater than $100\,m$.

DOP is calculated for every scenario and compared against position errors. The linear relationship between DOP, measurement range error, and position error is shown to exist for all scenarios. The eigenvalue trends of both DOP and position error standard deviation are consistent with one another. DOP is still applicable for use when calculating position with space-borne GPS receivers.

5.2 Recommendations for Future Research

There are a few recommendations for future research on this topic. Each of these recommendations revolves around adding more fidelity to the model:

- Fully implement a SDR to not only track the GPS signals, but also provide position estimates by decoding the RF signals from GPS signal simulator.
- Comparing the results of different position estimation algorithms currently used in navigation solutions, such as a Kalman Filter, against those resulting from the Newton-Raphson method.

- Consideration of non-isotropic receiver antenna models and the effect on existing errors due to antenna placement and orientation on a receiver satellite.
- Consideration of multi-GNSS receivers and regional space-based augmentation systems.

5.3 Summary

This chapter summarizes the results of the thesis research effort as well as presented future work opportunities. Chapter 1 provides the motivation for researching on-board satellite position estimation based on GPS measurements. Chapter 2 gave insight to the characteristics of the potential orbits for the GPS receiver to reside and current GNSS constellations. Errors affecting the GNSS signal and known techniques for estimating position from those noisy signals was also presented in Chapter 2. Chapter 3 presents the methodology behind creating a model that incorporates the location and velocities of GPS SVs and the user, errors affecting each, and transmitter/receiver models to simulate expected position error. Chapter 4 shows that the GPS and the Newton least squares algorithm for position estimation will result in errors under $10\,m$ for altitudes under that of the GPS constellation. For altitudes above the GPS constellation, the Newton least squares method no longer results in errors under $10\,m$. It also shows that the relationship for DOP and position error still holds for all these altitudes.

Appendix A. Additional Figures

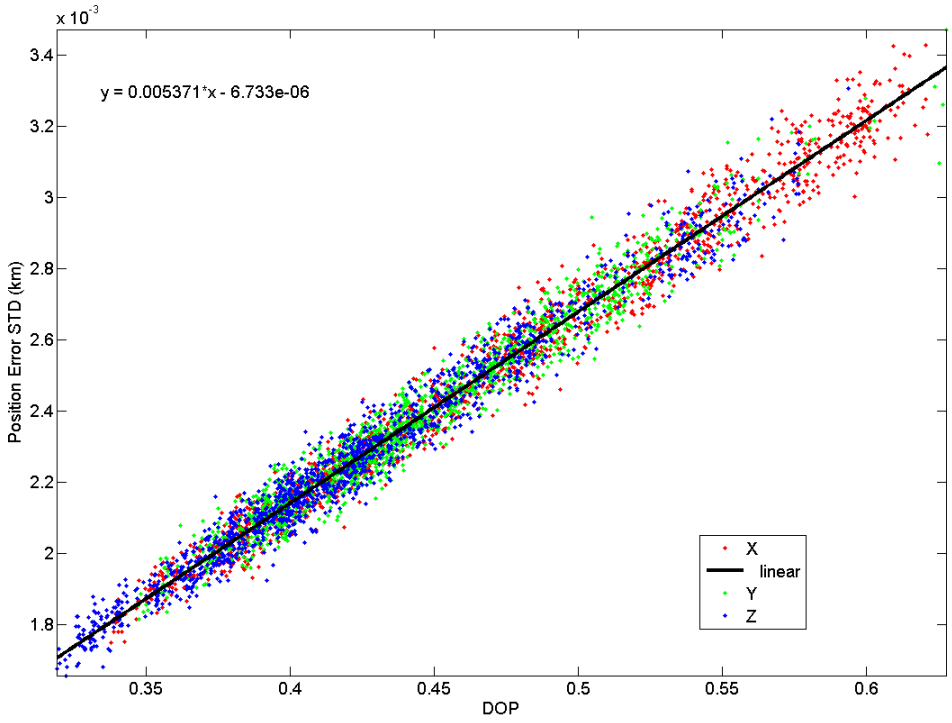

Figure 1.1. DOP vs Position Error STD at 15,150km

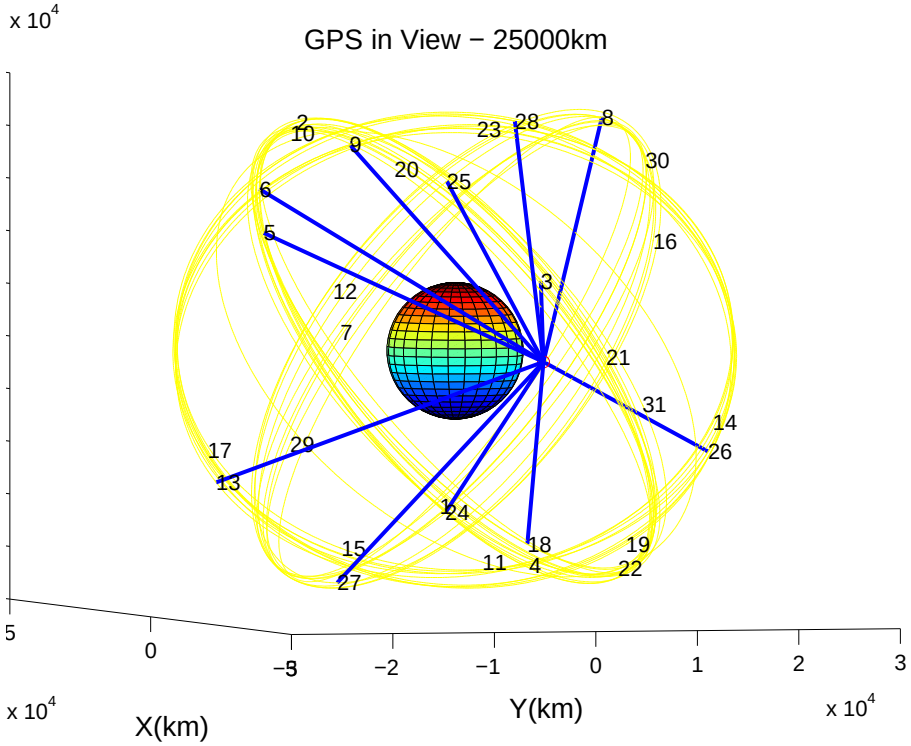

Figure 1.2. Different Angle of GPS in View at Scenario Start at 25,000km

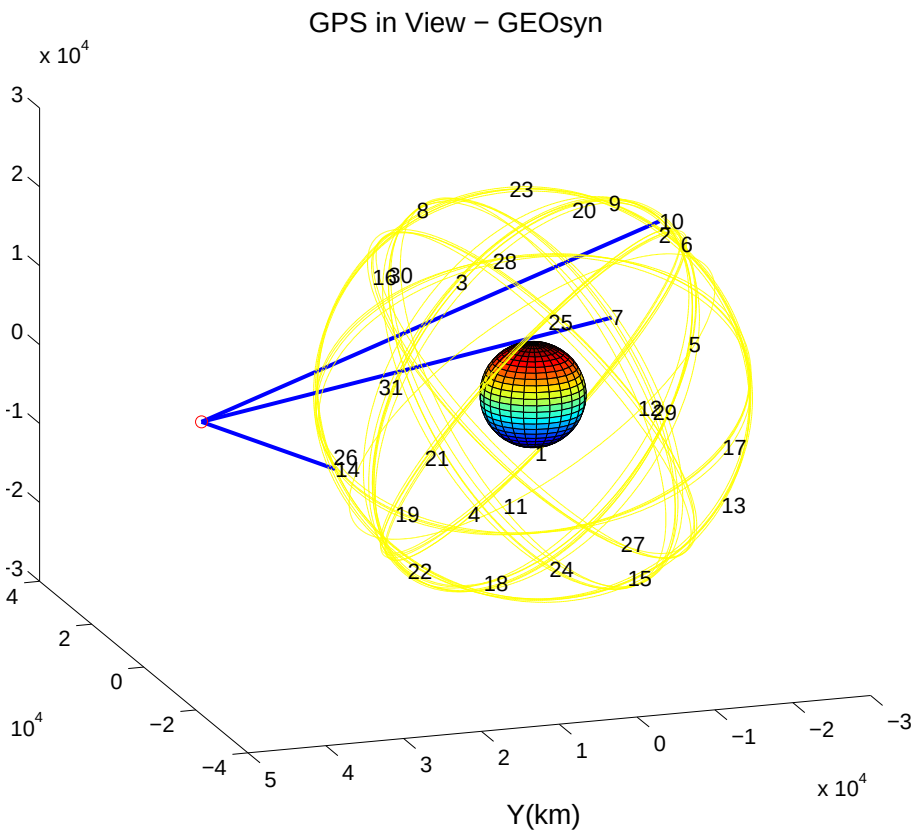

Figure 1.3. GPS in View Showing Side Lobe Connection

List of Acronyms

C/N0 Carrier Power to Noise Density Ratio

dB Decibels

DOP Dilution of Precision

ECEF Earth Centered Earth Fixed

ECI Earth Centered Inertial

ENU East-North-Up

GDOP Geometric Dilution of Precision

GEO Geostationary Orbit

GLONASS Global'naya Navigatsionnaya Sputnikovaya Sistema

GNSS Global Navigation Satellite System

GPS Global Positioning System

GTO Geostationary Transfer Orbit

GUI Graphic User Interface

HEO Highly Elliptical Orbit

ICD Interface Control Document

KF Kalman Filter

LEO Low Earth Orbit

LOS Line of Sight

MEO Medium Earth Orbit

PDOP Position Dilution of Precision

PIT Predetection Integration Time

PLL Phase Lock Loop

PNT Position, Navigation, and Timing

PRN Pseudo-Random Noise

RF Radio Frequency

SDR Software Defined Radio

SNR Signal to Noise Ratio

STK Systems Tool Kit

SV Space Vehicle

TLE Two-Line Element

UERE User Equivalent Range Error

Bibliography

1. *SIMGEN Software User Manual - Software for the SPIRENT Range of Satellite Navigation Simulator Products*. SPIRENT Communications, 2013. Document Number: DGP00686AAA.

2. Aeronautics, National and Space Administration. "Ancillary Description Writer's Guide, 2013", 2013. URL `http://gcmd.nasa.gov/add/ancillaryguide/platforms/orbit.html`.

3. Aghav, Sandip. "Development of On-Board Orbit Determination System for Low Earth Orbit (LEO) Satellite Using Global Navigation Satellite System (GNSS) Receiver Presentation". Department of Electronic Science, University of Pune, 2011.

4. Balbach, Oliver, Bernd Eissfeller, Guenter W Hein, Werner Enderle, Michael Schmidhuber, and Norbert Lemke. "Tracking GPS above GPS satellite altitude: first results of the GPS experiment on the HEO mission equator-S". *Position Location and Navigation Symposium, IEEE 1998*, 243–249. IEEE, 1998. ISSN 0780343301. DOI: 10.1109/PLANS.1998.670065.

5. Capuano, Vincenzo, Cyril Botteron, and Pierre-André Farine. "GNSS PERFORMANCES FOR MEO, GEO AND HEO". *SPACE COMMUNICATIONS AND NAVIGATION SYMPOSIUM-Space-Based Navigation Systems and Services*, EPFL-CONF-189830. 2013.

6. Filippi, Hannes, Eveline Gottzein, Christopher Kuehl, Carsten Mueller, Andrs Barrios-Montalvo, and Hugues Dauphin. "Feasibility of GNSS receivers for satellite navigation in GEO and higher altitudes". *Satellite Navigation Technologies and European Workshop on GNSS Signals and Signal Processing*

(NAVITEC), 2010 5th ESA Workshop on, 1–8. IEEE, 2010. ISSN 1424487404. DOI: 10.1109/NAVITEC.2010.5708023.

7. Hauschild, Andre, Markus Markgraf, and Oliver Montenbruck. "The Navigation and Occultation Experiment - GPS Receiver Performance On Board a LEO Satellite". *InsideGNSS*, 9(4):48–57, 2014. URL `http://insidegnss.com/node/4093`.

8. Henning, William. *User Guidelines for Single Base Real Time GNSS Positioning*. NOAA, 2011. URL `http://www.ngs.noaa.gov/PUBS_LIB/NGSRealTimeUserGuidelines.v2.1.pdf`.

9. Joseph, Angelo and Mark Petovello. "Measuring GNSS Signal Strength". 5(8):20–25, 2010. URL `http://www.insidegnss.com/node/2397`.

10. Kahr, Erin. "Prospects of Multi-GNSS Tracking for Formation Flying in Highly Elliptical Earth Orbits".

11. Kaplan, E. and C. Hegarty. *Understanding GPS: Principles and Applications, Second Edition*. Artech House, 2005. ISBN 9781580538954.

12. Kuang, Da, Willy Bertiger, Shailen Desai, Bruce Haines, Byron Iijima, and Thomas Meehan. "Precise orbit determination for COSMIC satellites using GPS data from two on-board antennas". *Position, Location and Navigation Symposium, 2008 IEEE/ION*, 720–730. IEEE, 2008. ISSN 1424415365. DOI: 10.1109/PLANS.2008.4570030.

13. Lorga, Jos FM, Pedro F Silva, Fabio Dovis, Andrea Di Cintio, Steeve Kowaltschek, David Jimenez, and Roger Jansson. "Autonomous orbit determination for future GEO and HEO missions". *Satellite Navigation Technologies and European Workshop on GNSS Signals and Signal Processing (NAVITEC),*

2010 5th ESA Workshop on, 1–14. IEEE, 2010. ISSN 1424487404. DOI: 10.1109/NAVITEC.2010.5708028.

14. Misra, P. and P. Enge. *Global Positioning System: Signals, Measurements, and Performance (Revised Second Edition)*. Ganga-Jamuna Press, 2012. URL `http://books.google.com/books?id=5WJOywAACAAJ`.

15. Person, Jon. "Writing Your Own GPS Applications: Part 2", 2008. URL `http://www.developerfusion.com/article/4652/writing-your-own-gps-applications-part-2/2/`.

16. Powell, Thomas D, Phillip D Martzen, Steven B Sedlacek, Chia-Chun Chao, and Randy Silva. *GPS Signals in a Geosynchronous Transfer Orbit:" Falcon Gold" Data Processing.* Technical report, 1999.

17. Riebeek, Holli. "Catalog of Earth Satellite Orbits", 2009. URL `http://earthobservatory.nasa.gov/Features/OrbitsCatalog/`.

18. Ruiz, Jennifer L and Charles H Frey. "Geosynchronous satellite use of GPS". *ION GNSS 18th*, 2005.

19. SMC, GPS. "NAVSTAR Global Positioning System Interface Specification". ARINC Engineering Services, LLC, 2004.

20. Won, Dae Hee, Jongsun Ahn, Seung-Woo Lee, Jiyun Lee, Sangkyung Sung, Heung-Won Park, Jun-Pyo Park, and Young Jae Lee. "Weighted DOP With Consideration on Elevation-Dependent Range Errors of GNSS Satellites". *Instrumentation and Measurement, IEEE Transactions on*, 61(12):3241–3250, 2012. ISSN 0018-9456. DOI: 10.1109/TIM.2012.2205512.

21. Yan, Junlin, Christian CJM Tiberius, Gerard JM Janssen, Peter JG Teunissen, and Giovanni Bellusci. "Review of range-based positioning algorithms".

Aerospace and Electronic Systems Magazine, IEEE, 28(8):2–27, 2013. ISSN 0885-8985. DOI: 10.1109/MAES.2013.6575420.

REPORT DOCUMENTATION PAGE

Form Approved
OMB No. 0704–0188

1. REPORT DATE *(DD–MM–YYYY)*	2. REPORT TYPE	3. DATES COVERED *(From — To)*
26–03–2015	Master's Thesis	Sept 2013 — Mar 2015

4. TITLE AND SUBTITLE

Expected Position Error for an Onboard Satellite GPS Receiver

5a. CONTRACT NUMBER

5b. GRANT NUMBER

5c. PROGRAM ELEMENT NUMBER

6. AUTHOR(S)

Williams, Anthony S., 1st Lt, USAF

5d. PROJECT NUMBER

15G167B

5e. TASK NUMBER

5f. WORK UNIT NUMBER

7. PERFORMING ORGANIZATION NAME(S) AND ADDRESS(ES)

Air Force Institute of Technology
Graduate School of Engineering and Management (AFIT/EN)
2950 Hobson Way
WPAFB OH 45433-7765

8. PERFORMING ORGANIZATION REPORT NUMBER

AFIT-ENY-MS-15-M-029

9. SPONSORING / MONITORING AGENCY NAME(S) AND ADDRESS(ES)

Intentionally Left Blank

10. SPONSOR/MONITOR'S ACRONYM(S)

11. SPONSOR/MONITOR'S REPORT NUMBER(S)

12. DISTRIBUTION / AVAILABILITY STATEMENT

Distribution Statement A:
Approved for Public Release; distribution unlimited.

13. SUPPLEMENTARY NOTES

14. ABSTRACT

The Global Positioning System (GPS) constellation provides ranging information that delivers inexpensive, high precision positioning for terrestrial users. Satellites in Low Earth Orbit (LEO) can use an onboard GPS receiver resulting in meter-level navigation solution accuracy. There are limitations to using GPS for positioning for satellites above LEO. The number of GPS satellites who's signal can be received decreases as the receivers altitude approaches that of the GPS constellation. Above the GPS constellation, the available GPS signals for ranging will originate from satellites on the opposite side of Earth. This research calculates the available GPS signals to the receiver and determines the expected position error, while considering the effects from a low signal to noise ratio, poor geometry, and signal shift caused by high relative velocity.

15. SUBJECT TERMS

GPS, Position Error, Dilution of Precision, Newton Least Squares

16. SECURITY CLASSIFICATION OF:			17. LIMITATION OF ABSTRACT	18. NUMBER OF PAGES	19a. NAME OF RESPONSIBLE PERSON
a. REPORT	b. ABSTRACT	c. THIS PAGE			Dr. Alan Jennings, AFIT/ENY
U	U	U	U	112	19b. TELEPHONE NUMBER *(include area code)* (937) 255-3636, x7495; alan.jennings.1@us.af.mil